Faculty of Engineering and Technology

Department of Mining and Geological Engineering

GROUNDWATER DEPLETION AT THE DUKWI WELLFIELD: CAUSES AND EFFECTS

by

ABIJAH DIPHOFU

Student ID number: 18100123

BSc (Soil and Water Conservation Engineering) (BUAN)

A Thesis Submitted to the Faculty of Engineering and Technology in Fulfilment of the Requirements for the Award of the Degree of Master of Engineering in Geological Engineering of BIUST

Supervisor: Dr. Jerome Anabannye Yendaw

Department of Mining and Geological Engineering

Faculty of Engineering and Technology, BIUST

BOTSWANA INTERNATIONAL UNIVERSITY OF SCIENCE & TECHNOLOGY

POSTGRADUATE SCHOOL

Declaration Regarding the Work and Copyright

FORM PGS - 320

DECLARATION REGARDING THE WORK AND COPYRIGHT

Candidate (please write in caps or type): ABIJAH DIPHOFU

Student ID: -18100123

Thesis Titled: - GROUNDWATER DEPLETION AT THE DUKWI WELLFIELD: CAUSES AND EFFECTS

I, the **Candidate**, certify that the Thesis is all my own original work and that I have not obtained a degree in this University or elsewhere on the basis of any of this work.

(If the thesis is based on a group project, then the student must indicate the extent of her / his contribution, with reference to any other theses submitted or published by each collaborator in the project, and a declaration to this effect must be included in the thesis)

Signed: ---------- Date: ------25/03/2022

Primary Supervisor (please write in caps or type): Dr. JEROME ANABANNYE YENDAW

I, the Candidate's **Primary Supervisor**, hereby confirm that I have inspected the above titled thesis and, to the best of my knowledge, it is based on the original work of the candidate.

Signed: ---------- Date: -25/03/2022----------

CERTIFICATION

The undersigned certifies that he has read and hereby recommends for acceptance by the Faculty of Engineering and Technology a thesis titled **Groundwater Depletion at the Dukwi Wellfield: Causes and Effects** in fulfilment of the requirements for the degree of Master of Engineering in Geological Engineering of the BIUST.

Dr. Jerome Anabannye Yendaw
(Supervisor)

Date: 22/06/2021

BIUST
BOTSWANA INTERNATIONAL UNIVERSITY OF SCIENCE & TECHNOLOGY

Plot 10071, Boseja Ward • Private Bag 16 , Palapye ,Botswana • Tel: +267493100/ 4900117 • Fax: +267 4900102

Postgraduate School

Antiplagiarism check

MEMORANDUM

Postgraduate candidate: Abijah Diphofu **Student ID**: 18100123

Degree level: Master **of Engineering in Geological Engineering**

Thesis Titled: Groundwater Depletion at the Dukwi Wellfield: Causes and Effects

The Anti-plagiarism Check had been completed and the results is detailed below.
Software and version used: **Turnitin Feedback Studio**

Outcome:

The final similarity index score stood at **11%** which is within a permissible range at BIUST.

Resolution: Comment from the Supervisor needed: YES [ ], or NOT [√] *(tick the appropriate)*
Officer who completed the check (please write in caps or type)

MR. KELEBONYE BAGAI

Signed: ---------- Date: 25/05/2021

COMMENTS BY THE PRIMARY SUPERVISOR (*if requested*):

_____

_____

_____

Primary supervisor (please write in caps or type)

_____

Signed: ---------- Date: 25/05/2021

ABSTRACT

The main issue associated with groundwater supply in Botswana are the rate of its replenishment relative to its extraction rate and quality. This study aims to identify the possible causes and effects of groundwater decline at the Dukwi Wellfield. Specifically, it aims to investigate the contributing variables for groundwater decline at the wellfield area; the trend and significance of groundwater level decline using the linear trend model; the influence of groundwater decline on water quality and chemistry change; the water quality and chemistry compliance based on the Botswana Bureau of Standard natural water specifications (BOS 262:2011) and to simulate and predict land subsidence using MODFLOW SUB and ModelMuse 4. The Pearson's correlation method was used to determine an association between various variables such as recharge and rainfall with the drop of water levels. The recharge rates were estimated using the hydrogeological model and were compared with abstraction rates. A piper plot was used for the geochemical characterization of groundwater at the wellfield area. The results from the hydrogeological model showed mean annual recharge rate of 1 149 691 m^3/year which is less than the mean annual total abstraction rate of 1 253 546 m^3/year. This influenced the decline of groundwater levels and a higher concentration of parameters such as Total Dissolved Solids and Electrical Conductivity. The simulated land subsidence of the study area from 2013 to 2019 ranged from 0.008 m to 0.022 m while the projected land subsidence from 2019 to 2031 will range from 0.015 m to 0.031 m. Overall, this study revealed that higher transmissivity estimates of 8.171 m^2/min, hydraulic conductivities of 0.0413 m/min and storativities of 0.0003299 were experienced at the study area, which influenced more extraction of groundwater resources and mean abstraction rates as high as 355 392 m^3/year. The statistical trends showed a declining water table with the coefficient of determination of 80% and above for most of the results from the trend model. The Electrical Conductivity and Total Dissolved Solids concentrations can be measured and monitored by implementing less energy consuming methods such as the Electromagnetic method.

ACKNOWLEDGEMENT

I would like to thank the All-Mighty God for giving me strength and guidance to complete this research work. Also, I would like to thank my supervisor Dr. Jerome Anabannye Yendaw for his continuous advice and help to complete this research work. I am grateful to the Department of Water Affairs and Water Utilities Corporation for allowing me to visit the Dukwi Wellfield and sharing with me the hydrological data of the wellfield. I also would like to thank the Botswana Meteorological Services for assisting me with the meteorological data in order to successfully complete this research work.

Lastly, I would like to thank my Mother Mrs. Kebatlhaole Ndiane for her kindness and devotion and her endless support throughout my years of studies.

TABLE OF CONTENTS

LIST OF FIGURES

LIST OF TABLES

CHAPTER 1

INTRODUCTION

1.1 Background Information

The crucial source of convenient water supply in Botswana is groundwater. About 65% of Botswana's water supply comes from groundwater resources for agriculture, industrial and household purposes, while the remaining 35 percent is from surface water (Du Plessis and Rowntree, 2003). The main issues associated with groundwater supply in Botswana are the rate of its replacement relative to the rate of extraction and its quality. Groundwater resource in Botswana is non-renewable and finite because its recharge is very little (Central Statistics Office, 2009). Groundwater depletion is a concern in Botswana, especially around mines and large settlements (Department of Environmental Affairs, 2006).

As an approach to groundwater resource management, identifying the causes of borehole failure is important and necessary when planning remedial measures for the wellfield as well as when appropriate water treatment methods are to be identified, if water quality deterioration exists due to borehole yield and water level decline. Chaoka *et al.* (2006) indicate that the determinants of groundwater depletion can reach about 80% of the total depletion in the wellfield. These determinants include water abstraction, discharge, low rainfall and higher evaporation rates due to extreme temperatures.

This investigation was necessitated by a continuous well yield decline in the Dukwi Wellfield which is located in the northeastern part of Botswana. The Dukwi Regional Wellfield has been identified by the Department of Water Affairs, Botswana, as one of the most important sources of potable water supply in the area. The Dukwi Regional Wellfield which was developed between 1985 and 1995 comprised of the Dukwi Wellfield Phase I, Dukwi Wellfield Phase II, Chidumela Wellfield and Soda Ash Botswana Boreholes (Geotechnical Consulting Services, 1998a).

The Dukwi Wellfield Phase II, which comprises of four production boreholes, is the only wellfield that is currently in operation, while the Dukwi Wellfield Phase I, Chidumela Wellfield and the Soda Ash Botswana Boreholes were shut down in 2008 due to their

diminishing water quality. The production boreholes of the Dukwi Wellfield Phase II were firstly operated in 1998 (Geotechnical Consulting Services, 1998a). Groundwater from the wellfield boreholes is abstracted from the Mea Arkose aquifer which is the main aquifer in north-eastern Botswana and part of the Karoo Supergroup (Geotechnical Consulting Services, 1998b; Legadiko, 2015).

1.2 Problem Statement

The Dukwi Wellfield is experiencing a continuous decline of groundwater levels. The Dukwi Wellfield Phase II shows no sustainable capacity to cope with the increasing demand for water supply to the centers which are dependent on it (Legadiko, 2015) therefore, indicating a need for proper and careful management of the wellfield.

Over abstraction in the Dukwi Wellfield leads to adverse effects in the environment such as lowering of the water table. Land subsidence due to excessive water table drawdown could be experienced around the Dukwi Wellfield, which could be detrimental to both human and animal life within and around the wellfield. This can lead to a permanent closure of the Dukwi Wellfield phase II which currently supplies the populace around the Dukwi area with potable water.

Water quality deterioration is being experienced at the Dukwi Wellfield Phase II. Poor groundwater quality was the main issue that resulted in the closure of the Dukwi Wellfield Phase I, Chidumela Wellfield and Soda Ash Botswana Boreholes, hence proper management of the remaining wellfield (Dukwi Wellfield phase II) has to be considered to avoid its closure. Therefore, this study is carried out to establish the causes of well yield decline at the Dukwi Wellfield which has led to poor water quality.

1.3 General Objectives

- To identify the possible determinants and effects of groundwater decline in the Dukwi Wellfield.

1.4 Specific Objectives

- To identify the contributing variables for groundwater decline at the Dukwi Wellfield.

- To determine the trend and significance of groundwater level decline in the Dukwi Wellfield.
- To determine the influence of groundwater decline on groundwater quality and chemistry change at the wellfield area.
- To evaluate the water quality of the study area for human consumption based on the Botswana Bureau of Standard natural water specification (BOS 262:2011).
- To predict land subsidence that can occur due to future groundwater exploitations.

1.5 Hypotheses

- Does the amount of rainfall and groundwater recharge significantly affect the groundwater level?
- Is the water quality change at the Dukwi Wellfield influenced by the hydro-geochemical parameters due to water level decline?
- Is the magnitude of land subsidence experienced at the wellfield area directly proportional to abstraction rates?

1.6 Significance of the Study

According to Du Plessis and Rowntree (2003), surface water in Botswana is a common resource that must be shared between a number of the Southern African Development Community (SADC) states that include Angola, Namibia, Zambia, Zimbabwe, South Africa and Mozambique. The development of surface water in Botswana is constrained by a number of factors such as high evaporation rates and lack of available dam sites. This indicates that water supply from surface water resources in Botswana is unreliable, hence groundwater management has to be considered to meet the increasing water demand in the country.

Earlier studies indicate that there is a decline of borehole yield and groundwater quality in most wellfields in Botswana, including the Dukwi Wellfield (Chaoka *et al.*, 2006; Central Statistics Office, 2009) but a limited research is done to determine the causes and effects of well yield decline. The last report done on the wellfield area was a modeling exercise by Legadiko (2015) to assess and quantify the available developed potable groundwater resources after a modeling exercise carried out by Water Surveys Botswana (Department of Water Affairs, 1995a, 1995b) between 1992 and 1995. This indicates that there is a need for a proper management of wellfields in Botswana, as they supply most potable water.

1.7 Thesis Outline

- Chapter 1 which is the introductory chapter contains the background information of the study, the problem statement, hypotheses, significance and objectives of the study.
- Chapter 2 presents the general information about the wellfield area.
- Chapter 3 presents a literature survey on factors that influence groundwater depletion and the effects of groundwater depletion. This chapter further describes and justifies the analytical methods used in this study to identify the causes and effects of groundwater depletion.
- Chapter 4 describes the overall methodology together with the models that were used to identify the causes and effects of groundwater depletion at the wellfield area.
- Chapter 5 presents results of the determinants of groundwater depletion as well as the outcomes that result from the depletion of groundwater. This chapter further discusses the results of the causes and effects of groundwater depletion.
- Chapter 6 summarises the main ideas from the study, together with the recommendations for future work.

CHAPTER 2

GENERAL INFORMATION ABOUT THE STUDY AREA

2.1 Study Area

The Dukwi Wellfield Phase II is located in the Central District, in the northeastern part of Botswana. The wellfield is located about 135 km northwest of Francistown and about 50 km Southeast of Nata. The study area is bound by longitudes 26˚21'E and 26˚29'E and latitudes 20˚31'S and 20˚35'S with a coverage area of approximately 483 km^2. Water from the wellfield is supplied to Dukwi, Nata, the Dukwi Refugee Camp and the Soda Ash Botswana (SAB) plant. The wellfield is administered by the Tutume Sub-District Council (Geotechnical Consulting Services, 1998a).

The wellfield consists of four production boreholes (BH 7674; BH 7675; BH 7678 and BH 7687); 32 private boreholes for abstraction of water for livestock and domestic purposes; 2 production boreholes owned by Soda Ash Botswana Mine and 28 monitoring wells for groundwater levels and water quality analysis (Geotechnical Consulting Services, 1998a; Legadiko, 2015) (Figure 2.1). The monitoring wells are used to detect and control the impact of groundwater abstraction from the production boreholes and contamination loading on the aquifer system (Brunner and Kinzelbach, 2008). Figure 2.2 indicates the location of the study area in the Central District of Botswana, while Table 2.1 shows the geographic coordinates of some of the monitoring wells and production boreholes located at the study area.

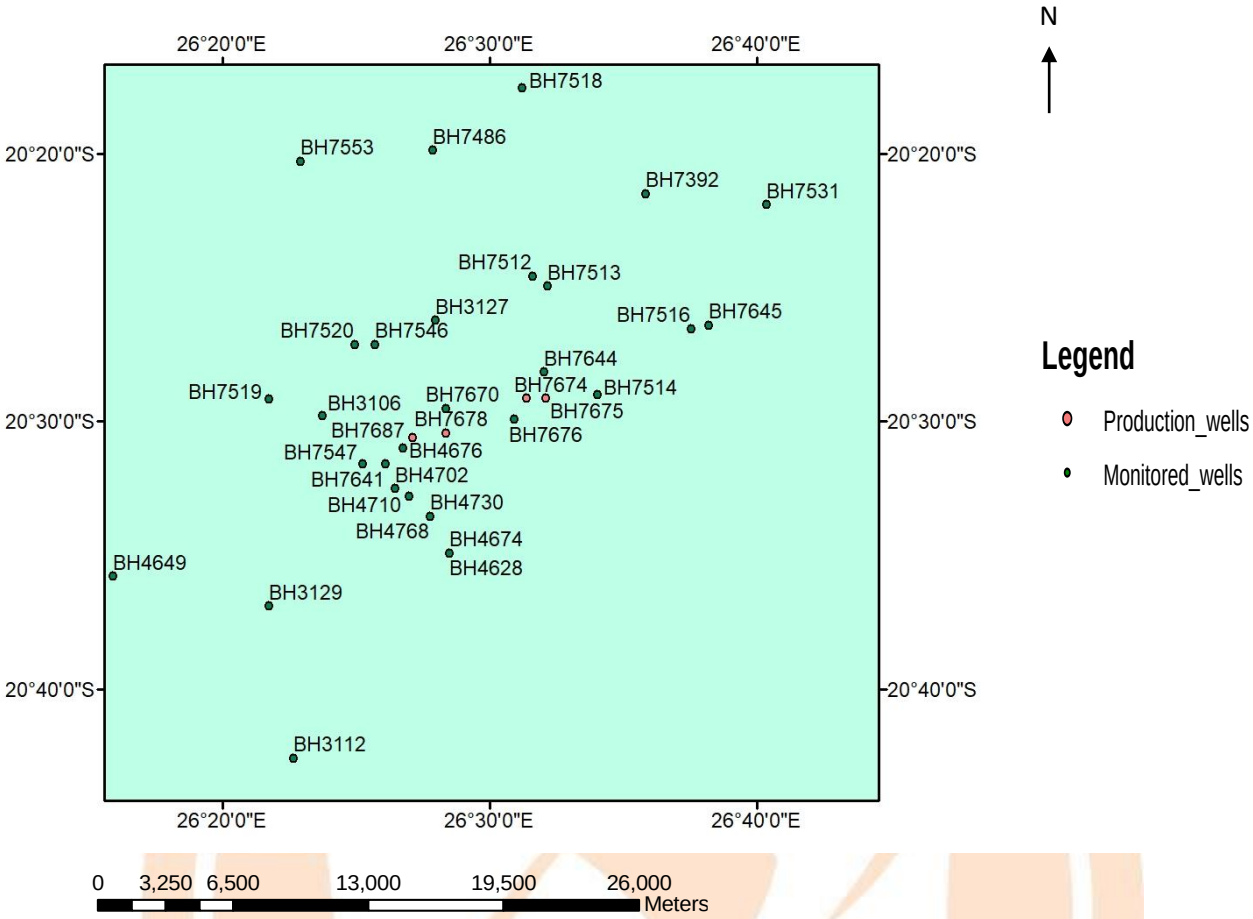

Figure 2.1 Monitoring wells and production boreholes in the project area (Department of Water Affairs, 2019a)

Table 2.1 Coordinates of the monitoring wells and production boreholes

Borehole Number	Northing (m)	Easting (m)	Latitude (deg:min:sec)	Longitude (deg:min:sec)
BH 7392	7734986.670	452501.990	20°29'05.61"S	26°32'40.32"E
BH 7486	7752468.583	442923.684	20°19'35.94"S	26°27'11.69"E
BH 7487	7758002.796	432794.545	20°16'34.72"S	26°21'23.14"E
BH 7512	7743309.759	450731.105	20°24'34.68"S	26°31'40.02"E
BH 7513	7741990.704	451619.380	20°25'17.68"S	26°32'10.54"E
BH 7514	7735165.546	454873.359	20°28'60.00"S	26°34'02.20"E
BH 7516	7739694.884	460963.777	20°26'33.14"S	26°37'32.80"E
BH 7518	7756280.021	449967.940	20°17'32.66"S	26°31'14.99"E
BH 7531	7748261.743	465857.240	20°21'54.78"S	26°40'22.27"E
BH 7549	7759124.976	462091.537	20°16'01.11"S	26°38'13.20"E
BH 7553	7751175.418	435539.228	20°20'17.16"S	26°22'56.88"E
BH 7641	7730294.980	439673.853	20°31'36.92"S	26°25'16.93"E
BH 7645	7739945.017	462134.581	20°26'25.09"S	26°38'13.22"E
BH 7674	7734870.434	450301.160	20°29'09.19"S	26°31'24.34"E
BH 7675	7734886.770	451507.962	20°29'08.77"S	26°32'06.00"E
BH 7676	7733403.436	449520.159	20°29'56.84"S	26°30'57.23"E
BH 7678	7732440.052	445065.036	20°30'27.73"S	26°28'23.32"E
BH 7686	7733628.244	447000.552	20°29'49.27"S	26°29'30.27"E
BH 7687	7732126.839	442906.418	20°30'37.69"S	26°27'08.76"E

Source for borehole location: Department of Water Affairs (2000)

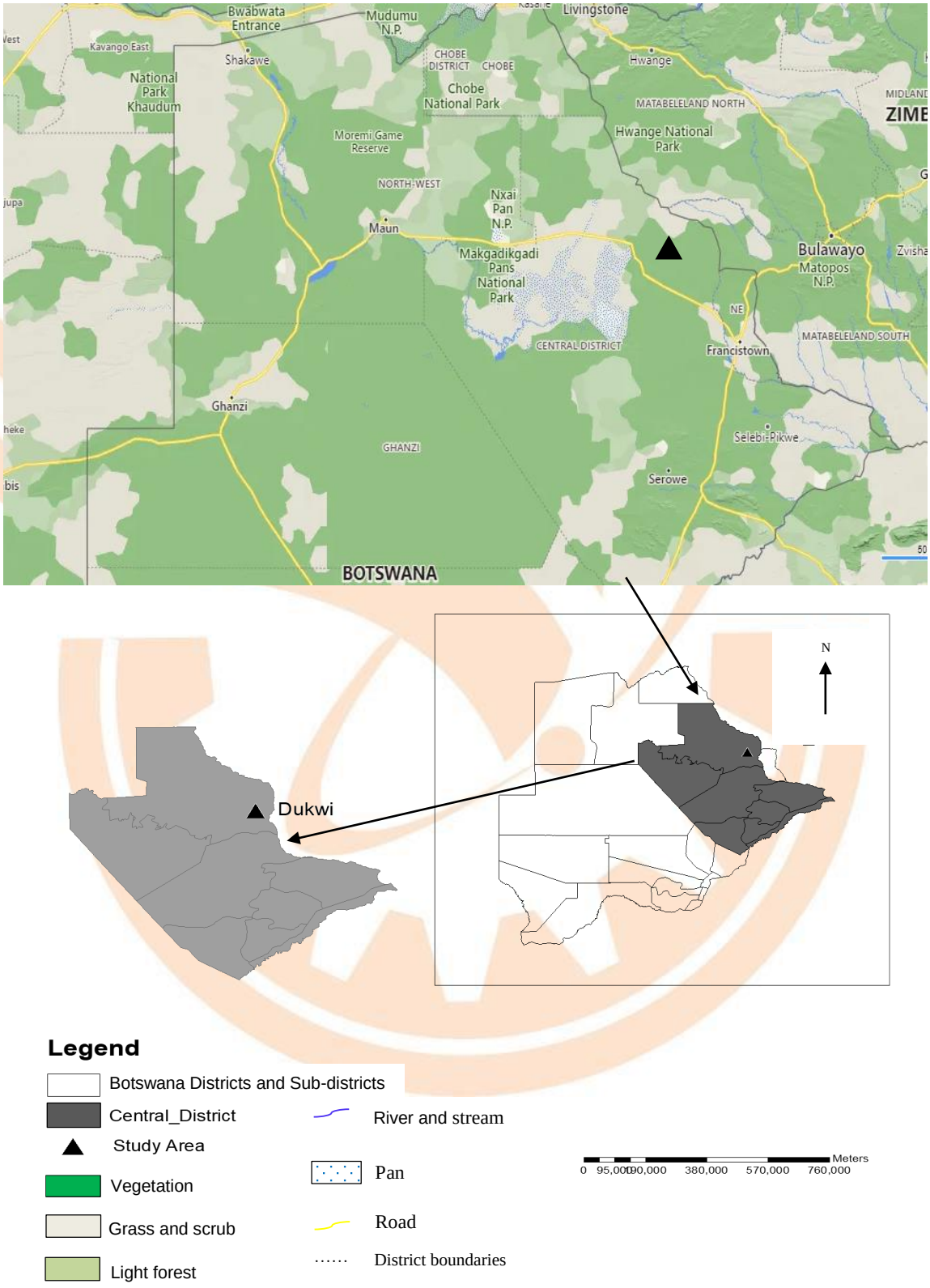

Figure 2.2 Location of the study area at the Central District

2.2 Physiography

The area is a plain that dips gently towards the Makgadikgadi depression to the west into which the aquifer system of the study area discharges. The ground elevation varies from approximately 900 meters above mean sea level (m amsl) at the edge of 'Sua Pan' to approximately 1000 m amsl in the east. The regional ground surface gradient is 1.7 m/km (Geotechnical Consulting Services, 1998a).

The Department of Water Affairs (1995) as cited in Legadiko (2015) indicates that the only significant topographic feature around the wellfield area occurs to the southeast of the study area, where 'Kgwana Hills', made up of a series of quartzitic inselbergs form a linear ridge aligned roughly north-south dominates part of the project area. The Kgwana hills which form the highest elevation in the study area, is 1065 m amsl. The eastern-most limit of the Paleo-Makgadikgadi Lake is represented by the 940 m amsl ground surface contour line. River channels are highly sinuous upstream of this elevation, whereas downstream the channels are anastomosing.

The boundaries of the aquifer area are defined by the Mosetse River that flows to the south and the Tutume, Nata and the Semowame Rivers that flow to the north of the wellfield. These rivers which are ephemeral, only flow after heavy rains into the Sua Pan. The rivers originate in the crystalline rocks to the east of the aquifer area. The deposition patterns of the rivers are controlled by low gradients, resulting in inland deltas and wide braided plains where the rivers enter the Sua Pan. Plains with a thick sand cover of up to 20 meters dominate the project area (Geotechnical Consulting Services, 1998a).

2.3 Climate

According to the Botswana Meteorological Services (2019a, 2019b), the area is semi-arid with cold, dry winter and very hot, wet summers. Rainfalls are unreliable and unevenly distributed, normally occurring in summer between September and April (Figure 2.3). There is a climatic transition period from wet to dry season around April and May and sometimes to early June. The dry period normally starts in June or sometime late May and ends in August or sometimes early September. The winter period normally starts towards the end of May to the beginning of August. The annual rainfall from 2010 to 2019 varied, ranging from 103.8 mm to 420.2 mm (Figure 2.4) (also see Appendix E).

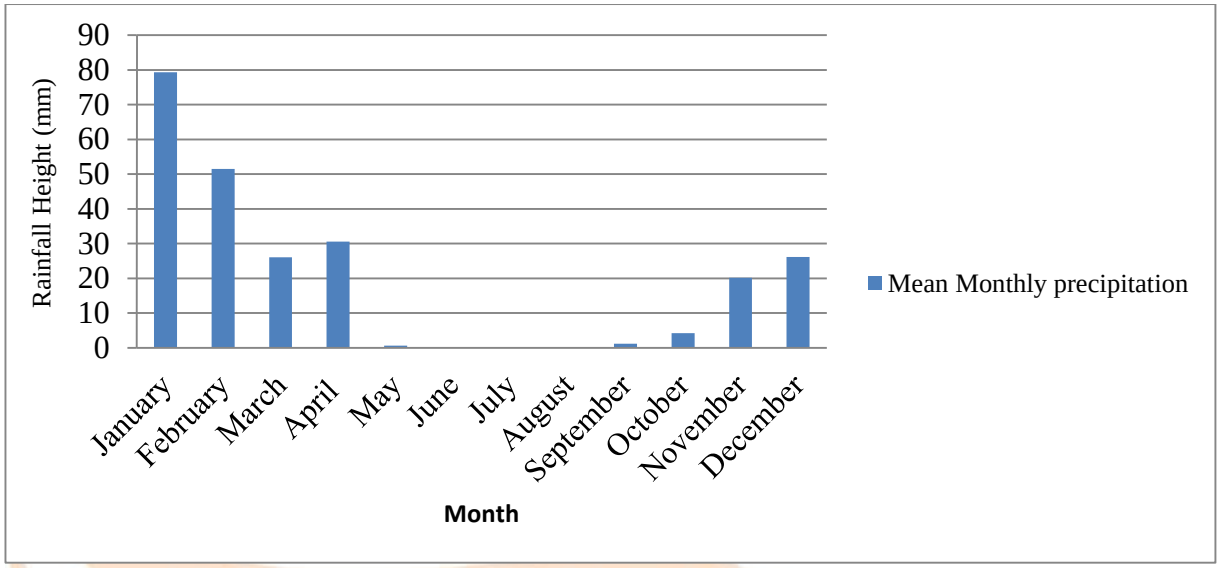

Figure 2.3 Mean Monthly Precipitation of the study area (2010-2019)

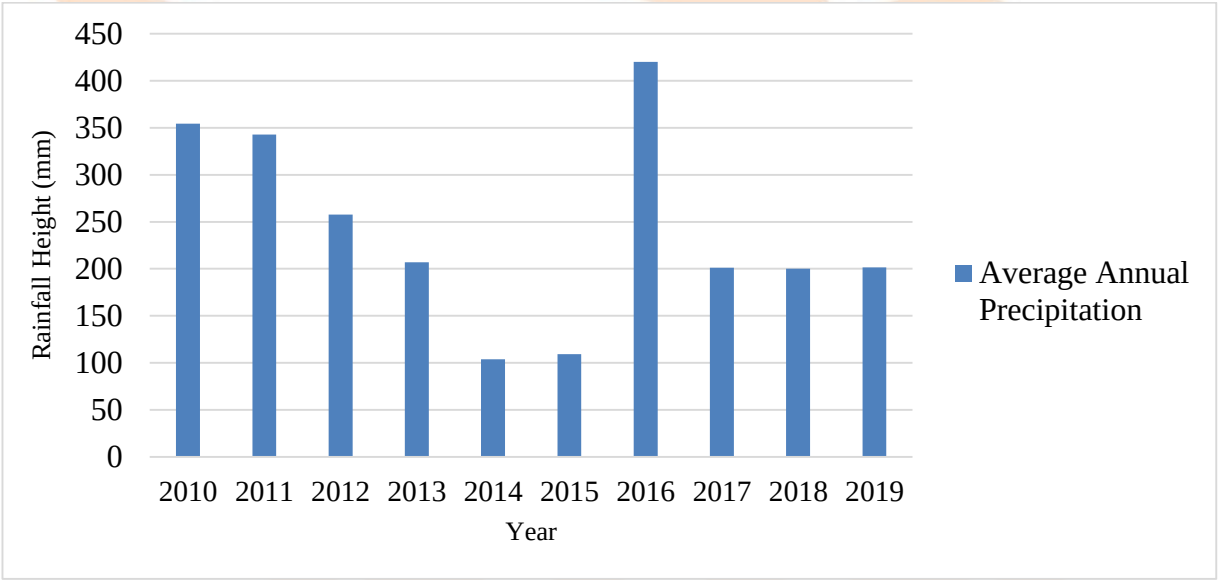

Figure 2.4 Annual Precipitation of the study area (2010-2019)

According to Bhalotra (1984) as cited in Geotechnical Consulting Services (1998a) rainfall in Botswana occurs due to three air streams namely: The Inter-tropical Convergence Zone; the south-eastern trade winds and the north-eastern monsoon winds. The Inter-tropical Convergence Zone winds mainly bring rain in January; the south-eastern trade winds in December while the north-eastern monsoon winds dominate the study area and are associated with the monsoon cycle of the Mozambique which occurs due to warm air that blows from the Indian ocean between April and September.

Figure 2.5 indicates the minimum temperatures of the study area during winter and the maximum temperatures during summer from 2010 to 2019. The winter temperatures (minimum temperatures) are normally below 18 ℃ with very low humidity and almost absent rainfall. Due to low amount of rainfall and humidity in winter, the area is often dry even when morning dews normally occur. Transition from winter to summer occurs around September and October, where the temperature starts to increase up to 40 ℃ in late October (Legadiko, 2015). The precipitation events are typically local high intensity events that occur in a short duration (Geotechnical Consulting Services, 1998a).

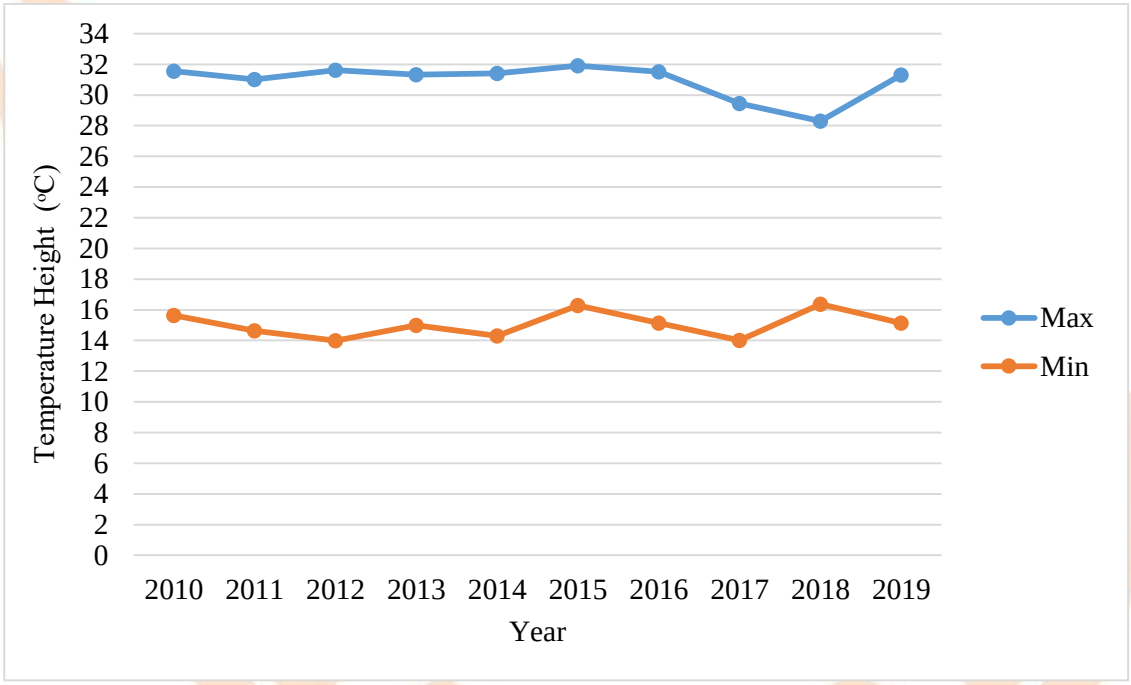

Figure 2.5 Annual maximum and minimum average temperatures of the study area (2010 to 2019).

2.4 Vegetation and Soils

According to the Department of Water Affairs (1995a) the area's vegetation is strongly influenced by major landforms. Mophane woodland mainly dominates the area, followed by shrubs species where the soils have poor drainage, or by mixed woodlands where there is drainage improvement, and the soils are deep. The vicinity of Sua Pan is characterized by grassland, where the occurrence of trees is inhibited by high salinity.

The soils in the area differ widely according to the parent material and the formational processes relating mainly to the Paleo Makgadikgadi Lake and the present-day pans. Saline

lacustrine clays and silts mainly as vertisols (black cotton soils) occur to the west of the study area, near Sua Pan. These soils grade into calcareous soils on the pan fringe areas and are gradually replaced by deeper sandy soils to the east (Geotechnical Consulting Services, 1998a).

2.5 Geology

Green (1966) and Stansfield (1973) indicate that the Dukwi Wellfield Phase II belongs to the eastern Karoo Sub-Basin portion of the Karoo Basin in Botswana. The pre-Karoo Basin lies at approximately 400 meters below the ground level. The western boundary of the Karoo Supergroup of the North-eastern part of Botswana, which is the faulted edge of the Stromberg Basalt, oversteps the Gantsi-Chobe fold belt marks, while the southern boundary of the Dukwi area is marked by Precambrian basement. The basement outcrops as ridges in the south and coincides with the Karoo dyke swarms through the Makgadikgadi Pans. The occurrence of ridges greatly influences sedimentation to occur in the study area. These ridges are recognized as the lower Karoo starter, hence the Ecca and the Dwyka stratigraphic units have been encountered in the southern part of the study area.

The geological map of the study area is shown in Figure 2.6 while the general regional stratigraphical succession for the Dukwi region is indicated in Table 2.2.

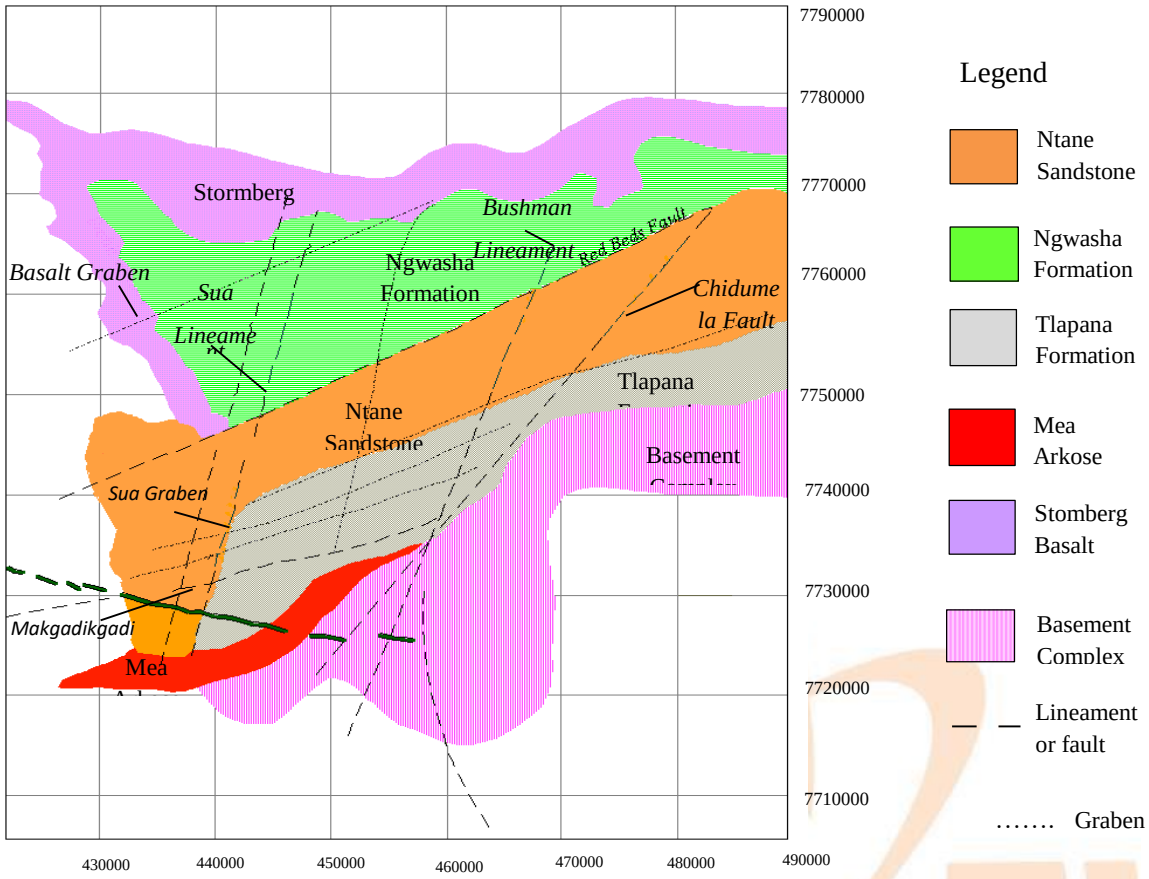

Figure 2.6 Geological map of the study area (Geotechnical Consulting Services, 1998a)

Table 2.2 Stratigraphic succession of the Dukwi area

Age	Stratigraphic Unit			Lithology
	Supergroup	Group	Formation	
Tertiary & Recent	-	Kalahari	-	Alluvium, calcrete and silcrete
Post-Karoo	Dolerite intrusions (dikes and sills)			
Lower Carboniferous to Upper Jurassic	Karoo	Stormberg		Basaltic flood lavas
		Lebung	Ntane Sandstone	Aeolian and fluviatile sandstones
			Ngwasha	Red to purple coloured mudstone and sandstone
			Pandamatenga	White coarse sandstone
		Ecca	Upper Tlapana	Variegated mudstones
			Lower Tlapana	Dark carbonic shales & coals
			Mea Arkose	Fluvio-deltaic sandstone with coals
		Dwyka	Dukwi	Grey varved mudstone and shale
Archaean Basement	Mosetse River Gneiss Group			Quartz, feldspar gneisses, migmatites and granitic gneisses
	Greenstone Belt Rocks			Chlorite-talc schists and green amphibolites

Source: Geotechnical Consulting Services (1998a)

Descriptions of the various stratigraphic units are provided below.

2.5.1 Archaean Basement

According to Reeves (1978) and Mason (1998), the Basement of the Dukwi area consists of two major units namely: the non-granitic schists/metasediments (referred to as greenstones) and the Mosetse River Gneiss Group. The Greenstone Belt rocks are encountered at a shallower depth eastwards and southwards and do not crop out within the area. These rocks trend NNE within the granitic basement and their composition is a combination of mafic and ultramafic rocks which are mainly chlorite-talc-schists and amphibolites and are characteristically green in colour.

The greenstone type rocks are part of the Archaean and Proterozoic belts of Zimbabwe, which truncate in the south against the Makgadikgadi Line. The Makgadikgadi Line, traceable across central and western Botswana separates Archaean cratonic rocks in the east from Proterozoic craton strata in the west.

The Mosetse River Gneiss Group is exposed in the southern part of the area and consists of quartz, feldspar gneisses, migmatites and granitic gneisses of sedimentary origin (Benett, 1970). The granitic gneisses predominate the area and are thought to be the result of granitization of fine-grained quartz-feldspar-biotite rich sediments. Throughout the gneiss group, amphibolites and subordinate schists and limestones occur widely but in limited amounts. The limestones are sheared and brecciated and show copper mineralization.

2.5.2 Karoo Supergroup

Identified as the "Nata Sub-Basin" by Smith (1984), the Karoo rocks of the north-eastern part of Botswana form part of a much larger sedimentary basin, which extends eastwards into Zimbabwe and northwards into Zambia and the Caprivi Strip. The Karoo Supergroup in the Dukwi area consists of four lithological units namely: the Dwyka, Eccra, Lebung and the Stormberg groups as described below.

The Dwyka Group represents the lowest member of the Karoo Supergroup. The sediments were deposited under glacial conditions and do not outcrop within the wellfield area. The group is represented by the Dukwi Formation in the Dukwi area (Stansfield, 1973). This formation is divided into a lower member of sedimentary rocks with beds of sandstone and tilloids and an upper member of varved shales occasionally covered by a thin bed of gritty pellet conglomerate.

The Ecca Group comprises the Mea Arkose Formation and the Tlapana Formation. The Mea Arkose Formation, also referred to as the "Middle Ecca" after Green (1966), outcrops in the southern part of the wellfield area and has an average thickness of 136 m. The formation comprises white, gritty arkoses and sub-arkoses, which frequently develop orange, iron stained bands in weathered outcrops. The feldspars are fresh in the unweathered rock, but when weathered they deteriorate to a white powder, probably kaolin. Pebbles are found throughout the sequence, either with a scattered distribution or confined to distinct beds. Fluviatile conditions prevailed during the sedimentation (Stransfield, 1973).

The Tlapana Formation is comprised of mudstones, siltstones and carbonaceous mudstones that overly the Mea Arkose Formation. The formation is subdivided into Lower Tlapana and Upper Tlapana Formation (Smith, 1984). The Lower Tlapana is characterized by the occurrence of coal and associated carbonaceous shales and mudstones with a mean thickness of 46 m in the wellfield area. Coals and carbonaceous horizons containing siderite and pyrite are generally subordinate in quantity to grey mudstones. A highly variable depositional environment is indicated by the lateral inhomogeneity of the formation.

The Upper Tlapana is the non-carbonaceous division of the formation and is distinguished by the complete absence of carbonaceous rocks. This formation has a mean thickness of 47 m and a maximum recorded thickness of 131 m in the wellfield area. The depositional conditions were such that a constant supply of argillaceous material was able to reach the shallow open waters in the area (Geotechnical Consulting Services, 1998a).

The mudstones outcrop over much of the southern part of the wellfield area. They are finely grained, massive and nodular, and vary in color ranging from purple, yellow, and brown to grey. The upper contact with the Pandamatenga Formation Sandstones is sharp.

According to Stansfield (1973), the Lebung Group is composed of the Pandamatenga, Ngwasha, and the Ntane Sandstone Formations. Pandamatenga Formation constitutes the bottom of the Lebung Group, lies unconformably on the Tlapana Formation, and does not outcrop within the wellfield area. The formation consists mainly of fine to medium grained calcareous sandstone and mud-flake breccias and conglomerates. The formation was probably deposited under fluviatile conditions in an arid continental environment as suggested by the presence of concretionary limestones.

The Ngwasha Formation also referred to as the “Red Beds” (Green, 1966) lies uncomfortably below the Ntane Sandstone Formation and consists of red thick, muddy siltstones with calcareous nodules. Both the color and the presence of calcareous nodules indicate oxidation of iron ores and evaporation of carbonate-rich groundwater in semi-arid conditions.

The Ntane Sandstone Formation which is equivalent to the Cave Sandstone (Green, 1966) covers much of the wellfield area and mainly comprises of coarse, gritty, cross-bedded

sandstones changing upwards to thinly bedded, medium to coarse-grained sandstones of cream-brown to red color. The sandstone is rich in quartz and contains feldspar and quartz pebbles up to 1 cm in diameter. The Ntane Sandstone Formation is suggested to be aeolian deposits (Smith, 1984).

The Stormberg Group comprises the youngest rocks of the Karoo Supergroup and is represented by basaltic lavas. The group is present mainly to the north of the wellfield area. A narrow graben controlled by NW trending lineament extends south-eastwards from the north into the wellfield area. Within this basalt graben some 30 m of highly weathered tuffaceous lava are present. The lavas are typically grey-green to purple-grey, are fine-grained, and contain amygdales and vesicles. Their widespread distribution suggests a non-explosive deposition (Geotechnical Consulting Services, 1998a).

2.5.3 Post-Karoo Intrusions

The intrusion of dolerite, mainly as dikes took place during the Post-Karoo. These intrusions, which are present throughout the area, predominantly trend in a west-northwest direction (Geotechnical Consulting Services, 1998a).

2.5.4 Tertiary and Recent Deposits

The Kalahari Group in the area consists of sandstones (especially in the northern part of the Sua Pan), calcrete and silcrete, and alluvial sands along the riverbeds. The older Tertiary Aeolian Sands and semi-consolidated sandstones, which form the basal member of the Kalahari Beds Formation, do not exist in the wellfield area (Geotechnical Consulting Services, 1998a).

2.6 Geological Structure

Stansfield (1973) described the geological structure of the area based on the tectonic past events of the Dukwi area. The geological structure is due to three tectonic episodic events namely, the Ancient Episodes, Inter-Karoo Episodes and the Post-Karoo Episodes which occurred around the area. The Ancient Episode Tectonics affected the rocks of the basement only and changed the pile of sediments that existed before to gneisses which the basement comprises of. The Inter-Karoo Episodes were accountable for the unconformity that occurred at the base of the Mea Arkose and the Ntane Sandstone. The Post-Karoo Episodes were responsible for the displacement of the Karoo Formations in the study area.

Fault traces across the study area were revealed by examination of aerial photographs of the area by Stansfield (1973). The most prominent structures are the Bushman and the Sua Lineaments (see Figure 2.6, Section 2.5).

Tectonic structures and the basin sedimentary infilling essentially determine the groundwater hydrodynamics (Geotechnical Consulting Services, 1998a). The major structural features that influence the hydrogeology of the study area are indicated in Table 2.3.

Table 2.3 The Main Structures and Lineaments within the Wellfield Area

Structure	Trend	Age of Structure	Age of Reactivation
Sua Lineament	NNE	Pre-Cambrian	Carboniferous, Permian Quaternary
Bushman Lineament	NNE	Pre-Cambrian	Carboniferous to Quaternary
Chidumela Fault	NE	Pre-Cambrian	Carboniferous, Permian Quaternary
Makgadikgadi Line	ENE	Pre-Cambrian	Carboniferous and Permian
Basalt Graben	NW	Permian	Triassic and Jurassic
Red Beds Fault	ENE	Permian	Triassic
Dolerite Dykes (Tuli Swarm)	WNW	Jurassic	Jurassic

Source: Department of Water Affairs (1995a).

The Department of Water Affairs, (1995a) through satellite imagery, regional geophysics, and drilling activities drew the following conclusions with regards to the geological structures of the wellfield area as shown in Figure 2.7, Section 2.7.3:

- North to south trending faults that are parallel to amphibolites and meta-limestones of the Matsitama Greenstone occur mainly to the eastern part of the area.
- North to north-northeast trending lineaments occur across the whole area. The most significant structure with this trend is the Sua Lineament, which defines the western edge of the Dukwi Basin. This lineament, which is clearly visible on the satellite imagery, was confirmed by an aeromagnetic low and can be explained as a narrow graben. This fault zone coincides with the maximum extension of the Makgadikgadi Palaeo Lake in the quaternary period.

- Northeast trending faults define the south-eastern boundary of the Dukwi Basin. The Chidumela Fault belongs to this group and is coincident with a change in basement type, from paragneisses to the east to metasedimentary/volcanic greenstones to the west.
- East-northeast trending fractures parallel to the Makgadikgadi Line identified in the center of the area which can be traced north-eastwards until it curves and becomes parallel to the northeast trending faults. It defines the southern edge of the basin.
- East-southeast to west-northwest trending lineaments mainly present in the southern part of the area. These lineaments represent the northern edge of the Tuli Dyke Swarm, which extends some 1000 km across northern Botswana from Zimbabwe. The dykes intersect the Makgadikgadi Line and are evidence of a major crustal rifting event (Reeves, 1978).
- Northwest to southeast trending lineaments in the northern part of the area which form a graben structure to the west of the wellfield area.
- North-northwest to south-southeast trending faults perpendicular to the Bushman Lineament and define the eastern edge of the Dukwi Basin.

2.7 Wellfield Hydrogeology

2.7.1 Current Wellfield Layout

The Dukwi Wellfield Phase II is the only wellfield that is currently in operation, while the other two wellfields comprising Dukwi Wellfield Phase I, Chidumela Wellfield and the Soda Ash Botswana Boreholes that make up the Dukwi Regional Wellfield were decommissioned due to their deteriorating water quality. The Dukwi Wellfield Phase II comprises of four production boreholes, namely BH 7674, BH 7675, BH7678 and BH7687 (Geotechnical Consulting Services, 1998a).

The production boreholes are connected by 160 mm, 200 mm, 250 mm and 315 mm diameter pipelines that transfer water to a reservoir, a lip tank and a booster tank, in order to supply water to Sua Pan (Sowa Town), Nata, Dukwi and the Dukwi Quarantine Camp areas (Geotechnical Consulting Services, 1998a). Water level and chemistry monitoring is done on 28 monitoring wells that are well distributed across the project area. The monitoring process is done on a monthly basis (Legadiko, 2015). Abstraction in the four production boreholes is done by some electrical submersible pumps which are connected to Telemetry system (Geotechnical Consulting Services, 1998a).

2.7.2 Drilling and Construction Details of Boreholes

The drilling and construction details for the Dukwi Wellfield Phase II are presented in Table 2.3. The details include the borehole depths, diameters drilled, pump intake, casing and screening.

The production boreholes range in depth of 125 meters below ground level (mbgl) to 198 mbgl. The boreholes are cased and screened for the total length of each borehole. The boreholes are packed with gravel to the top of the Mea Arkose and pressure grouted to the surface. In some of the boreholes, 20 slot stainless steel wire wound screens with 18% open area and a diameter of 205 mm were installed, while in other boreholes, slotted casing was used (Legadiko, 2015). The construction details are summarised in Table 2.4.

Table 2.4 Drilling and Construction Details for the Production Boreholes

Borehole Number	Depth (mbgl)	Drilling Details (Interval (m)/ Diameter (mm))	Casing Details (Interval (m)/ Diameter (mm))	Screen Details (Interval (m)/ Diameter (mm))	Pump Intake (mbgl)
BH 7674	197	0 – 91 m / 381 mm 91 – 197 m / 305 mm	0 – 2 m / 381 mm 0 – 91 m / 305mm 0 – 90 m / 205 mm 125 – 191 m / 205 mm	90 – 125 m / 205 mm	90.20
BH 7675	198	0 – 100 m / 381 mm 100 – 198 m / 305 mm	0 – 2 m / 381 mm 0 – 100 m / 305 mm 0 – 103 m / 254 mm 159 – 190 m / 205 mm	103 – 135 m / 205 mm 135 – 159 m / 205 mm	87.30
BH 7678	125	0 – 38 m / 381 mm 38 – 124 m / 305 mm	0 – 1 m / 381 mm 0 – 38 m / 305 mm 0 – 70 m / 205 mm 93 – 115 m / 205 mm	70 – 93 m / 205 mm	73.80
BH 7687	145	0 – 59 m / 381 mm 59 -145 m / 305 mm	0 – 1 m / 432 mm 0 – 59 m / 305 mm 0 – 63 m / 205 mm 112 – 142 m / 205 mm	63 – 86 m / 205 mm 86 – 112 m / 205 mm	69.70

Source: Geotechnical Consulting Services (1998a)

2.7.3 Groundwater Occurrences and Movement

Geotechnical Consulting Services (1998a) identified the Mea Arkose formation in the project area as the major aquifer capable of providing portable groundwater. Limited quantities of groundwater also occur within the following formations;

- Calcrete and silcrete horizons of the Kalahari Group and montmorillonite-rich soils which facilitate the occurrence of localized perched aquifers that are used by hand dug wells along the Semowame River;
- Stormberg Group Basalts which consist of extremely high saline water (Total Dissolved Solids (TDS) > 20 000 mg/l);
- Ntane Sandstone Formation which contains moderately high saline water (Total Dissolved Solids up to 2 500 mg/l)
- Tlapana Formation which consists of portable water.

Table 2.5 presents the number of water strikes, the formations in which the strikes were encountered and the average yield per formation.

Table 2.5 Groundwater occurrence and yields from wellfield water points

Formation	Number of Water Strikes	Average Yield (m^3/h)
Mea Arkose	98	22
Stormberg	3	2
Ntane Sandstone	7	6
Ngwasha	12	11
Pandamatenga	2	9
Tlapana	21	5
Dwyka	2	3
Basement Complex	4	2

Source: Geotechnical Consulting Services (1998a)

Based on the average yield and the number of water strikes, the Mea Arkose is categorized as the main aquifer in the study area, while the Ngwasha and the Pandamatenga formations come second and third respectively. Other formations reflect low yields and low

probabilities of water interceptions, such as the Pandamatenga and the Dwyka formations with only two water interceptions each.

The Department of Water Affairs (1976) earlier reported that the Mea Arkose Aquifer, the major aquifer in the study area is highly heterogeneous and anisotropic due to the variability and a broad range of transmissivity values recorded in the aquifer, ranging from 1.5 m^2/day to 1760 m^2/day. The bottom of the Mea Arkose Aquifer is defined by the mudstones of the Dwyka Formation and the basement rocks (granites and gneisses). The Mea Arkose Aquifer is confined towards the north by the overlying Tlapana Mudstones over most of the area. The confinement degree increases towards the north, where the overlying silts and mudstones of the Ngwasha Formation increase the thickness of the confining layer.

The truncation of the aquifer against the basement rocks (depositional control) and the major faults offsets (post depositional control) which effectively divide the aquifer into compartments control the geometry and the dimensions of the Mea Arkose Aquifer. Department of Water Affairs (1995a) proposed the division of the aquifer into four major compartments (Figure 2.7).

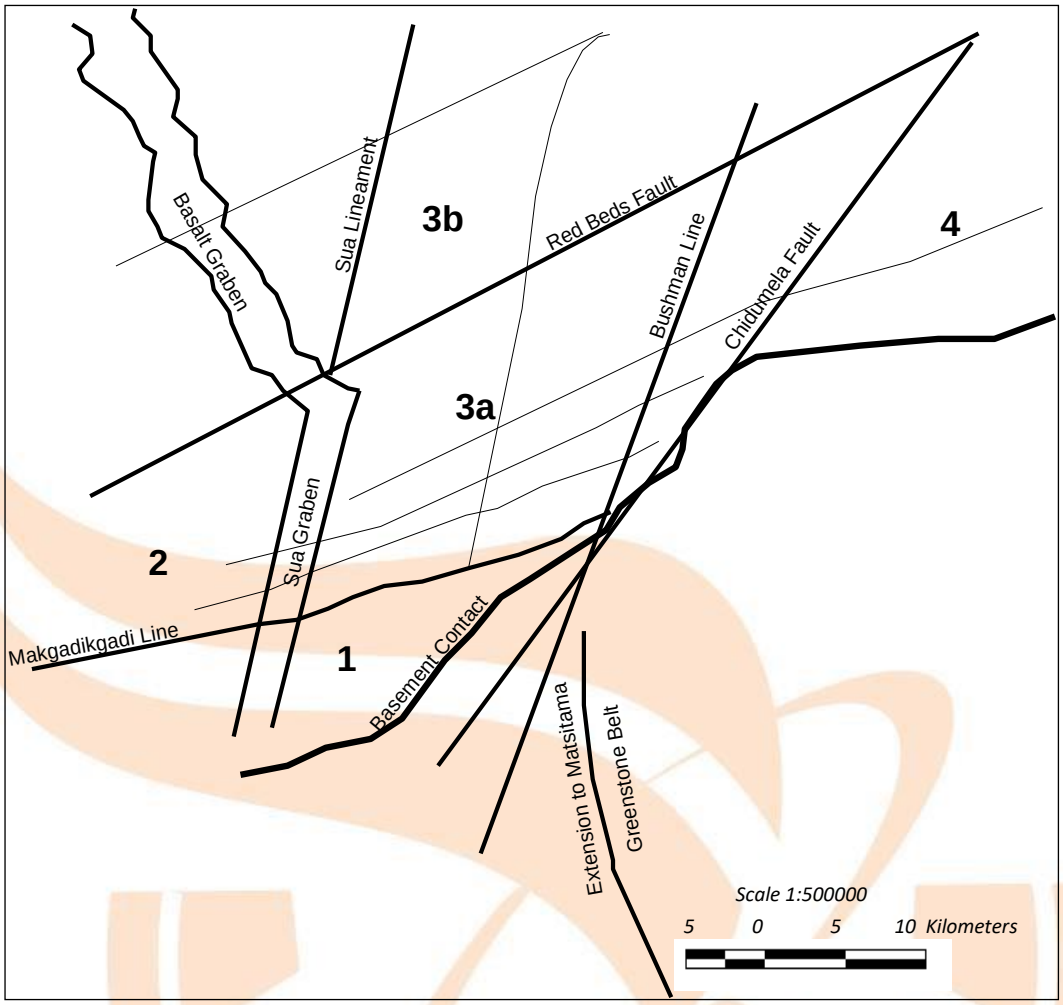

Figure 2.7 Aquifer Compartments (Department of Water Affairs, 1995a)

The Dukwi basin is controlled on its eastern boundary by the northeast trending Chidumela Fault, which acts as a flow barrier that separates Compartments 3 and 4. The northern part of the wellfield is represented by Compartment 3, while the Chidumela Wellfield occupies Compartment 4. Another northeast trending fault, the Bushman Fault appears to be the basement feature that does not affect the Karoo Sediments. The east-northeast trending extensional growth faults on the southern margin and within the basin control down stepping to the north of the Mea Arkose Aquifer.

The Makgadikgadi Line which extends over approximately 12 km along the edge of a steep basement gradient is the most important structure in the Wellfield. This fault coincides with the transition from granites and gneisses in the south, to greenstones and metadolerites in the north. Compartment 1 is separated from Compartment 3 by a high transmissivity zone

along the southern edge of the fault. The southern limit of the Ngwasha Formation is defined by the Red Beds Fault, which lies further to the north. This fault divides Compartment 3 into 3A and 3B.

The north-northeast orientated Sua Graben truncates against a northwest trending basalt graben along the western margin. The Sua Graben continues to the north as the Sua Lineament, which is located immediately to the west of the Wellfield. Drilling across the Sua Lineament has indicated the Sua Graben as a narrow feature which totally displaces the aquifer. The graben defines the western boundary of Compartment 3, separating it from the westerly Compartment 2. In the north of the Dukwi Wellfield, the groundwater heads which are 20 m lower to the west act as flow barriers. This effect is not noticeable in the southern part of the wellfield.

The dikes belonging to the Tuli Dike Swarms are considered to form partial flow barriers as they intersect the area in a west-north-westerly direction. Regionally, groundwater flows across the area in a westerly direction and discharges at Sua Pan. Locally, more complex flow patterns can occur due to the compartmentalization of the aquifer. Based on the conceptual model developed by the Department of Water Affairs (1995a) and potentiometric contours plotted in 1998 considering boreholes that obtained water from the Mea Arkose Aquifer, the following observations were made:

- The general flow direction in the southern part of the Dukwi Basin continues to the southwest, with flows that are parallel to the east-northeast structural features like the Makgadikgadi Line.
- In the north (Compartment 2 in Figure 2.7) groundwater flows westwards towards Sua Pan.
- Groundwater Compartment 1 is formed by the south-eastern part of the area up to the zone with high transmissivity. The hydraulic gradient was found to be very small (approximately 5×10^{-4}) and it is even lower in Compartment 2.
- Compartment 3, which is located to the north of Compartment 1 is an almost isolated sub-basin which contains old water that discharges slowly towards the southwest.

- Compartment 4, which is located in the NE, is comprised of the Chidumela Wellfield. This compartment is isolated from the other compartments by the Chidumela Fault.

CHAPTER 3

LITERATURE REVIEW

3.1 Definition of Groundwater

Groundwater is defined as the water that appears in pore spaces of the soil and fractures of rock formations beneath the Earth's surface (Nelson, 2015) or the water that saturates the void spaces of rocks or sediments below the earth's surface (California Department of Water Resources, 2003)**.** Groundwater is part of the hydrological cycle, as precipitation water (rainfall/snow water) infiltrates down into the ground and adds to the groundwater reservoir. Part of groundwater in the reservoir will laterally flow and be discharged to the rivers, lakes or oceans due to hydraulic gradient as base flow, while part of it will evaporate to the atmosphere and condense to form precipitation. A reverse flow (water flowing from stream to groundwater reservoir) can occur when the stream's water level rises compared to groundwater level, resulting in a bank storage. Water level drop in the stream will cause water from the bank storage to flow back to the stream (Singhal and Gupta, 2010).

Subsurface water can be classified according to two depth zones, depending on the degree of saturation. These zones are the vadose zone (zone of aeration) and the zone of saturation (groundwater/phreatic zone). The vadose zone is located between the water table and the land surface. This zone is occupied by both air and water, which partly fill the intergranular spaces. The lower subdivision of the vadose zone is known as the capillary fringe, where water is held by surface tension in the voids. The zone of saturation, also known as the groundwater zone is saturated only with water, air being excluded. The upper portion of the zone of saturation in an unconfined aquifer is represented by the water table. The thickness of the two subzones can be affected by the water table fluctuations due to natural and man-made conditions (Singhal and Gupta, 2010), hence these water table fluctuations have to be monitored as groundwater is considered as the major supply of water to wells and springs.

Figure 3.1 illustrates the two subsurface water zones (vadose zone and the zone of saturation); the capillary fringe which is the lower subdivision of the vadose zone, where water is held by surface tension in the voids (Fitts, 2013) and the water table.

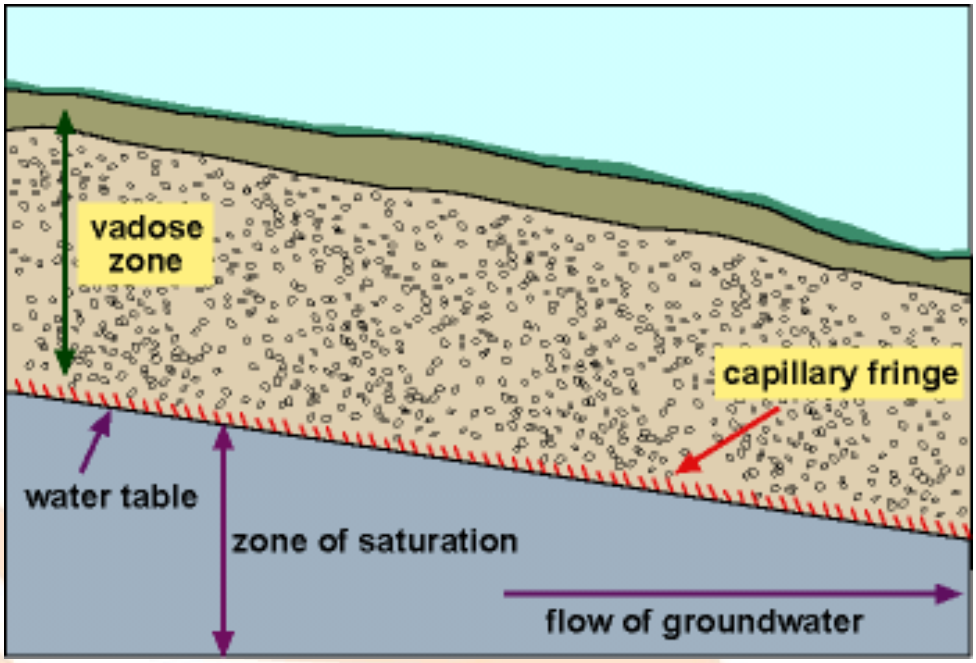

Figure 3.1 The subsurface water zones, the Capillary fringe and the water table (Iqbal, 2015)

California Department of Water Resources (2003) states that for a rock to function as a groundwater resource, it is determined by different characteristics such as its porosity, transmissivity and hydraulic conductivity. Various methods can be used to determine these rock properties. These methods include performing laboratory and aquifer tests with varying degrees of accuracy or by doing lithologic and geophysical observation such as using the electromagnetic geophysical method to determine the electrical conductivity of rocks (Zhdanov, 2015).

3.1.1 Description of the Rock Properties

3.1.1.1. Hydraulic conductivity

Harter (2003) defines hydraulic conductivity as the ability of a geologic material to move groundwater measured in different units of length per time, such as in feet per day, meters per day or in gallons per day per square foot. Higher hydraulic conductivity leads to greater amount of groundwater flow. Hydraulic conductivity of sandy or gravel aquifers is much higher than the hydraulic conductivity of clays. Sandy and gravel aquifers have a hydraulic conductivity of approximately 3.048 meters per day to 30.48 meters per day while that of clays is 3.048×10^{-5} meters day, which is a very tiny fraction of the hydraulic conductivity

of the sandy and gravel aquifers. The hydraulic conductivity of fractured rocks is approximately 0.3048 to 3.048 meters per day, depending on the degree of fracturing.

According to Oosterbaan and Nijland (1986), hydraulic conductivity can be calculated using Darcy's equation (Equation 3.1)

$$K = V/S \quad (3.1)$$

where: V = velocity of groundwater
k = hydraulic conductivity
S = hydraulic gradient

3.1.1.2 Porosity

According to California Department of Water Resources (2003), porosity is defined as the ratio of voids in a formation to the total volume of the material. It is used to measure the amount of groundwater that can be stored in the void space of the material. Porosity is determined by the shape and the uniformity of grain sizes in sediments therefore finer grained sediments have higher porosity than coarser sediments, due to their difference in grain size uniformity and shapes. Porosity equals to specific yield, which is the fractional amount of water that can freely drain due to gravity and can be extracted from sediments and specific retention, which is described as the groundwater portion that can be retained as films on grains or in small pore spaces of sediments.

The Porosity of sediments can be determined from Equation 3.2 based on the specific yield and specific retention.

$$n = S_Y + S_r \quad (3.2)$$

where: n = total porosity
S_Y = Specific Yield
S_r = Specific retention

3.1.1.3 Transmissivity

Transmissivity is the measure of the capability of the aquifer to convey groundwater through its entire thickness that is saturated (California Department of Water Resources, 2003) or can be defined as the result of the hydraulic conductivity and the saturated thickness of an aquifer expressed as the rate at which groundwater flows through a unit width of an aquifer. Based on the relationship between the pumping rate and the resultant drawdown of the water level in the aquifer, different methods are used to calculate transmissivity. These methods include the graphical method which is based on the data collected from aquifer tests and the method of using specific capacity data based on unadjusted drawdown. Specific capacity tests for calculating the transmissivity are less expensive than the graphical method, as drawdown in the pumped well is measured once, while the graphical method involves installation of observation wells and conducting the test, which is much expensive (Kelbe *et al.*, 2011).

Transmissivity of the aquifer can be determined from the product of the hydraulic conductivity and the aquifer's thickness as indicated by Equation 3.3 (Heath, 2009).

$$T = kb \tag{3.3}$$

where: T = transmissivity

b = aquifer's thickness

k = hydraulic Conductivity

3.2 Factors that Influence Groundwater Movement

The movement of groundwater is determined by elevation and the pressure points. Groundwater moves from areas of higher elevation to areas of lower elevation and from higher pressure points to lower pressure points. This movement is quite slow (between 0.3 to 3.05 meters/day), because it moves through small pore spaces between the rocks. The force that influences groundwater movement is the hydraulic head, which is the surface water pressure and the water table elevation. The movement of groundwater is always in the lower direction of the hydraulic head gradient (Harter, 2003) indicating that if there is no hydraulic head gradient, there will be no groundwater flow.

Groundwater occurrences and movement also depends on the geo-hydrological characteristics (such as lithology, texture and structure) of the geological formations

(Singhal and Gupta,1999). The three types of identified geologic formations are the aquifer, aquitard and the aquiclude (Zreda, 2007).

3.2.1 Aquifer

According to the California Department of Water Resources (2003) an aquifer is a saturated and permeable geological formation from which significant amount of groundwater can be pumped or a geologic unit with good hydraulic conductivity of more than 10^{-6} m/s to supply wells and springs with water of reasonable quantity (Singhal and Gupta, 2010). Aquifers are classified into different categories, namely unconfined, confined or leaky/semi confined, depending on their hydraulic characteristics. Unconfined aquifers are aquifers in which the water table forms the upper part and the pressure is equal to zero (Zreda, 2007) or where the atmospheric pressure is equal to the pressure on the top surface of groundwater (California Department of Water Resources, 2003). In unconfined aquifers, the water table is exposed to the atmosphere, through the vadose zone. The vadose zone allows water to enter through the soil , then filters down to the phreatic zone, where the top of this zone is the water table (Nelson, 2015).

Aquifers are defined as confined or artesian aquifers if they are bounded by impermeable strata (aquitards) at the upper part of the saturated zone (Nelson, 2015). In confined aquifers, the water is subjected to pressure which is greater than the atmospheric pressure (Singhal and Gupta, 2010). This means that when the aquitard is penetrated by a well under this condition, the water will spring above the top of the aquifer (California Department of Water Resources, 2003). Confined aquifers can be created under three types of geological formations, namely: stratiform multilayered formations; fractures and joints and solution cavities. Confined aquifers can change to unconfined aquifers with time and space, depending on the position of the potentiometric surface (Singhal and Gupta, 2010). This indicates that groundwater can rise out of the confined aquifer, to balance with the pressure outside the aquifer (atmospheric pressure) when the aquifer is penetrated.

3.2.2 Aquitards

Aquitards are semi-pervious formations such as silt, clay and shale, which cannot transmit sufficiently great amount of water but only small quantities (Zreda, 2007). These formations do not have enough permeability but due to vertical leakage, allows groundwater to interchange between adjacent aquifers.

3.2.3 Aquicludes

An aquiclude is described as a geologic formation that contains water but does not transmit water because it is impermeable. Aquiclude formations include unfractured crystalline rocks and shales. Every geologic formation has hydraulic conductivity (ability to transmit water) (Singhal and Gupta, 2010). This means that aquicludes cannot be found in nature.

3.3 Understanding Groundwater Depletion

Groundwater is the most important component of fresh water supply in various regions around the world, and it is of vital importance to the water security of many communities (Taylor *et al.*, 2013). Chilton (1996) states that about 95 percent of the readily available freshwater around the world is represented by groundwater stores, while 3.5 percent is from lakes, swamps, reservoirs and rivers and the remaining 1.5 percent is represented by soil moisture. From Giordano (2010), about 50 percent of the world's portable water is supplied by groundwater and nearly half of the world's population (between 1.5 to 2.8 billion people) depends on groundwater as their vital source for drinking. In Botswana, the main water supply (65 percentage) comes from groundwater resources whereas the least water supply (35 percentage) is from surface water resources (Du Plessis and Rowntree, 2003). This emphasizes the significance of groundwater resource as many communities depend on it.

However, more dependency on the groundwater system can cause it to be depleted. Fitch *et al.* (2016) states that in many parts around the world, the use of groundwater exceeds surface water usage and this is expected to increase more with improvement of drilling and pumping activities. Groundwater usage has been less observed than surface water due to its hidden nature and its difficulty to conceptualize. The time frame for groundwater system to reach thresholds of concern is longer than many time frames used in societal decision making and as a result, groundwater remains a minor player in water resources management. In various parts around the world, groundwater replenishment rates cannot match with the past and current depletion rates, which can lead to the groundwater system being degraded and once the system is degraded, it is not quick, cheap or easy to recover due to its hidden nature. This indicates that a precaution has to be taken when it comes to managing the groundwater resources to avoid the expenses that can be encountered once the groundwater system has degraded.

According to Konikow and Kendy (2005) groundwater depletion is being experienced in different regions such as in Africa, Asia, Australia, China, America and localized areas around the world. Taylor *et al*. (2013) states that the risk of overutilization of groundwater resources is noticeable in semi-arid regions where groundwater demand will intensify, due to the projected increase in frequency and intensity of droughts, rising population and standards of living and expansion of irrigated areas. Wada *et al.* (2010) indicates that the global groundwater depletion increased from 126 (± 32) km^3/year in 1960 to 283 (± 40) km^3 /year in 2000. Other factors that can lead to groundwater depletion around the world include sustained groundwater pumping; urbanization and climate variation (Mustafa *et al.,* 2017).

Wada *et al.* (2010) and Fitch *et al.* (2016) state that groundwater depletion or over exploitation occurs when groundwater abstraction exceeds recharge over a long period of time. Central Statistics Office (2009) defines water abstraction as the permanent or temporal removal of water from any source (soil) during a specified period of time while water recharge according to Nimmo *et al.* (2005) and Matthews (2014) is whereby the saturated zone of the aquifer system is filled with a defined volume of water replenishing the groundwater reservoir. According to Konikow and Kendy (2005), the depletion of groundwater can be observed from two different perspectives, which are the depletion of groundwater as a lowering of the volume of water in the saturated zone, not considering the water quality change and as the reduction of the volume of fresh groundwater stored that can be used.

3.4 Factors that Influence Groundwater Depletion

3.4.1 Sustained Groundwater Pumping

There is evidence that the primary cause of groundwater depletion around the world is due to sustained groundwater pumping, that is when groundwater pumping surpasses groundwater recharge for a long period of time. Harter (2003) and Bartolino and Cunningham (2003) indicate that groundwater can be recharged by infiltration from precipitation, surface water or through deep percolation from irrigation. This water can be stored underground or be naturally discharged to streams, springs or be transpired by plants. The storage water volume remains relatively constant or is in equilibrium once the groundwater system is developed. This equilibrium is however changed once pumping begins which causes groundwater level to decline. Groundwater withdrawals therefore,

must be balanced by some combination of increased recharge, decreased discharge and removal from storage (Bartolino and Cunningham, 2003). This indicates that more groundwater withdrawal due to pumping will result in the groundwater system being depleted or the water level declining over a long period of time.

It is indicated that more groundwater abstraction than recharge is being experienced around the world. Qureshi *et al.* (2010) have shown that the annual global groundwater abstraction is approximately 4,430 km^3, while the total groundwater recharge is approximately between 750 to 800 km^3 which is about one sixth of the total fresh water abstractions. Du Plessis and Rowntree (2003) indicate that the potential of groundwater resources in Botswana is estimated to be 1.7×10^9 m^3/year and 1.0×10^9 m^3/year is extractable while 17×10^6 m^3/year is rechargeable volume. Lower groundwater recharge rates than abstraction rates which are experienced worldwide can lead to groundwater resources being depleted.

3.4.2 Population Growth and Urbanisation

Much evidence indicates that population growth and urbanization also leads to groundwater depletion around the world. Population Action International (2011) indicates that approximately 2 million people around the world are currently living in areas faced with water scarcity (where less than 1000 cubic meter of renewable fresh water is available per person per year) and affected with water stress (where fresh water that is available per person in a year is between 1000 to 1667 cubic meters) due to population growth.

Bierkens (2019) states that currently the global population has quadrupled, exceeding 7 billion with more than 50 percent of people living in urban areas. In Botswana, the population is estimated to be 2.3 million (Trading Economics, 2019) and the Dukwi population to be 6,507 and expected to rise annually (Statistics Botswana, 2015). As a result of population growth, the abstracted volume of water for human needs has increased over the previous 100 years from about 500 km^3/year to approximately 4000 km^3/year worldwide (Bierkens, 2019). A continual rise in population numbers will contribute to a rising demand and competition of water for different purposes such as for domestic, industrial and agricultural purposes.

Erickson and Stefan (2009) have observed that urbanization can affect the quantity of groundwater recharge and have shown that annual recharge can be decreased by 30-40

percent, due to urbanization. Urbanization makes the land surface impermeable through building roads, buildings, driveways and parking lots which significantly reduce direct infiltration of excess rainfall and accelerates surface runoff therefore decreasing groundwater recharge rates. Erickson and Stefan (2009) also states that imperviousness from 18 to 36 percent can greatly reduce the available area for infiltration of precipitation, therefore reducing the water available for groundwater recharge. Less groundwater recharge due to urbanization will limit the available water for drinking and also reduce base flow resulting in higher water temperatures experienced in cold water streams (New Hampshire Fish and Game, 2013). This will pose a threat to different aquatic species that cannot live and adapt to warmer temperatures; hence this will threaten the livelihood of most citizens as they depend on these aquatic species as source of food and income.

3.4.3 Climatic Variation

Studies indicate that climate variation is also one of the factors that affect groundwater recharge. According to Tomlinson *et al.* (2016) climate variation, is defined as the orderly shifting in the long-term statistics of weather elements that last for decades or for a longer period of time. Kumar (2012) states that the major cause of climatic variation is due to increasing concentrations of greenhouse gases found in the atmosphere, such as carbon dioxide gas, which had continually increased since the 1950s, due to anthropogenic activities such as cutting trees and burning fossil fuels and natural influences. Kumar (2012) further states that an increased concentration of the atmospheric gases leads to the modification of the global and local climate characteristics, such as temperature and precipitation. Based on Legadiko (2015), the mean annual rainfalls that are experienced at the study area highly differ, ranging from 100 mm to 800 mm.

Understanding the effects of global change of climate on groundwater resources is poorly understood than on surface water resources, because of their hidden nature and they are not easily accessed hence making it difficult to recognize the impact of climatic change on them. Insufficient monitoring data in many regions around the world due to lack of necessary tools also makes it difficult to detect the correlation between groundwater levels and climate change (Green *et al.*, 2011). This will result in insufficient research being done on the climate change impacts on groundwater resources, even though it is indicated that the hydrogeological processes and the groundwater resources can be directly and indirectly

affected by change of climate, which means that these groundwater resources will be left vulnerable to effects of climate change in various regions around the world.

Taylor *et al.* (2013) explains that groundwater recharge occurs from both diffuse rain fed recharge and focused recharge that occurs due to leakage from surface water bodies. Focused recharge normally occurs at locations where surface water flow is concentrated at the land surface such as in stream channels, lakes, topographic depressions, irrigated agricultural land and other preferential flow paths (Green, 2016). Groundwater recharge dependents more on climate, land cover and geology. Climate and land cover determine precipitation and evapotranspiration, whereas geology determines whether the water surplus (precipitation minus evapotranspiration) can be transmitted and stored in the subsurface (Taylor *et al.,* 2013). This indicates that climate plays a major role in groundwater recharge as it determines the groundwater amount that will reach the surface, infiltrate into the groundwater system and become base flow to streams and rivers.

According to Kumar and Singh (2016), various aquifers are recharged differently depending on the permeability of rocks and soils that overlie them. Unconfined aquifers are sensitive to climate change and directly recharged by rainfall and surface water bodies such as rivers and lakes, while confined aquifers are not recharged by direct rainfall as they are characterized by impermeable overlying bed but by rivers, lakes and rainfall that occurs at a larger distance (up to a thousand kilometers).

The Intergovernment Panel on Climate Change (2007a) and Krinner *et al.* (2013) estimated an increase of 0.6 ± 0.2 °C in the global mean surface temperature since 1861 and predicts an increase of 2 to 4 °C over the next 100 years. These changes will be influenced by many factors such as global warming (Green, 2016) and how solar radiation is taken in by the atmosphere and the earth's surface (Todd and Mays, 2005). The hydrologic cycle will be significantly modified by temperature changes, that is precipitation and evaporation rates will be altered with a higher likelihood of flooding that will contribute to disproportional groundwater recharge and droughts which will lead to a sharp groundwater decline (Taylor *et al.,* 2013). Due to the projected increase in temperature, evapotranspiration is expected to rise reducing runoff and water content in some regions (Green, 2016), thus resulting in more groundwater resources to be further stressed worldwide.

It is indicated that the effects of climate change will be severe in developing countries as more than 70 percent decrease in groundwater recharge will be experienced in some parts of Africa, Brazil and along the south rim of the Mediterranean Sea and a more than 30 percent potential increase will be encountered in the Sahel, Middle East, Northern China, Siberia and the Western United States by the year 2050, due to climatic changes (Intergovernmental Panel on Climate Change, 2007b). Climatic changes will also account for 20 percent increase in water scarcity globally, which will severely affect the ecosystem and the society (Green, 2016). These changes due to recharge rates were concluded using some climatic models such as the ECHAM4, HadCM3 and General Circulation Models (GCM) which project the global recharge rates. The models predict that groundwater recharge will decrease by more than 10 percent in most areas with high population densities and highly sensitive to groundwater recharge reductions (Taylor *et al.,* 2013). These recharge projections are closely related to changes in precipitation because precipitation directly affects the recharge rates.

Climate changes can lead to other severe effects in an area in addition to change in groundwater recharge and discharge. Taylor *et al.* (2013) indicates that climate variation can lead to a change in irrigation demand. In 1995, a global study of the consequences of climate variation on irrigation demand estimated that by 2070, two thirds of the irrigated land will be subjected to increased demand of water for irrigation due to persistent droughts (Doll, 2002). This will lead to a change from surface water to groundwater supply for agriculture and will stress further the limited groundwater resources, leading to more groundwater depletion around the globe and contributing to severe secondary effects of groundwater depletion, such as land subsidence which cannot be easily reversed once occurred. Other factors that will be affected by climate change include surface groundwater interactions and water quality (Green, 2016).

However, it is indicated that wetter conditions do not always result in more groundwater recharge as they can enhance evapotranspiration from desert blooms which can entirely consume the water surplus while less rainfall can lead to increased groundwater recharge due to reduced leaf area and less stomata opening resulting in less evapotranspiration. Less continental runoff and more infiltration which enhances groundwater recharge can also occur from lower rainfall, while higher rainfall that occurs in a short period of time can lead to less groundwater recharge due to lower infiltration rate and more surface runoff (Taylor

et al., 2013). Higher evaporation rates that result from higher temperatures can also offset groundwater recharge that can result from increase in total effective rainfall. The available water that can be infiltrated into the soil can be modified by the construction of water management systems such as reservoirs and boreholes (Kumar, 2012).

3.4.4 Land Use Change

Evidence indicates that the change of land use such as expansion of agriculture (rain fed or irrigated) also can affect the quality and amount of groundwater. Taylor *et al.* (2013) indicates that changes in irrigation demand can contribute to severe indirect effects of climate on groundwater resources than the direct effects of climate on groundwater resources. For example, surface water irrigation can increase groundwater recharge, replenishing the previously depleted aquifers and raising groundwater levels which can result in degrading the groundwater quality due to mobilization of salts and other contaminants accumulated in the unsaturated soil profiles. Sharma's 1989 study (as cited in Green, 2016) concludes that recharge is influenced by land use by indicating that a ±20 percent change in recharge will result in a ±30 percent change in recharge beneath the natural grassland and ±80 percent change in recharge beneath the pine plantation. These studies indicate that changing the use of land can influence the recharge and quality of the groundwater resources.

3.5 Effects of Groundwater Depletion

3.5.1 Groundwater Quality and Chemistry Change

Groundwater quality and chemistry change can occur when groundwater levels decrease. Todd and Mays (2005) states that groundwater naturally contains dissolved solids of 1000 mg/l and dissolved salt content of 25 mg/l in quartzine springs and 300 000 mg/l in brines. However, the concentration of these dissolved solids and salts can increase due to the evapotranspiration process, which causes groundwater level declines. An increase in the concentration of dissolved solids and salts will result in the use of the groundwater resource being undermined and in some instances become risky to human and plant life and hazardous to the environment (Fitch *et al.*, 2016). Other factors which can increase the accumulation of dissolved solutes and salts in groundwater include the contact of groundwater with highly soluble minerals, such as gypsum and when it is heated geothermally (Todd and Mays, 2005).

Todd and Mays (2005) and Delleur (2006) state that the type and concentration of salts which can occur in groundwater is determined by the travel time, the source of groundwater and the chemical composition of the aquifer system. Chemical equilibrium between the water and the rock medium can happen if the minerals of the rocks are relatively soluble. A greater exposure of groundwater to soluble materials in the geologic strata and its slow velocity can result in more concentration of dissolved constituents.

Different ranges of groundwater occur due to different flow velocities, surface area and chemical structure of the aquifer (Delleur, 2006). Groundwater salinity increases with depth. This is because water becomes denser at deeper depths, as compared to shallow depths, hence leading to higher salinity with increasing depth as density and salinity are directly related (Wattez, 2020). In a larger aquifer, groundwater at the top (about 100 m to 500 m) is mostly expected to be fresh, with the Total Dissolved Solids (TDS) of less than 1 g/l , while groundwater below this depth is most likely to be brackish with TDS of between 1 mg/l to 10 mg/l, saline with TDS concentration that ranges between 10 mg/l to 35 mg/l or hyper-saline with TDS concentration of more than 35 mg/l (Bierkens, 2019).

A common geochemical sequence found in groundwater is the occurrence of bicarbonate waters found near the ground surface which is different from the chloride waters found in the deepest parts of formations (Todd and Mays, 2005). The Bicarbonate waters are mainly due to the dissolution of carbon dioxide in the soil, which is formed by biological activity, by atmospheric precipitation. This results in the formation of carbonic acid, which dissolves soluble minerals such as alumino-silicates found in igneous rocks which are mostly found in the earth crust. The chloride water encountered at greater depth is mainly due to the dissolution of old sedimentary formations (Chilton, 1996).

Motevalli *et al.* (2019) states that groundwater with more chloride concentration and more changes in the cation concentration such as sodium, that results from the cation exchange reaction between the aquifer and saltwater intrusion are the important factors in groundwater salinization. De Louw (2013) also indicates that more chloride concentration is used to represent the salinity of water, because chloride is the major stable anion found in saline groundwater bodies. This indicates that reducing groundwater levels will lead to more salinity being reached in the deeper depths, where there is a high concentration of chloride anions.

Bierkens (2019) indicates that increasing salinization occurs in many parts around the world due to excessive pumping which mainly causes the upcoming of the fresh-salt groundwater interface. According to Zhou and Bear *et al*. (2005), the upcoming and well contamination quickly occur when the fresh-salt water interface is nearer the well screen below. Bierkens (2019) states that if salt groundwater occurs closely below the well screen, the withdrawal of groundwater will not only result in the shutdown of the well within a short time period, but will also make groundwater unsuitable for use over a large area located several km^2 away for many decades.

Groundwater recharge that occurs through the soil zone with a higher amount of carbon than the atmosphere leads to a recharged groundwater with a higher concentration of organic carbon (Todd and Mays, 2005). Vissers (2004) states that the presence of the minor and trace elements found in groundwater is mainly due to the presence of these elements in the sorption and redox state. Some of the trace elements found in groundwater can be due to recharge by precipitation that contains these elements from anthropogenic sources.

Precipitation usually contains some dissolved mineral matter in small quantities which react with the minerals found in the rocks and soil, once in contact with them. The concentration of the hydrogen-ion (pH) and the redox potential (Eh) of water determines the amount and type of mineral that can be dissolved in the rocks and soil. The carbon dioxide derived from the atmosphere and organic processes in the soil assists the solvent action of rain as it moves underground (Todd and Mays, 2005).

Todd and Mays (2005) states that the quality of groundwater can be affected by recharge from alluvial stream channels or artificial recharge areas where recharge of water underground occurs in large volume. The soluble products that result from soil weathering and erosion caused by rainfall and flowing water can cause salts to be added to groundwater as it passes through the soil. Large quantities of salts in the water table can occur due to excess irrigation, as water percolates down the water table. The increase of salts during irrigation depends on soil permeability, drainage, the amount of water applied to crops and on climate. Groundwater found in arid climates usually contains more salts because leaching by rainwater is ineffective to dilute salt solutions.

Igneous rocks are less soluble than sedimentary rocks, hence the sedimentary rocks are mainly found in groundwater due to their high solubility and greater abundance on the earth's crust. Sedimentary rocks, such as sandstone and mudstone can lead to a higher concentration of total dissolved solids in groundwater. This is mainly due to the presence of a soluble cement, such as calcite, in these rocks (Chilton, 1996). The common cations added to groundwater are sodium and calcium, while bicarbonate and sulphate are the corresponding anions. Dissolution of igneous rocks often results in silica being added to groundwater due to the presence of silicate minerals that occur in these rocks. Nitrate and chloride are naturally occurring minerals in groundwater, but a higher concentration however can indicate pollution from highly concentrated sources such as from sewages and connate water (Todd and Mays, 2005).

3.5.1.1 Transportation of dissolved contaminations in groundwater

Dissolved contaminants in groundwater are transported by different mechanisms of diffusion, mechanical dispersion, advection and sorption. In diffusion, the solutes move from a higher concentrated zone to a lower concentrated zone due to Brownian motion of ions and molecules. Mechanical dispersion occurs due to the heterogeneities of the aquifer, resulting in the plume spreading along and across the major flow direction. Factors that lead to the occurrence of dispersion include more flow rate occurring at the center of the pores than at the edges, longer pathways and larger flow velocities in smaller pores than in larger pores. Advection is the transportation of solutes by the bulk groundwater and occurs mostly in sand and gravel aquifers with significant groundwater. Sorption mechanism involves the exchange of ions and molecules between the solid and liquid phases through adsorption and desorption processes (Delleur, 2006).

3.5.2 Land Subsidence.

Studies indicate that more groundwater pumping than recharge can result in land subsidence or consolidation**.** Land subsidence involves the earth's surface suddenly sinking or settling gradually due to subsurface movement of the earth materials, such as groundwater exploitation. Land subsidence occurs when the support given to the ground by the pore-fluid pressure from the aquifer system is transferred to the skeleton of the aquifer, leading to its compression (Todd and Mays, 2005).

According to Waltham (2015), land subsidence in many areas around the world such as in Santa Clara found in Carlifornia, Shanghai in China and Bangkok in Tailand occurs mainly due to more groundwater extraction or over exploitation of groundwater resources which results in the lowering of the water table. These areas have been experiencing land subsidence that ranges from 1.0 m to 2.63 m since 1920 due to higher abstraction rates from sand aquifers than the recharge rates.

Holzer and Johnson (1985) states that at least 8 urban areas such as Bangkok in Tailand, Houston and San Jose in United States, Mexico City in Mexico, Osaka and Tokyo in Japan, Shanghai in China and Venice in Italy have been experiencing land subsidence due to higher groundwater pumping from unconsolidated sediment for municipal and industrial water supply. These areas experienced land subsidence that ranges from 0.2 m to 8.5 m, which caused significant economic losses influenced by flooding and damage of structures, such as buildings and water well casing.

Minderhoud *et al*. (2017) states that land subsidence that ranges from 1.1 cm/year to 2.5 cm/year has been occurring in Mekong Delta, Vietnam mainly due to higher abstraction rates of groundwater resources. This delta sank on average of approximately 18 cm in the past 25 years due to higher groundwater withdrawals. Subsidence in this area increased the vulnerability to flooding, storm surges and intrusion of saltwater in the channels.

Delleur (2006) states that when the water table lowers, the hydrostatic pressure decreases while the inter-granular pressure increases. Land subsidence therefore is determined by the inter-granular pressures which occur before and after the water table drop; the thickness of the soil layer and the rocks and soil's modulus of elasticity which differs in each type of rock and soil. Delleur (2006) further indicates that land subsidence occurs mostly in clayed layers than on sand or gravel because the modulus of elasticity of clayed materials is less than of sand and gravel. The modulus of elasticity of clay ranges from 50 N/cm^2 to 1470 N/cm^2, while for sand, it ranges from 980 N/cm^2 to 7850 N/cm^2. The range of values for gravel is from 9806 N/cm^2 to 19620 N/cm^2.

Land subsidence (S_u) is calculated by Equation (3.4) based on inter-granular pressures and moduli of elasticity for rocks and soils (Delleur, 2006).

$$S_U = Z(P_{i2} + P_{i1})/E \quad (3.4)$$

where: P_{i1} and P_{i2} = the inter-granular pressures that occur before and after the water table drop

Z = thickness of the soil layer

E- = modulus of elasticity of rocks and soils.

Land subsidence can result in severe damage to structures including roads, buildings, transportation networks, and hydraulic structures such as pumping stations, river embankments and sewage systems within the area of occurrence of the subsidence (Delleur, 2006). This will result in significant economic losses leading to high maintenance costs estimated annually to be billions of dollars worldwide (Waltham, 2015). Land subsidence could also lead to increased flood risk due to ineffective drainage systems and lowered surface levels (Bierkens, 2019). Water management disruptions and related effects such as changing of stream gradients, drains and an increased need for groundwater pumping can occur due to land subsidence (Waltham, 2015).

According to Delleur (2006) land subsidence occurs mostly in aquitards that comprise of inter-bedded layers of silt and clays. This occurs when the drainage of the aquitard that squeezes the fluid from its interior causes the internal stress to increase. The aquifer compressibility will also increase by a factor of 20 to 100, which can lead to unrecoverable aquifer compaction. Bierkens (2019) states that some part of land subsidence can be elastic while some part can be inelastic. In inelastic subsidence (often regarded as plastic instantaneous deformation), the storage capacity of the aquifer will be greatly reduced and not possible to fully recover it.

3.5.3 Drying Up of Adjacent Wells

Studies indicate that excessive pumping can result in the drying up of adjacent wells due to the formation of the cone of depression. Jones (2006) indicates that when water from the aquifer is pumped by a well, the level of groundwater around the well declines, forming a cone of depression. These water level declines are higher at the well that is pumping and reduce to zero at some radial depth from the well. The hydraulic gradient established within the cone of depression will cause water to move from the aquifer to the well. The shape of the cone of depression depends on the hydraulic conductivity and the groundwater extraction rate (Orica, 2014).

Orica (2014) states that more groundwater pumping from the extraction wells will result in the depth of the cone of depression increasing and the edges broadening. The groundwater divide will move further downwards. More pumping in a series of wells that are placed adjacent to each other will result in the cones of depression formed around the wells to overlap and merge, the groundwater table to be lowered and the hydraulic containment line to be formed. No groundwater will flow past these points and excessive water table drawdown will result in the drying up of other wells that are adjacent to the extraction well. Figures 3.2 (a) and (b) illustrates the water level of adjacent wells (Well A and Well B) decreasing when the depth and edges of the cone of depression increase due to pumping.

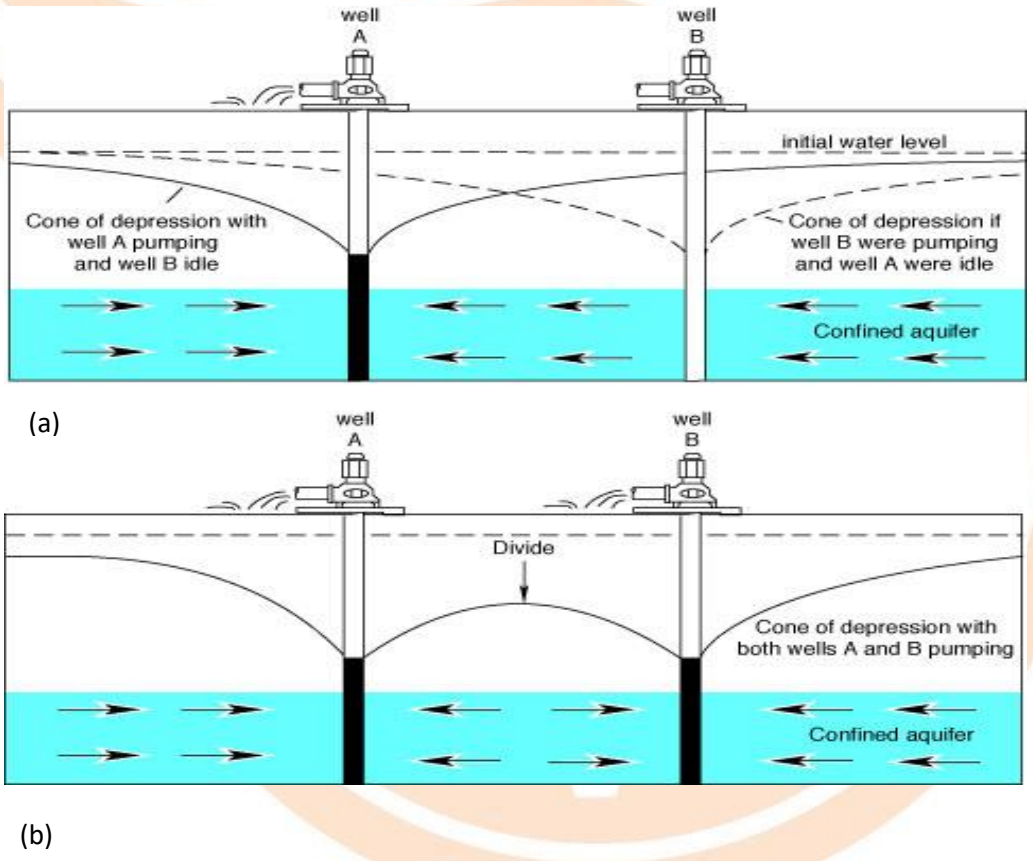

Figures 3.2 (a) and (b) The formation of cone of depression in adjacent wells (Buchanan and Buddemeir, 1993)

3.5.4 Induced Recharge

It has been observed that increase in groundwater withdrawal can reduce groundwater discharge to the surface water bodies, hence reducing their flow. Barlow and Leake (2012) indicates that excessive groundwater pumping can lead to induced recharge of surface water

into the aquifer to the pumping well and captured groundwater discharge. The total amount of the surface water body will be greatly reduced or depleted in both processes. Pumping for a prolonged period of time will result in the water source being pumped coming from surface water depletion with no contributions from the groundwater storage. This will lead to the aquifer being in a new state of equilibrium, whereby the pumping rate will be equal to the surface water depletion, and the cone of depression will no longer expand further.

Bierkens (2019) indicates that a reduction of the flow of the surface water can lead to adverse effects on the environment such as degrading of the quality of water due to less dilution of toxins and pathogens in water, increased surface water temperatures and enhancement of the hydrological drought. Less surface water will also lead to more water shortages for some activities that require adequate water such as in agriculture. This will further lead to more depletion of the groundwater resources in order to meet increasing water demands.

Figure 3.3 indicates an example of a cone of depression produced by over pumping in a well. A hydraulic gradient between the aquifer and a stream will be produced, leading to an induced recharge.

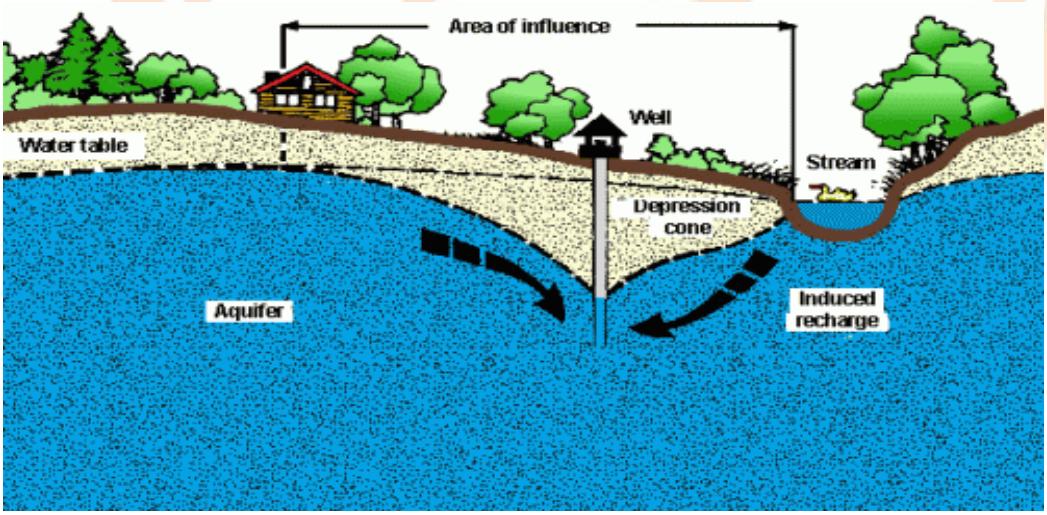

Figure 3.3 Induced recharge due to over pumping a well (Oregon State University, 2020)

There are various analytical methods that can be used to identify the determinants of groundwater depletion and the outcomes that can result from the depletion of groundwater

resources. The methods include the Cooper and Jacob (1946) straight line method, the Pearson's correlation analysis method, the linear trend modeling method, a piper diagram, the linear interpolation method, MODFLOW SUB and the hydrogeological model.

3.6 Data Analysis Methods

3.6.1 The Cooper and Jacob (1946) method

The Cooper and Jacob (1946) method is a semi logarithmic, time-drawdown analysis method for the estimation of the hydraulic properties such as transmissivity and storativity of the aquifer (Neuman *et al.*, 2007) and the radii of influence that can occur due to pumping in a constant pumping test (Dragoni, 1998).

Studies indicate that the Cooper and Jacob (1946)'s analysis method forms an appropriate method to estimate the hydraulic properties of most heterogeneous formations. According to Meier *et al.* (1998) and Sfinchez-vila *et al.* (1999) transmissivity estimates obtained through the Cooper and Jacob (1946) method, provide an important information about the aquifer. The method also provides a good estimation of the hydraulic properties in heterogeneous formations.

Butler (1991) states that the transmissivity values obtained using the standard techniques such as the Cooper and Jacob (1946) method in heterogeneous systems and multi-well tests, represents transmissivity at a regional scale as the values are nearer the geometric mean of transmissivity fields. Schad and Teutsch (1994) and Meier *et al.* (1998) used the Cooper and Jacob (1946) method to analyze data from wells in heterogeneous formations. They concluded that applying this method resulted in almost homogeneous transmissivity estimates and strong spatial variation of storativity estimates.

The Cooper and Jacob (1946) method is based on the fact that the Theis well function can be plotted on a semi logarithmic paper as a straight line for large values of times (Meier *et al.*, 1998) and when the well radius is small and well function smaller than or equal to 0.01 (Dinu *et al.*, 2017). The method can be used in measurements of drawdown versus radial distance to the observation well or drawdown versus effective radius of the well if the measured drawdowns are done on the pumping well (Meier *et al.*, 1998). Equation (3.5) indicates the Cooper and Jacob (1946) drawdown solution (Brikowski, 2013).

$$s = \frac{2.3Q}{4\pi T}\log\left(\frac{2.25Tt}{r^2S}\right) \quad (3.5)$$

where: s = drawdown

Q = constant discharge

T = transmissivity

t = time

r = effective radius of the pumping well or radial distance to the observation well

S = storativity

If the discharge and the distance from the well that is pumped or effective radius are constant, Equation 3.5 results in a straight-line equation with slope A and intercept B (Equation 3.6).

$$s = A\ logt + B \quad (3.6)$$

where: $A = \frac{2.3Q}{4\pi T}$

$B = \frac{2.3Q}{4\pi T}\log(2.25T/r^2)$

3.6.2 Pearson's Correlation Analysis

The Pearson's correlation analysis method established by Karl Pearson in 1948 is the most frequently used method to measure the strength, direction and probability of association between two variables (Chee and Queen, 2016). The method is commonly used as the primary statistical method of analysis as it is the most efficient method in predicting a single variable with many independent variables (Moore *et al.*, 2002).

According to Gingrich (2004), Pearson's Correlation analysis method involves summarising the relation between two variables into one number called Correlation Coefficient (r). Correlation Coefficients usually range from -1 to +1. A Correlation Coefficient close to zero indicates small relation between the dependent and independent variables while a Correlation Coefficient above 0 indicates evidence of a positive association between the variables under consideration. A larger positive correlation between the two variables occurs

if “r” is nearer to 1 while a larger negative association between the two variables is indicated by a negative “r”.

The correlation method is widely used in the earth sciences. Moore *et al.* (2002) used this analysis method to find the association between well yield and geological features such as lineaments, bedrock lithology and topography in New Hampshire, England. The well yields used ranged from 0 to more than 113.56 m^3/hour. The results showed a positive correlation of the yield of the well with the well depth of 0.53 indicating that the well yield increased with the total depth. The correlation between the drainage area and well yield was positive at 0.024 showing that large drainage areas led to higher yields. The correlations between the well yield and the well sites identified within 30.48 m of lineaments was positive and ranged from 0.37 to 1.23 indicating that these lineaments were associated with higher well yields. The correlation between the well yield and the curvature of the land surface is negative (-2.15), thus, indicating that the concave downward surfaces were associated with higher well yields.

Manoj *et al.* (2013) used the correlation analysis method to determine the interrelationship between the chemical parameters such as TDS, chloride, bicarbonate, potassium, Dissolved Oxygen (DO) and Biochemical Oxygen Demand (BOD) found in ponds located at Santiniketan-Bolpur-Sriniketan zone, Birbhum District, West Bengal, India. Most of the parameters displayed a positive and strong correlation among each other, hence indicating a high interaction of the chemical parameters in surface waters.

There was a positive correlation of TDS with various cations such as calcium, magnesium, sodium and potassium that ranged from 0.862 to 0.987 whereas it was negatively correlated with DO at -0.828. This showed that high TDS concentrations were associated with high concentrations of cations and less associated with the amount of oxygen found in surface waters. There was a negative correlation of DO with BOD of -0.670 and phosphate (-0.695) while BOD was positively correlated with phosphate at 0.982. Thus, illustrating that the oxygen concentration in surface water was not associated with oxygen that was available to be consumed by bacteria and microorganisms, in order to decompose organic material in water. The correlation between DO and phosphate was negative (-0.695) indicating that a higher phosphate concentration contributed to less concentration of oxygen dissolved in the surface water.

3.6.3 Linear Trend Modeling

According to Remy *et al.* (2005) a linear trend method of analysis is used to calculate the best line that describes the fit between a dependent variable such as water levels and independent variable such as years. The trend model slope is used to indicate the rate of change that occurs over time. The linear trend modeling was used to find the existence and significance of declining trends in the groundwater levels at the Dukwi Well Field. This technique has been widely applied to study variability of many types of hydrogeological variables (Chaoka *et al.*, 2006). The existence and the significance of the declining trends were measured by using the coefficient of determination (R^2).

Siva Prasad and Venkateswara Rao (2018) used the linear trend method to study the relationship between the pre-monsoon groundwater level and the rise in groundwater levels in Kandivalasa river sub-basin of Eastern Ghats of India from 2013 to 2015. The results from the trend model showed that there was a linear correlation between the pre-monsoon groundwater level and the rise in groundwater levels with R^2 that ranged from 0.34 to 0.68 and positive slopes that ranged from 0.322 to 0.611. This showed an increase in groundwater recharge occurred with increase in the water table depth.

Fanta, *et al.* (2002) used the linear trend model to study the annual river flow variability of Southern Africa by identifying the trends of annual runoff in rivers located in the Southern African regions. The study analyzed the temporal variability of time series of annual runoff of 502 rivers in the southern African regions such as Botswana, Malawi, South Africa, Swaziland and Tanzania from 1940 to 2000. The majority of the slope from the trend model was negative and ranged from -0.028 to -0.002 in areas of Southeastern Namibia, Southern Botswana and Northwestern South Africa. This showed the existence of declining trends of annual river flow in the Southern African Region which were likely associated with climatic factors such as rainfall variability and anthropogenic sources such as local abstractions for agricultural and industrial purposes.

The linear trend was used by Mastrocicco *et al.* (2018) to assess the effects of atmospheric temperatures on the underlying unconfined aquifer in the Campanian Plain in Southern Italy from 2004 to 2016. The results from the model indicated an increasing trend of the minimum air and groundwater temperatures with R^2 of 0.867 therefore, indicating a good correlation of the annual mean minimum air temperature with the average groundwater temperature.

3.6.4 Piper Diagram

A piper diagram is commonly used for geo-chemical characterization of water in many regions worldwide. It is used to indicate the hydrochemical composition of water with respect to the presence of ions such as Na^+, K^+, Ca^{2+}, Mg^{2+}, HCO_3^-, CO_3^{2-}, Cl- and SO_4^{2-} (Purushotham *et al.*, 2011).

Sadashivaiah *et al.* (2008) used the piper plot for hydrochemical analysis and evaluation of groundwater quality in Tumkur Taluk, Karnataka State, India on 269 water samples collected during the pre-monsoon season in February 2006 and 279 water samples collected during the post-monsoon season in December 2006. The study revealed that the calcium magnesium water type dominated the study area during the pre-monsoon period with 90 % of the representative water samples. The anion concentration showed that the bicarbonate water type was represented by 87.5 % of the water samples during the pre-monsoon season and 91 % during the post-monsoon period. This showed that groundwater at the study area was generally of the calcium-magnesium-bicarbonate type mainly due to the presence of igneous rocks of crystalline nature such as granites and metamorphic rocks such as gneisses.

Purushotham *et al.* (2011) used a piper plot to study the depletion of groundwater and quality decline caused by impacts of the environment in Maheshwaram catchment located in Andhra Pradesh district, India. The study indicated that the depletion of groundwater and water quality decline at the Maheshwaram catchment was caused by lack of perennial surface water, little rainfall and groundwater overexploitation. Water quality decline was mainly caused by human-induced activities such as the use of fertilizers and pesticides for crop production.

Purushotham *et al.* (2011) designed a piper plot using analytical data obtained from hydrochemical analysis on 20 groundwater samples obtained during the pre- and post-monsoon seasons of 2007 and 2008. The cation ternary diagram indicated that the concentration of calcium was dominant at concentrations that ranged between 38.8 mg/l and 805.7 mg/l followed by sodium with concentrations ranging between 35.9 mg/l and 684.4 mg/l, magnesium with concentrations ranging between 20.4 mg/l and 264.9 mg/l and potassium with concentrations that ranged from 0.6 mg/l to 12.7 mg/l. The concentration of calcium, sodium and magnesium was likely due to the weathering of rock-forming minerals such as pyroxenes and plagioclase feldspar in igneous rocks found at the study area such as

granites and alaskites, while the potassium concentrations were likely due to silicate minerals such as amphiboles and pyroxenes found in the igneous rocks.

The anion ternary diagram for the study area showed that the bicarbonate ion was dominant at concentrations that ranged from 170.7 mg/l to 909.8 mg/l followed by chloride at concentrations that ranged from 23 mg/l to 3 024 mg/l, sulfate at concentrations that ranged from 10 mg/l to 1 796 mg/l, nitrate at concentrations that ranged from 8 mg/l to 415.1 mg/l and fluoride at concentrations that ranged from 0.44 mg/l to 1.88 mg/l. The bicarbonate concentrations were influenced by the dissolution of carbon dioxide due to organic matter decomposition in the soil. The chloride concentrations were influenced by the domestic sewage and industrial pollutants at the study area. Sulfate in groundwater was influenced by sulfides in igneous rocks such as aplite and pegmatite found at the study area.

A piper plot was used by Manoj *et al.* (2013) in the characterization and classification of surface water chemistry in India. The hydrochemistry of some ponds in Santiniketan-Bolpur-Sriniketan zone, Birbhum district, west Bengal, India was investigated together with the effect of an annual fair and festival - Pous Mela, on water chemistry change on 15 samples of 5 surface water bodies (namely, Ponds 1, 2, 3, 4 and 5) located near the fair ground. The samples were obtained before and during the Pous Mela festival (on the third week and fourth week of December 2012).

Manoj *et al.* (2013) showed that the measured concentrations of Dissolved Oxygen (DO) and Biochemical Oxygen Demand (BOD) from the ponds increased before and during Pous Mela. The DO concentrations ranged between 2.7 mg/l and 3.8 mg/l while the BOD concentrations ranged between 10 mg/l and 90 mg/l. The BOD concentrations were higher than the maximum recommended BOD value of 3 mg/l (Central Pollution Control Board , 2007). This showed the presence of organic pollution in the ponds influenced by human activities during the Pous Mela festival such as bathing, washing of clothes and utensils.

3.6.5 The Hydrogeological Model

The hydrogeological model is the recharge estimation method that is based on the infiltration coefficients of specific rocks such as limestones and sandstones (Rahmani *et al.*, 2017). Studies indicate that the recharge estimation methods that are determined from the infiltration coefficients provide appropriate results for estimating groundwater recharge at

semi-arid regions as compared to other methods of recharge estimations such as using the Chaturvedi equation and the model of Chibane *et al.* (Rahmani *et al*., 2017; Patil *et al.*, 2019).

Patil *et al.* 2019 used Rainfall Infiltration Factor (RIF) method which uses the geological infiltration coefficients to assess the recharge from rainfall in Mandri river watershed, Kanker district, Chhattisgarh, India. The study area comprised of various rocks such as epidiorite, granite and schists with infiltration coefficients that ranged from 6% to 11%. The estimated recharge was for a ten year duration from 2006-2007 to 2015-2016. The study showed that the ten year average recharge that was determined from the RIF method was 890.22 ha/m and was closer to the recharge estimation of 1079 ha/m that was determined from the water table fluctuation method which is mostly used to estimate groundwater recharge worldwide.

Siva Prasad and Venkateswara Rao (2018) used the RIF method to assess the groundwater recharge in the Kandivalasa river sub-basin at the east coast of India from 2013 to 2016. The recharge was estimated using the infiltration coefficient of 11% due to the geology of the study area which comprised of weathered and fractured khondalic formation, granite gneiss and the soil. The study showed that the annual rainfall was around 1000 mm and the per cent of rainfall that converted to groundwater recharge was 11.12%, 13.18%. 9.51% and 12.80% for the years 2013, 2014, 2015 and 2016 respectively. The estimated recharge from RIF method indicated that the least recharge of 11.47 MCM occurred in 2016, while the highest estimated recharge of 13.86 MCM occurred in 2013. The highest recharge at the study area was influenced by a continuous high precipitation event of more than 300 mm that occurred within a year.

3.6.6 The Linear Interpolation Method

The linear interpolation method is used to determine the analytical function *f(x)* that passes through the given data points in order to approximate the desired unknown value (Howard, 2018). This method is widely used in the field of science and engineering and found to be reliable in estimating the missing data (Chen and Claridge, 2000). The linear interpolation method uses the straight-line equation that represent a straight line that connects the given data points (Howard, 2018).

Anjomshoaa (2019) used the linear interpolation analysis method to fill the missing meteorological data in the heating and cooling seasons at Kerman, Iran from 2009 to 2011. About 5% of the data was missing due to instant equipment failure. The missing weather data that was interpolated was temperature, pressure and relative humidity. The linear interpolation method was tested for its accuracy by introducing artificial gaps into the hourly data to make it a 3-hour data. The accuracy of the linear interpolation method was checked by comparing the original data set and the interpolated data set. The results showed that the interpolated data set of the percentage relative humidity that ranged from approximately 77.5% to 99% was closer to the real data set that ranged from 77.5% to 100%.

Baltazar and Claridge (2002) determined the accuracy of the cubic spline and Fourier series techniques for filling the missing building energy use and weather data at the United States of America from 1989 to 1994, by comparing these techniques with the linear interpolation method. The data set that was used included the dry-bulb temperature and the cooling and heating data and 20 samples of hourly data. These data sets were collected from different locations in the United States of America.

The evaluated pseudo gaps for the dry bulb temperature data collected at one of the locations in Texas ranged from 4474 to 6042. The results showed that the linear interpolation method was a better approach for filling the gaps of the temperature data of the dry bulb. The linear interpolation method had the highest percentage of the estimated dry-bulb temperature data that ranged from 72% to 99% while the Fourier technique had the least percentage of the estimated dry-bulb temperature data that ranged from 19% to 65%.

North (2012) assessed the influence of climate change on the occurrence of Hypoxia in Swiss Lakes from 1976 to 2010 by using the linear interpolation method to interpolate the historical lake water profiles such as temperature, oxygen, phosphorus and chloride profiles. The water temperature profile ranged from approximately 2 ^{o}C to 24 ^{o}C, the oxygen concentration ranged from 1 mg/l to 14 mg/l, the total phosphorus concentration ranged from approximately 10 µg/l to 280 µg/l while the chloride concentration ranged from 2.5 mg/l to 4.0 mg/l. The results from the linear interpolation method was compared with the interpolated results from the cubic spline method and the accuracy of each method was assessed using the Root Mean Square Error (RMSE) and the Maximum Absolute BIAS Error (MABE).

Pseudo gaps of various sizes that represent the number of missing data points were created by removing the measured data from the water column profile. The pseudo gap sizes ranged from 1 to 3 and were then filled using each of the interpolation method. The results indicated that the RMSE associated with both the cubic spline and the linear interpolation method increased with the pseudo gaps. The MABE for the cubic spline method ranged from 7.5 to 27.8 while the MABE for the linear interpolation method ranged from 5.3 to 8.7. This showed that the errors associated with the cubic spline method increased faster as compared to the errors associated with the linear interpolation method, hence indicating the linear interpolation method can be best used for estimating the historical water profiles.

3.6.7 MODFLOW

MODFLOW is a three-dimensional model that uses the method of finite-difference. It is commonly used to simulate groundwater flow systems. MODFLOW model consists of the package of the Subsidence and Aquifer-System Compaction (SUB Package). The SUB Package is based on Terzaghi (1925)'s principle of effective stress, where effective stress is expressed as the difference between the total stress and the pore pressure. Equation (3.7) indicates the effective stress principle used by the SUB Package (Hoffmann *et al.,* 2000).

$$\sigma' = \sigma - p \tag{3.7}$$

where: σ' = effective stress

σ = total stress

p = pore pressure

The SUB Package was created to simulate compaction and storage changes that result from changes in effective stress for a given head change. Equation (3.8) indicates the effective stress formula used by the SUB Package in MODFLOW model to simulate changes of compaction and storage in confined aquifer systems (Hoffmann *et al.,* 2000).

$$\Delta\sigma_{zz} = \rho w g \Delta h \tag{3.8}$$

where: $\Delta\sigma_{zz}$ = change in effective stress

ρw = density of water

Δh = change in head

g = gravitational acceleration

Hofmann *et al.* (2003) states that MODFLOW is widely used and legally tested to simulate groundwater models. MODFLOW model is used to initiate groundwater management strategies and to provide scientific foundation for controlling land subsidence (Cui *et al.*, 2014). It has been indicated that the main factor leading to land subsidence is contributed by groundwater withdrawals with the confined aquifers being the main withdrawal targets (Hofmann *et al.*, 2003; Cui *et al.*, 2014; Deng *et al.*, 2018; Ghazavi and Ebrahimi, 2018).

Deng *et al.* (2018) used MODFLOW to simulate and forecast land subsidence to monitor the intake of groundwater during the water transfer project of the South to North in Tianjin, China. The results from the MODFLOW model showed that the groundwater tables from six confined and unconfined aquifers (Aquifers I, II, III, IV, V, VI) in Tianjin and land subsidence were successfully managed and improved under the application of three management plans of groundwater exploitation namely, the high, medium and low plans. The predicted results from the model showed a rise of the water table of more than 25 m from the aquifers and an average annual land rebound of 2.41 mm/year in the simulation period of 2006 to 2030 and 6.04 mm/year in the simulation period of 2006 and 2020. The results from the MODFLOW model showed that the application of the three schemes in Tianjin was effective in regulating groundwater exploitations.

Cui *et al.* (2014) used MODFLOW model to investigate groundwater resources and their changes in the plain of Tianjin from 1998 to 2008. The model indicated that the groundwater withdrawals contributed to 96.37% of the total discharge rate of 1 761.89 × 10^6 m^3/year, while the lateral boundary outflow contributed to 3.63% of the total discharge rate. The model showed that the crossflow recharge contributed to 44.43% of the total recharge rate of 1 626.15 ×10^6 m^3/year, while the compression release and the lateral boundary flow contributed to 32.14% and 21.88% respectively of the total recharge rate. This showed that there was a negative balance of -135.72 ×10^6 m^3/year between the recharge and discharge rates.

Cui *et al.* (2014) also used the simulated water heads from 1998 to 2008 to predict the groundwater level changing patterns and the associated land subsidence variations under the controlled groundwater exploitation after the execution of the south to north water diversion project in Tianjin. The predicted results showed that the groundwater levels may increase annually if the abstraction rates decreased below 1 150 × 10^6 m^3/year. The predicted model

results indicated that there will be an average land rebound rate of 2-3 mm/year over 11 years period from 2009 to 2020 in areas that were dominated by land subsidence and the cumulative land subsidence would decrease from 1000 mm to 62 mm.

The MODFLOW model was also used by Ghazavi and Ebrahimi (2018) to study the interactive effects of land subsidence and construction of dams on Mosian Aquifer, located in North East of Iran. The results indicated that MODFLOW model was an appropriate model to be used as a groundwater management tool with a coefficient of determination (R^2) for groundwater levels of 0.96 from 1991 to 2006 and 0.93 from 2007 to 2014.
Ghazavi and Ebrahimi (2018) estimated the impact of dam construction on the recharge and discharge rates from river leakage and return flow of irrigation using annual flows of the Doiraj River from 1991 to 2012. The MODFLOW model showed that the estimated annual groundwater recharge through the Doiraj River for this period was about 10.5 million cubic meters (MCM) and decreased through the construction of the dam to about 7 MCM. The return flow increased from 7.1 MCM in 1991 to 13.6 MCM in 2012, while the discharge through pumping increased from 18 MCM in 1991 to more than 60 MCM in 2012. The results from the model indicated that the dam construction had no significant effects on land subsidence at the study area as it normally occurred at around 5 to 36 cm.

CHAPTER 4

METHODOLOGY

4.1 Stages of Investigation Employed

The methodology of investigation has been categorized into Pre-fieldwork, Fieldwork and the Post-fieldwork. The Pre-fieldwork undertaken in the initial stage involved problem identification and collection of hydrological and meteorological data from departments including Water Utilities Corporation and Botswana Meteorological Services. The hydrological and meteorological data collected from these departments were used to analyze the determinants of groundwater depletion at the wellfield area.

The Fieldwork involved hydro sampling from production boreholes and monitoring wells within the study area with the view of determining the water types in the project area and the effects of groundwater depletion on water quality and water chemistry change. The hydro sampling exercise was carried out on the 27th of July 2019 and on the 28th of October 2019, as studies indicate that most of the chemical changes in groundwater occur approximately after a 3-month period (Botswana Bureau of Standards, 2016).

The Post-fieldwork involved the analysis of data obtained using different methods that include trend and correlation analyses to identify the determinants of groundwater level decline in the wellfield area and the significance of the declining trends; Piper Plots for geochemical characterization of groundwater in the wellfield area and the simulation of the occurrence of land subsidence by means of ModelMuse and MODFLOW-2005 software. Other software programs, such as Arc GIS, Microsoft Excel, Surfer and the hybrid model were employed for data processing. Based on the results obtained, the conclusions and recommendations were then drawn.

Figure 4.1 indicates a flow chart of the three stages and activities that were performed in order to meet the objectives of the study.

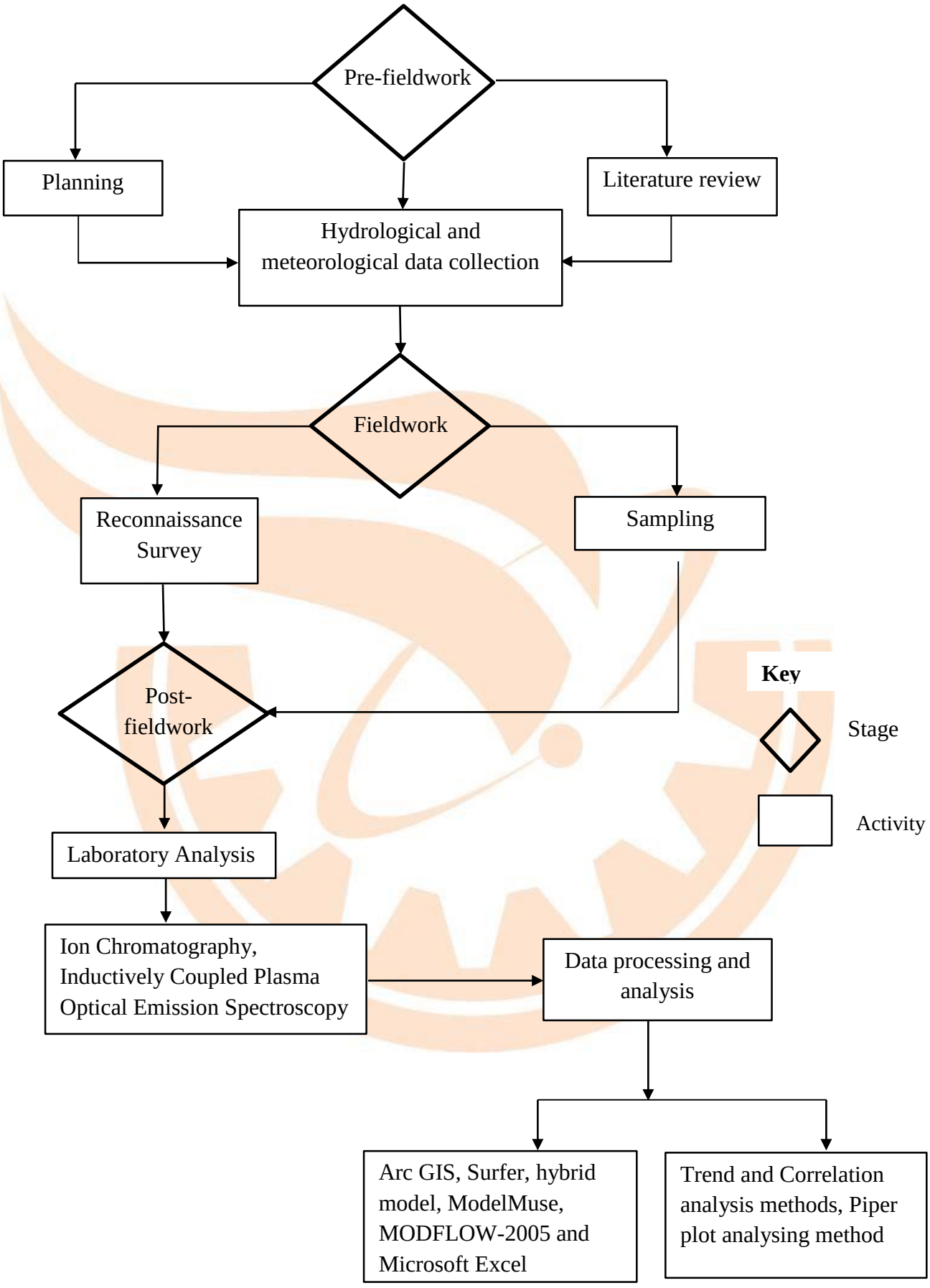

Figure 4.1 Stages and activities employed during the study

4.1.1 Pre- Fieldwork

4.1.1.1 Project planning

The problem statement and the justification of the study were outlined after a review of previous reports related to the project topic on the study area by the Central Statistics Office (2009) and the Department of Environmental Affairs (2006). These reports verified the occurrence of the depletion of groundwater at the wellfield area, hence indicating a need to investigate the causes of the decline of groundwater and the environmental consequences of the water decline. The objectives of the research project were stated, so that the purpose of conducting the research project was clearly defined to help guide the research work.

4.1.1.2 Literature review

In order to acquire the available wellfield data, different sources of data such as Department of Water Affairs, Geological Surveys and Water Utilities Corporation were consulted. Other data sources included unpublished postgraduate studies reports related to wellfields in Botswana. The availability and affordability of the analysis tools used in the study such as trend analysis and correlation analysis were also assessed during the literature review.

4.1.1.3 Hydrological and meteorological data collection

Hydrological data such as groundwater occurrences, movements and groundwater levels time series and meteorological data covering temperature and rainfall were obtained from the Department of Water Affairs, Water Utilities Corporation and the Botswana Meteorological Services. The data acquired was used in analyzing the determinants of groundwater depletion and the impact they had on the wellfield area.

4.1.2 Fieldwork

4.1.2.1 Reconnaissance survey

The survey involved the acquisition and study of existing maps and aerial images of the project area to assess existing routes, identification of geological features such as main aquifers and lineaments and the land topography. The aerial topographic maps were used in determining the groundwater flow directions. The reconnaissance survey also assisted in eliminating unfeasible routes to the study area when performing fieldwork thus saving time and costs.

4.1.2.2 Hydro sampling

Water samples were collected in July 2019 and October 2019 from different monitoring wells and the four production boreholes of the Dukwi Wellfield namely, BH7674, BH7675, BH7678 and BH7687 for this study. The Electrical Conductivity (EC), Total Dissolved Solids (TDS), pH, temperature and turbidity of groundwater samples were measured in-situ using a multiparameter waterproof meter (Hanna HI9829). Water samples collected from the boreholes (Figure 4.2) were stored in appropriate plastic bottles and transported using ice chests (Figure 4.3) to avoid further chemical reactions due to heat during transportation as higher temperatures increase the chemical reaction rate of substances (Taoukis *et al.*, 2014). The water samples were submitted to the Department of Water Affairs, Water Utilities Corporation and BIUST Department of Earth and Environment Sciences laboratories for water chemistry and quality analysis. This was because some of the ions such as chloride and sulphate could not be analyzed at the Department of Water Affairs and Water Utilities Corporation due to lack of facilities, hence analysis for these constituents at the BIUST Department of Earth and Environment Sciences laboratories where the facilities are available. It is worth noting that all the laboratories use the Botswana Bureau of Standard specifications for natural water (BOS 262. 2011) for water quality analysis.

Figure 4.2 Collection of water samples from borehole sampling point

Figure 4.3 Water samples stored in ice chest during transportation

4.1.2.3 Water level measurements

Water level readings were recorded on a monthly basis from April to December 2019 from the monitoring wells and production boreholes within the study area. The groundwater levels were determined by lowering the water level indicator instrument into the borehole through an access tube installed on top of the borehole (Figure 4.4).

Figure 4.4 Measurement of borehole water level using water level indicator instrument

4.1.3 Post-Fieldwork

4.1.3.1 Laboratory testing analytical techniques employed

Upon arrival at the BIUST Department of Earth and Environment Sciences laboratories, the groundwater samples were filtered using a 0.45 μm filter to remove some sediments. The filtrate was then collected using a vial which was thoroughly rinsed with distilled water to reduce the potential of contaminating the sample before tests were run. The concentrations of major cations such as sodium and potassium and major anions such as chloride and sulphate were determined using an ion chromatography (Thermo Scientific Dionex Chromeleon) while the heavy metals such as iron and lead were determined by the Inductively Coupled Plasma Optical Emission Spectroscopy (Thermo Scientific iCAP PRO ICP-OES).

The water chemistry results of some ions such as bromine and carbonate and heavy metals such as aluminum and manganese were determined by the Department of Water Affairs and Water Utilities Corporation. The water chemistry results of bromine, carbonate, aluminum and manganese from the monitoring wells of the study area (BH 2985, BH 4649, BH 7516, BH 7521, BH 7639 and BH 7546) were obtained from the Department of Water Affairs, while the water chemistry results of bromine, carbonate, aluminum and manganese from the production boreholes of the study area (BH 7674, BH 7675, BH 7678 and BH 7687) were collected from the Water Utilities Corporation.

4.1.3.2 Pearson's correlation analysis

The method was used in identifying the determinants of groundwater level decline. Various variables recorded from the study area in a 10-year period, from 2010 to 2019 were used. These variables include independent variables (abstractions, rainfall, recharge, and temperature) and dependent variable (water level drop). Seasonal and yearly variations in determinants of groundwater depletion during the years were traced. The results were linked with the decline in groundwater levels and the correlation between them was analyzed.

Pearson's Coefficient (r) is indicated by Equation 4.1 (Gingrich, 2004)

$$r = Sxy/\sqrt{SxxSyy} \quad (4.1)$$

where: $Sxx = \sum X^2 - (X)^2/n$

$Syy = \sum Y^2 - (\sum Y)^2/n$

$Sxy = \sum XY - (\sum X)(\sum Y)/n$

Y = dependent variable values

X = values of each independent variable

n = number of values for X and Y variables

4.1.3.3 Linear trend modeling

This method was used to determine the existence and significance of declining trends in the groundwater levels at the Dukwi Wellfield. In the linear trend analysis, the best fit line to describe the independent variable (e.g. time in years) and the dependent variables (e.g. groundwater level readings) was determined. The existence and the significance of the declining trends were measured by using the coefficient of determination (R^2) (Chaoka *et al.*, 2006). R^2 was determined using Microsoft excel.

4.1.3.4 Geochemical characterization of groundwater

A Piper Plot was used to classify the concentration of different cations and anions and their interrelationship in different representative water samples taken from production boreholes and monitoring wells located in the study area. The piper plot consists of three graphs: A ternary graph located in the bottom left (see Figure 4.5) which represents the cations, a ternary graph located in the bottom right which represents the anions, and the diamond graph located in the center, representing the combination of the anions and cations determined from the ternary graphs (Mills *et al.*, 2019).

The cation ternary diagram represents different water types, such as the calcium, magnesium and sodium and potassium types, while the anion ternary diagram represents the sulphate, bicarbonate, chloride and the no-dominant water types (Mills *et al.*, 2019). In the diamond plot the upper quartile constitutes the calcium sulphate waters (gypsum groundwater and mine drainage), the left quartile represents the calcium bicarbonate waters (shallow and fresh groundwater), the right quadrant represents the sodium chloride waters (marine and deep ancient groundwater) and the bottom quadrant represents the sodium bicarbonate waters (deep groundwater influenced by ion exchange) (Anon., 2020b).

The mill equivalent percentages of the major cations (Mg, Ca, Na and K) and anions (Cl, SO_4, CO_3 and HCO3) were plotted in the two ternary diagrams which were then projected into the middle diamond plot to indicate the overall character of water. Figure 4.5 indicates the hydrochemical facies in the cation and anion ternary diagrams and in the diamond plot.

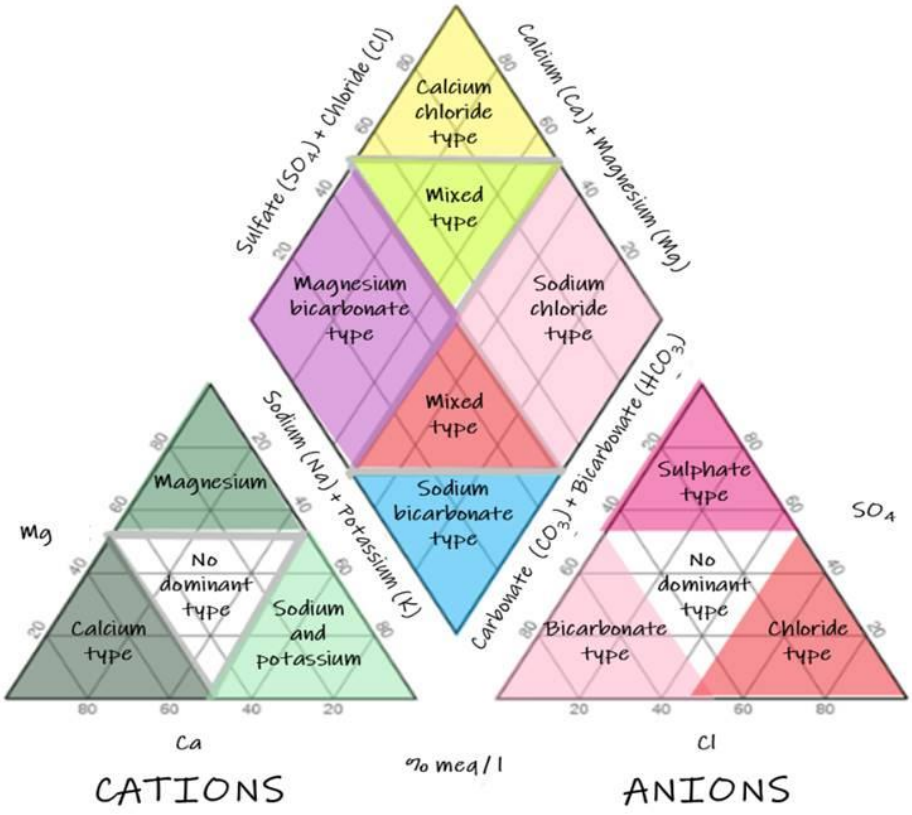

Figure 4.5 Hydrochemical facies in the cation and anion triangles and in the diamond plot (after Montoya and Carita, 2018)

4.1.3.5 Water quality and chemistry compliance

The analyzed water chemistry of the study area was compared with the Botswana Bureau of Standard natural water specifications (BOS 262:2011) to determine if the water quality and chemistry in the Dukwi Wellfield as established in this study comply with the recommended standards (Appendix A) used in Botswana.

4.1.3.6 Determination of aquifer parameters

The aquifer's storativity was estimated from the aquifer's thickness and specific storage of lithologies, since the aquifer is confined over most part of the area by the overlying silt and

mudstones of the Ngwasha Formation and the Tlapana Mudstones as indicated in Section 2.7.3. The aquifer's thickness in each borehole was obtained from the geological logs table (Appendix B), which indicates the geology and the depth of each lithological unit found in the production boreholes of the project area, while the specific storage values were obtained from Table 4.1, which indicates specific storage for various lithologies and aquifer's compressibility (α). The aquifer storativity (S) was then estimated using Equation (4.2) (Younger, 2000).

Table 4.1 Specific storage values for various lithological units and aquifer compressibility

Lithological unit	Aquifer compressibility (α m S/kg)	Specific Storage (m^{-1})
Clay	0.000001	0.00981
Silt, fine sand	0.0000001	0.000982
Medium Sand, fine gravel	0.00000001	0.0000987
Coarse sand, medium gravel, highly fissured rock	0.000000001	0.000105
Coarse gravel, moderately fissured rock	0.0000000001	0.00000163
Unfissured rock	0.00000000001	0.000000746

Source: (Freeze and Cherry, 1979; Younger, 2000)

$$S = S_S \times b \quad (4.2)$$

where: S = storativity

S_S = specific storage of various lithology

b = saturated thickness

The drawdown data of the four pumping wells of the wellfield area was used to estimate the aquifer's transmissivity (T) and radius of influence (R) derived by employing the Cooper and Jacob (1946) method. The drawdown data was acquired from pumping tests of the production boreholes that were conducted in 1994 (see Appendix C).

Equation (4.3) indicates the Cooper and Jacob (1946) formula as cited in Dinu *et al.* (2017) that was used to estimate transmissivity of the aquifer in the study area.

$$T = \frac{2.3Q}{4\pi\Delta s} \quad (4.3)$$

where: T = aquifer transmissivity (m^2/min)

Q = constant discharge of the pumping well (m^3/min)

Δs = gradient of a straight line between 1 log cycle (m)

The radius of influence (R) of the pumping wells at any given time t, was estimated from Equation (4.4), derived from the Cooper and Jacob (1946) equation.

$$R = \sqrt{\frac{2.24584Tt}{S}} \quad (4.4)$$

where: R = radius of influence (m)

t = time (min)

Other terms have their usual meanings as in Equations (4.2) and (4.3)

4.1.3.7 Estimation of Hydraulic Conductivity

The hydraulic conductivity (k) was determined by dividing the estimated transmissivities acquired from the Cooper and Jacob method (Equation 4.3) by the aquifer thicknesses. The aquifer thicknesses were attained from the geological logs table (Appendix B). The aquifer hydraulic conductivity was determined using Equation (4.5).

$$k = T/b \quad (4.5)$$

where: k = hydraulic conductivity

b = aquifer's thickness

4.1.3.8 Estimation of groundwater recharge

Groundwater recharge in the wellfield area was estimated using the hydrogeological model which depends on the geological infiltration coefficients and the precipitation (Rahmani *et al.*, 2017) experienced in the study area. The geological coefficients used were obtained from Table 4.2 which indicates the infiltration coefficients of geological materials found at the study area. The model is represented by Equation (4.6).

Table 4.2 Infiltration coefficients of rocks

Type of rock	Infiltration coefficient%
Soil	1
Clay	1
Sand	4
Sandstone	4
Calcrete	5
Mudstone	5
Siltstone	5
Shale	5
Arkose	5

Source: Rahmani *et al.* 2017; Siva *et al*. 2018

$$GWR = \frac{\emptyset \times P}{100} \quad (4.6)$$

where: GWR = estimated groundwater recharge

Ø = geological infiltration coefficient

P = annual average rainfall

A linear association between the geological coefficients and the annual average precipitation was derived after making uniform the geological coefficients following Rahmani *et al.(* 2017) as indicated by Equation (4.7).

$$\mathrm{GWR} = 0.034 \times \mathrm{P} \quad (4.7)$$

All the terms have their usual meanings as in Equation (4.6)

The recharge estimations determined in equation (4.7) were converted to the annual incoming water volume by multiplying the recharge with the recharge area (Prasad and Rao, 2018) as indicated by Equation (4.8). This was done for easy comparison with the recorded abstractions rates of the wellfield measured in cubic meters per year. Three recharge zones were identified for the aquifer at the study area. The identified recharge zones are along the Mea Arkose Formation; the contact between the Mea Arkose Formation and the Basement

Complex and along Ntane Formation. These recharge zones occupied an area of approximately 164 km^2 (Geotechnical Consulting Services, 1998b). The recharge along the Mea Arkose and Ntane Formations is mainly through the river courses of the Tutume River, Gwedebi River and the Mosetse River which is located at a distance of about 3 km away from the wellfield area (Geotechnical Consulting Services, 1998a).

$$\mathrm{GWR} = (0.034 \times \mathrm{P})\mathrm{A} \quad (4.8)$$

where: A = recharge area (164 km^2)
All other terms have their usual meaning as in Equation (4.6)

4.1.3.9 Estimation of Abstraction Rates

The recorded abstraction rates of the production boreholes were from 2013 to 2019 due to missing abstraction records from 2010 to 2012. There were some gaps in the abstraction records from 2016 to 2018. A linear interpolation method Equation 4.9 (Noor *et al*., 2004) was employed to estimate the missing abstraction rates from 2016 to 2018 by using the available abstraction rates and recorded water levels of the production boreholes from 2013 to 2019.

$$f(x) = f(x_0) + \frac{f(x_1) - f(x_0)}{X_1 - X_0}(x - x_0) \quad (4.9)$$

where: $f(x)$ = the estimated abstraction rates (2016, 2017 and 2018)
x = recorded water levels (2016, 2017 and 2018)
$f(x_0)$ = initial recorded abstraction rates in 2013
$f(x_1)$ = last recorded abstraction rates in 2019
x_0 = initial recorded water levels in 2013
x_1 = last recorded water levels in 2019

4.1.3.10 Simulation of land subsidence

The Mea Arkose aquifer, the major aquifer in the wellfield area from which all the four production boreholes extract potable water, was used in the modeling exercise for this study. Due to the heterogeneous and anisotropic characteristics of the aquifer system, the simulation of land subsidence was done using the Subsidence and Aquifer-System

Compaction package in MODFLOW-2005 (MODFLOW SUB) and ModelMuse 4. MODFLOW SUB simulates interbeds compaction based on Terzaghi (1925)'s principle of effective stress.

The model domain was homogeneously discretized using a one-kilometer grid based on previous studies of the wellfield area (Geotechnical Consulting Services, 1998b). The reference datum for the measurement of the hydraulic heads that was used in the model was 1000 m amsl which is the maximum ground elevation of the study area as indicated in Section 2.2. The model boundaries were set in accordance with the two rivers found in the study area namely, the Semoane River which bounds the aquifer to the north and the Mosetse River which confines the aquifer to the South (Geotechnical Consulting Services, 1998b). The simulation of the two rivers was done using the General Head Boundary Package in the model while the four pumping wells were simulated using the Well Package.

The specific yield and porosity of the aquifer were set to be 140.53% and 231.41% respectively. The porosity was estimated by summing the average porosities of different geological materials found in the boreholes (see Appendix G), while the specific yield was determined by multiplying the porosity fraction accounted for by specific yield of the different lithologies (see Appendix H) by their average porosities determined from Appendix G (Younger, 2000).

To determine land subsidence in the study area, two simulation periods of 6 years (2013-2019) and 12 years (2019-2031) were used for this study. A simulation period of 6 years was used to simulate land subsidence that occurred due to pumping in the production boreholes (BH 7674, BH 7675, BH 7678 and BH 7687) from 2013 to 2019 while the simulation period of 12 years (2019 to 2031) was used to simulate land subsidence that can result from future groundwater exploitation.

4.1.3.11 Calculation of land subsidence

Land subsidence induced by pumping was calculated to compare it with the simulated land subsidence from MODFLOW SUB. Land subsidence was calculated using the specific storage and the hydraulic head variations. The change in hydraulic heads was obtained by subtracting the recorded water levels in 2019 from the recorded water levels in 2013. The

specific storage of each borehole was obtained from adding the specific storage of various lithologies intercepted by the boreholes (see Table 4.1, Section 4.1.3.6).
Land subsidence was calculated using Equation (4.10) (Chen *et al.*, 2003).

$$S = S_S \Delta H M \quad (4.10)$$

where: S = amount of land subsidence

S_s = specific storage

ΔH = change in head

M = thickness of the layer

CHAPTER 5

RESULTS AND DISCUSSIONS

5.1 Results

5.1.1 Estimation of Recharge

The average annual rainfall and the estimated groundwater recharge of the study area from 2013 to 2019 based on the hydrogeological model (Equation 4.8) are presented in Table 5.1. From the table, the least estimated recharge of 578 789 m^3/year occurred in 2014, while the highest estimated groundwater recharge of 2 343 035 m^3/year for the period under consideration happened in 2016 corresponding with the highest average rainfall. The mean annual groundwater recharge was 1 149 691 m^3/year. Variation in the groundwater recharge of the study area is observed to be dependent upon the variations in annual rainfall of the study area that ranged from 103.8 mm to 420.2 mm.

Table 5.1 Annual Rainfall and Estimated Recharge of the study area (2013-2019)

Year	Annual Rainfall (mm) (Botswana Meteorological Services, 2019a)	Recharge (m^3/year)
2013	207.1	1 154 789
2014	103.8	578 789
2015	109.2	608 899
2016	420.2	2 343 035
2017	201.2	1 121 891
2018	200.3	1 116 873
2019	201.5	1 123 564
Average	206.2	1 149 691

5.1.2 Estimation of Aquifer Parameters and Radius of Influence

Estimates of the aquifer storativity was determined by summing up the storativity values for the individual strata in a borehole as exemplified by the aquifer storativity for Production Borehole BH 7678 (Table 5.2). The total storativity of this borehole following the estimation procedure as spelt out is 0.00021262.

Table 5.2 Estimation of aquifer storativity (Borehole BH 7678)

Borehole Number	Lithology (Department of Water Affairs, 1995b)	Estimated Specific Storage	Saturated thickness (m) (Department of Water Affairs, 1995b)	Storativity
BH 7678	Sand	0.00001050	1.00	0.00001050
	White calcrete	0.00000163	4.00	0.00000652
	Coloured Mudstone	0.00000163	30.0	0.00004890
	Buff, yellow, white arkose	0.00000163	51.0	0.00008313
	Brown, purple, grey sandstone	0.00000163	15.0	0.00002445
	Tillite	0.00000163	2.00	0.00000326
	Pale grey siltstone	0.00000163	16.0	0.00002608
	Schist	0.00000163	6.00	0.00000978
Total		0.00002191	125	0.00021262

Note: The specific storage estimates from this table are from Younger (2000)

Drawdown data of the pumping wells in the project area based on the Cooper and Jacob (1946) method for the determination of the aquifer hydraulic properties are presented in Figures 5.1 to 5.4. The analysis was based on the pumping test data of the production boreholes BH 7674, BH 7675, BH 7678 and BH 7687 that was performed at discharge rates ranging from 0.750 m^3/min to 3.75 m^3/min (see Appendix C).

At the beginning of the pumping test, Borehole BH 7675 had the least drawdown of 0.010 m, while BH 7687 had the highest drawdown of 2.95 m. At the end of the pumping test, (120 minutes), Borehole BH 7687 had the highest drawdown of 21.81 m, while Borehole BH 7675 had the least drawdown of 0.200 m (see Appendix C).

The Production Borehole BH 7687 experienced some progressive increase in drawdown from 2.95 m to 21.06 m within the first 16.00 minutes. Thereafter, there was marginal drawdown from 21.11 m to 21.81 m with time to the end of the pumping test at 120.00 minutes.

The Production Borehole BH 7675 experienced some marginal drawdown from 0.010 m to 0.140 m for 55.00 minutes followed by some gradual increase in drawdown from 0.170 m to 0.200 m with time to the end of pumping test at 120.00 minutes.

The gradients for the time drawdown straight line plots (see Figures 5.1 to 5.4) range from 0.084 meters per log cycle to 17.3 meters per log cycle. Borehole BH 7675 has the least gradient of 0.084 meters per log cycle, while Borehole BH 7687 has the highest gradient of 17.3 meters per log cycle. The variations in gradient have been influenced by the different drawdowns experienced in the Production Boreholes (BH 7678, BH 7687, BH 7674 and BH 7675) which range between 0.010 m and 21.8 m.

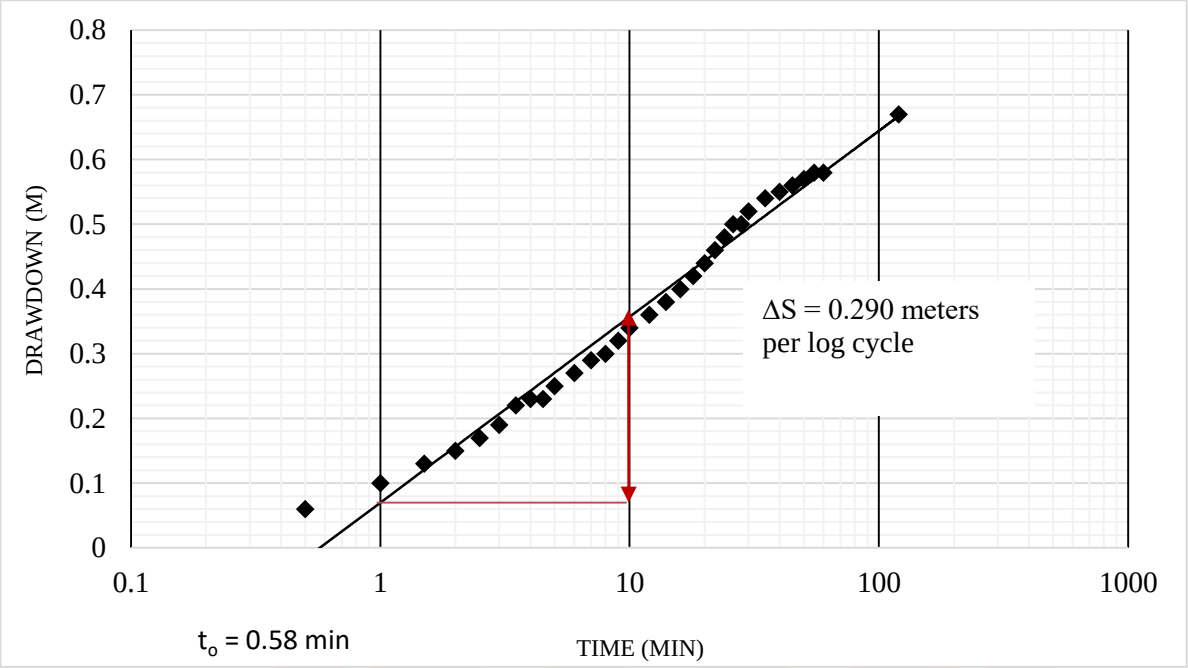

Figure 5.1 Time drawdown straight line plot for BH 7674

(◆ = Drawdown)

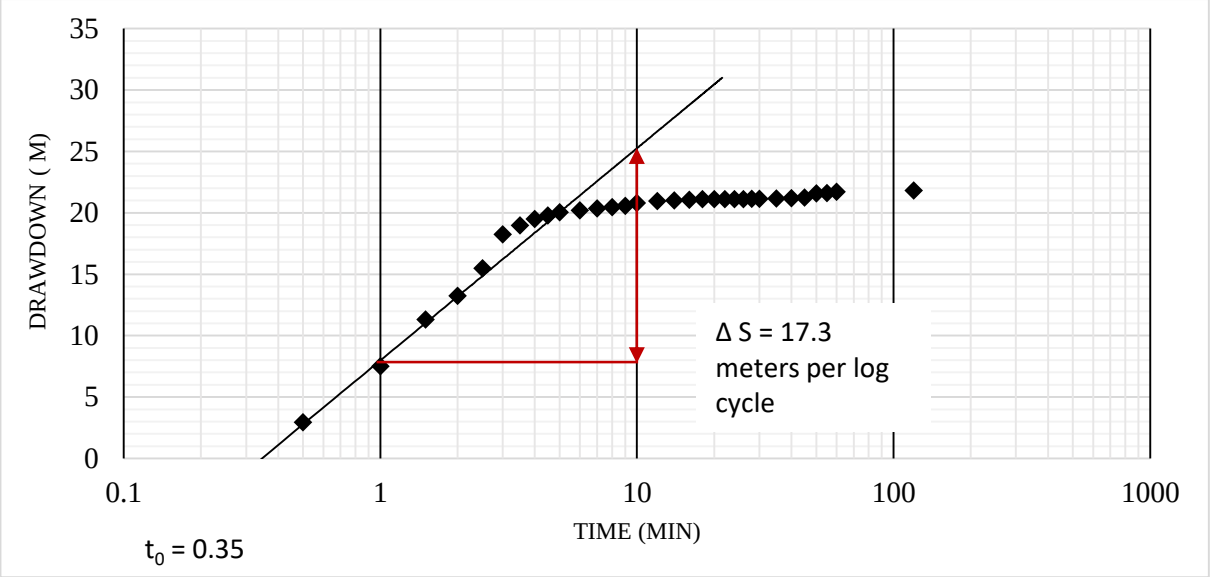

Figure 5.2 Time drawdown straight line plot for BH 7687

(◆ = Drawdown)

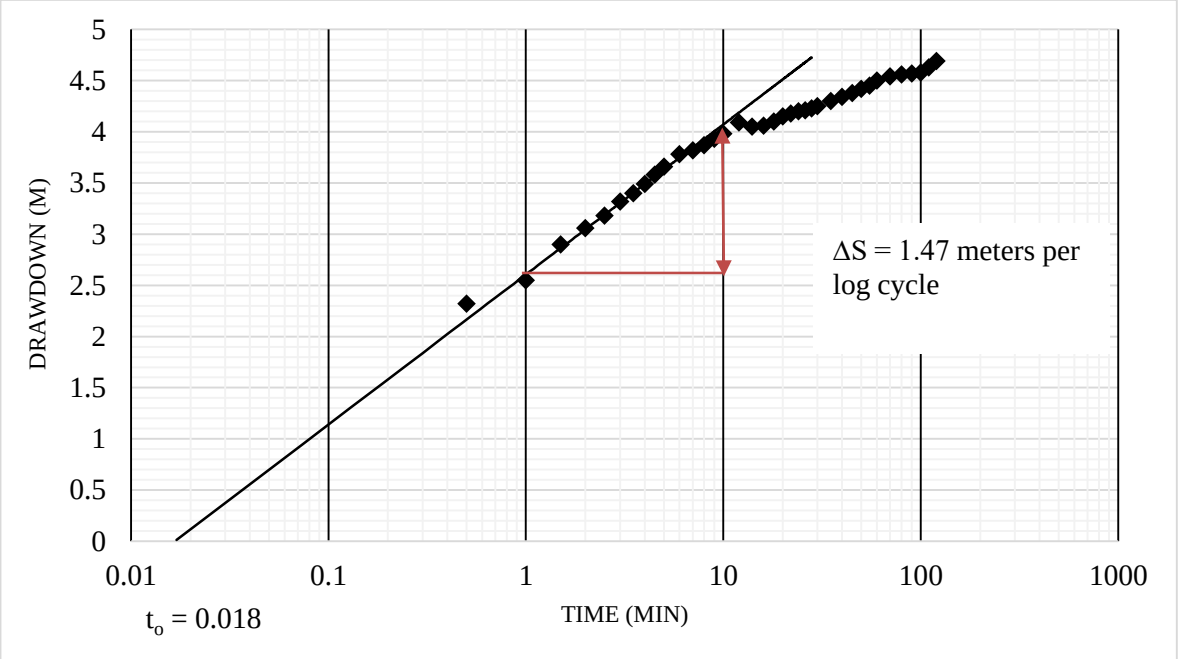

Figure 5.3 Time drawdown straight line plot for BH 7678

(◆ = Drawdown)

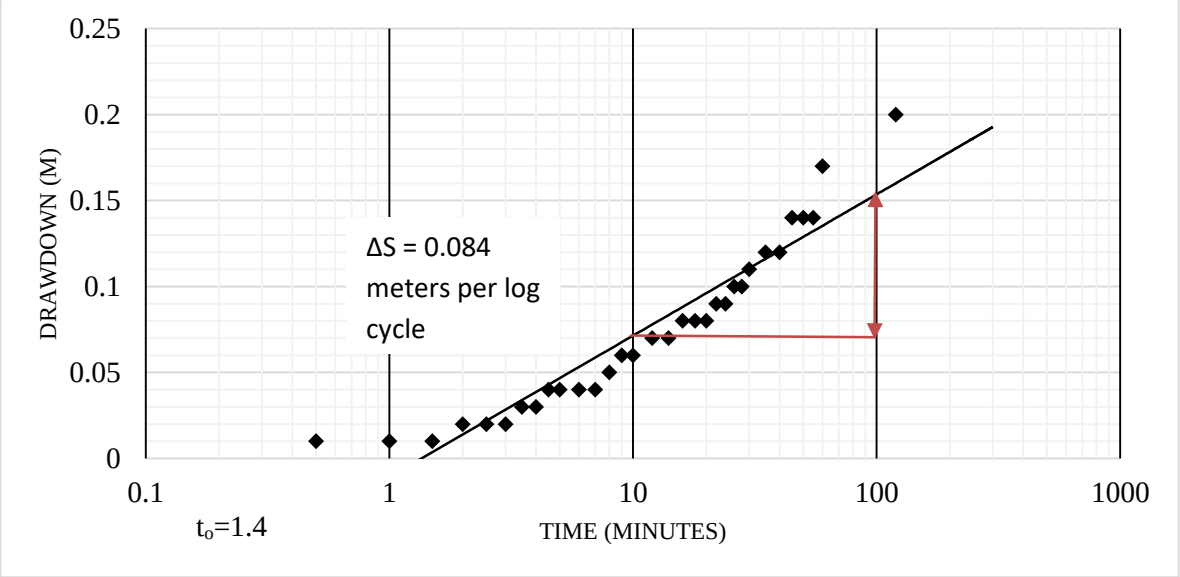

Figure 5.4 Time drawdown straight line plot for BH 7675

(◆ = Drawdown)

The calculated storativity, transmissivity, radius of influence and the hydraulic conductivity of the pumping wells after 2 hours of pumping from Equations (4.2) to (4.5) respectively are presented in Table 5.3.

Transmissivity (T) estimates as indicated in Table 5.3 range from 0.01587 m^2/min to 8.171 m^2/min, with Borehole BH 7675 having the highest transmissivity and Borehole BH 7687 having the least transmissivity. Borehole BH 7687 has the highest gradient of the time drawdown straight line plot of 17.3 meters per log cycle (see Figure 5.2), while Borehole BH 7675 has the least gradient of the time drawdown straight line plot of 0.084 meters per log cycle (see Figure 5.4). This shows that the transmissivity estimates of the production boreholes are indirectly related to the gradients of the time drawdown straight line plots. The average transmissivity of the production boreholes is 2.228 m^2/min.

The hydraulic conductivities (k) range from 0.000109 m/min to 0.0413 m/min, Borehole BH 7675 has the highest hydraulic conductivity while Borehole BH 7687 has the least hydraulic conductivity. Borehole BH 7675 has the least gradient of the time drawdown straight line plot of 0.084 meters per log cycle (see Figure 5.4), while Borehole BH 7687 has the highest gradient of the time drawdown straight line plot of 17.3 meters per log cycle (see Figure 5.2). This indicates that the estimated hydraulic conductivities of the production boreholes are indirectly related to the gradients of the time drawdown straight line plots.

In terms of radius of influence, Borehole BH 7687 has the least radius of influence of 135.16 m, while Borehole BH 7675 has the highest radius of influence of 2 583.6 m. Borehole BH 7687 has the highest gradient of the time drawdown straight line plot of 17.3 meters per log cycle (see Figure 5.2), while Borehole BH 7675 has the least gradient of the time drawdown straight line plot of 0.084 meters per log cycle (see Figure 5.4). This shows that the estimated radius of influence are indirectly related to the gradients of the time drawdown straight line plots. The average radius of influence is 1 001.0 m. The storativity estimates ranges between 0.0002126 and 0.0003299. Borehole BH 7675 has the highest storativity estimates while Borehole BH 7678 has the least storativity.

Table 5.3. Estimated aquifer parameters and radius of influence

Borehole ID.	Thickness (m) (DWA, 2000)	Q (m^3/min) (DWA, 2000)	T (m^2/min)	k (m/min)	S	R (m)
BH 7674	197	0.750	0.4733	0.00240	0.0002456	720.70
BH 7675	198	3.75	8.171	0.0413	0.0003299	2 583.6
BH 7678	125	2.02	0.2515	0.00201	0.0002126	564.64
BH 7687	145	1.50	0.01587	0.000109	0.0002341	135.16
Average	166	2.00	2.228	0.0114	0.0002556	1 001.0

Legend: Q = Constant Discharge; S = Storativity; T = Transmissivity; R = Radius of influence; k = Hydraulic Conductivity; DWA = Department of Water Affairs

5.1.3 Abstractions Rates

The annual abstraction rates in the study area from 2013 to 2019 are presented in Table 5.4. There were some gaps in the abstraction rate records from 2016 to 2018, hence, these rates have been estimated using the linear interpolation method (see Equation 4.9). The mean abstraction rates of the production boreholes ranged from 261 368 m^3/year to 355 392 m^3/year, with Borehole BH 7675 having the highest mean abstraction rate and Borehole BH 7687 with the least mean abstraction rate. The highest total abstraction rate of 1 366 612 m^3/year occurred in 2014, while the least abstraction rate of 1 132 531 m^3/year occurred in 2013. The mean annual total abstraction rate of the production boreholes is 1 253 546 m^3/year. The variations in the abstraction rates within the study area may be attributed to a

decrease in subsistence farming activities such as crop production as suggested by Legadiko (2015) and population increase according to Central Statistics Office (2009).

Table 5.4 Abstraction Rates of the Production Boreholes (2013-2019)

Borehole Number	Abstraction rates (m^3/year)							Mean Abstractions (m^3/year)
	Year							
	2013	2014	2015	2016	2017	2018	2019	
BH 7674	228 151	374 079	254 837	277 729	262 439	308 310	385 689	298 748
BH 7675	337 635	388 680	371 326	352 900	339 076	345 226	352 900	355 392
BH 7678	342 210	305 455	380 918	327 213	328 660	328 414	353 402	338 039
BH 7687	224 535	298 398	261 114	256 195	263 558	254 852	270 921	261 368
Total	1 132 531	1 366 612	1 268 195	1 214 037	1 193 733	1 236 802	1 362 912	1 253 546

Source: Water Utilities Corporation (2019b)

5.1.4 Record of Water Levels

Table 5.5 presents the initial and average water levels of the monitoring wells and production boreholes of the project area. The initial water levels were recorded in 1993 while the average water levels were recorded between 2010 and 2019. From the table, the Monitoring Well BH 7639 had the highest initial water level of 983.33 m amsl, while Monitoring Well BH 7520 had the least recorded initial water level of 942.72 m amsl. The height of the groundwater table corresponds to the topographic heights of 1000 m amsl to the east of the study area and topographic lows of approximately 900 m amsl at the edge of Sua Pan located to the west of the study area.

The table indicates that for the period under consideration (2010 to 2019), the production and monitoring wells in the study area experienced different head variations ranging from 2.39 m amsl to 47.93 m amsl. The Monitoring Well BH 7641 had the highest head variation of 47.93 m amsl, while the Monitoring Well BH 4768 had the least head change of 2.78 m amsl. For the Production Boreholes, Borehole BH 7675 had the highest head variation of 11.93 m amsl. Production Borehole BH 7687 had the least head variation of 2.39 m amsl in comparison with other production boreholes of the study area.

Table 5.5 Record of water levels in the study area from 2010-2019

Borehole Number	Initial Water Level (m amsl) 1993 (DWA, 2000)	Average Water Level (m amsl)										
		Year										ΔH (m amsl)
		2010	2011	2012	2013	2014	2015	2016	2017	2018	2019	
BH 4768 (Obs)	957.19	905.39	905.01	904.85	904.55	904.17	903.75	904.10	903.03	902.74	902.64	2.75
BH 7516 (Obs)	975.46	916.49	914.61	913.60	912.43	909.41	908.09	909.37	909.56	907.33	905.62	10.87
BH 7520 (Obs)	942.72	916.30	915.00	914.45	913.73	913.01	911.75	912.24	910.73	909.75	908.78	7.52
BH 7521 (Obs)	945.08	916.21	915.08	914.22	913.37	912.53	911.67	911.86	910.38	909.17	908.63	7.58
BH 7546 (Obs)	948.15	917.29	915.05	914.22	913.39	912.49	910.11	909.99	883.91	881.67	881.21	36.08
BH 7639 (Obs)	983.33	914.36	913.13	911.66	910.21	908.40	906.79	907.79	907.21	905.46	904.56	9.8
BH 7641 (Obs)	951.24	909.49	905.35	904.83	904.46	904.10	903.55	903.60	903.16	902.68	901.56	7.93
BH 7645 (Obs)	977.25	918.24	917.49	915.77	914.48	914.04	912.61	913.10	912.13	910.75	910.32	7.92
BH 7669 (Obs)	962.32	924.73	923.42	922.79	922.31	921.75	920.72	921.31	919.79	919.27	916.78	7.95
BH 7674 (Prod)	976.84	918.24	916.73	915.83	914.48	914.05	913.13	913.41	913.74	912.75	911.08	7.16
BH 7675 (Prod)	980.11	916.49	914.46	913.07	910.07	909.42	909.41	909.82	909.55	907.33	904.56	11.93
BH 7678 (Prod)	960.00	905.11	904.98	905.02	904.20	903.74	903.48	903.10	902.57	902.66	900.10	5.01
BH 7687 (Prod)	962.62	905.49	905.35	904.83	904.46	904.10	903.55	903.60	903.40	903.20	903.10	2.39

Notes: Obs = Observation Well; Prod = Production Borehole; ΔH = Head Variation, DWA = Department of Water Affairs

(Source: Water Utilities Corporation, 2019a; Department of Water Affairs, 2019b)

5.1.5 Drawdown Curves

The calculated drawdowns per year of the production boreholes and monitoring wells of the study area are presented in Figures 5.5 to 5.8. The drawdowns were obtained based on the dynamic average water levels of the monitoring wells (BH 4768 and BH 7521) and the production boreholes (BH 7678 and BH 7687) from 2010 to 2019. The drawdowns of each borehole were determined by subtracting the dynamic average water levels of each year from those determined in 2010. The average water levels ranged from 881.21 m amsl to 924.73 m amsl (see Table 5.5, Section 5.1.4). Drawdowns for the production boreholes and the monitoring wells ranged from 0.00 m to 7.58 m and generally increased over the years.

Although the drawdowns are observed to be directly proportional to time as indicated by the figures, Observation Wells BH 4768 and BH 7521 and Production Borehole BH 7687 experienced drawdown decrease of 0.35 m, 0.19 m and 0.05 m respectively between 2015 and 2016. Production Borehole BH 7678 experienced drawdown decrease of 0.04 m between 2011 and 2012 and 0.09 m between 2017 and 2018. This borehole experienced an increase of drawdown of 2.56 m between 2018 and 2019. Borehole BH 7687 experienced a drawdown increase of 0.1 m between 2018 and 2019, while Observation Well BH 4768 experienced a drawdown increase of 0.1 m between 2018 and 2019.

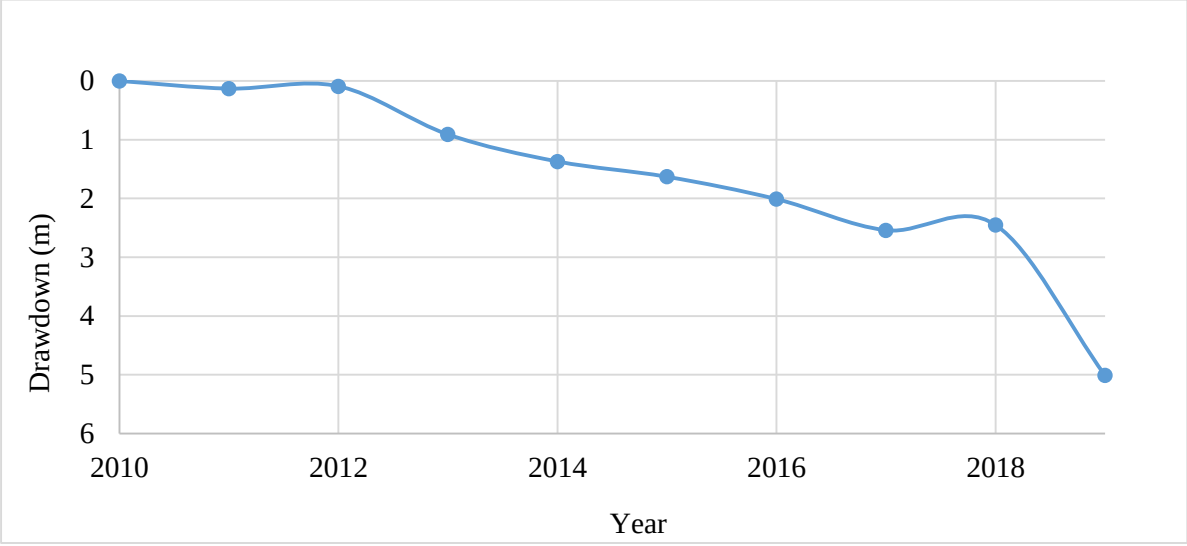

Figure 5.5 Drawdown for production borehole BH 7678

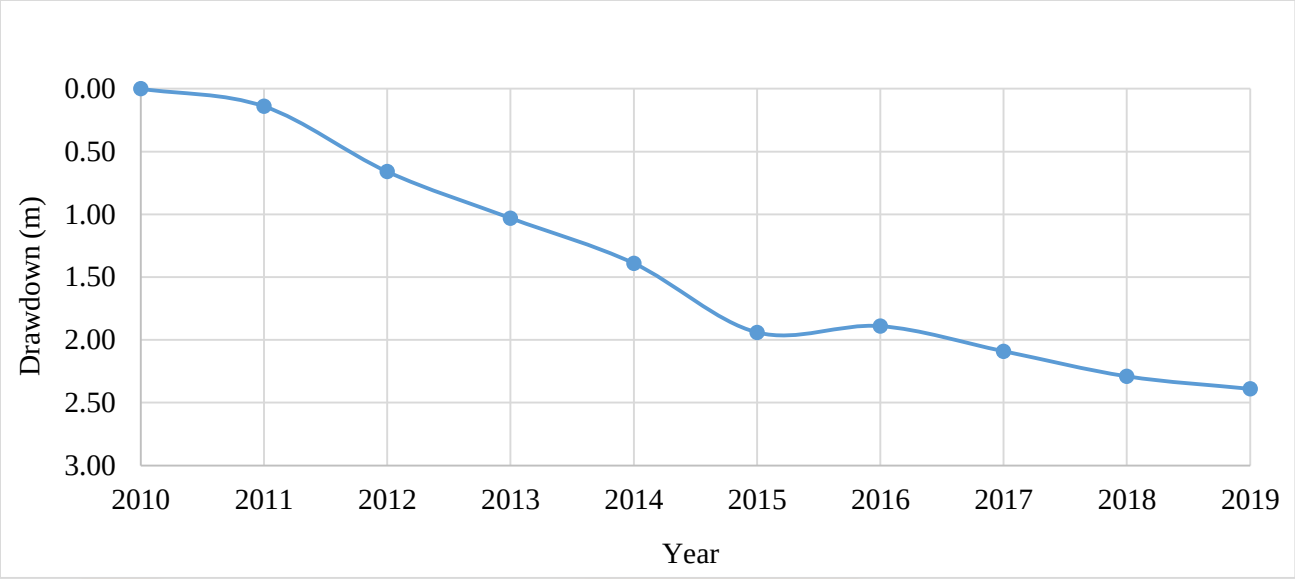

Figure 5.6 Drawdown for production borehole BH 7687

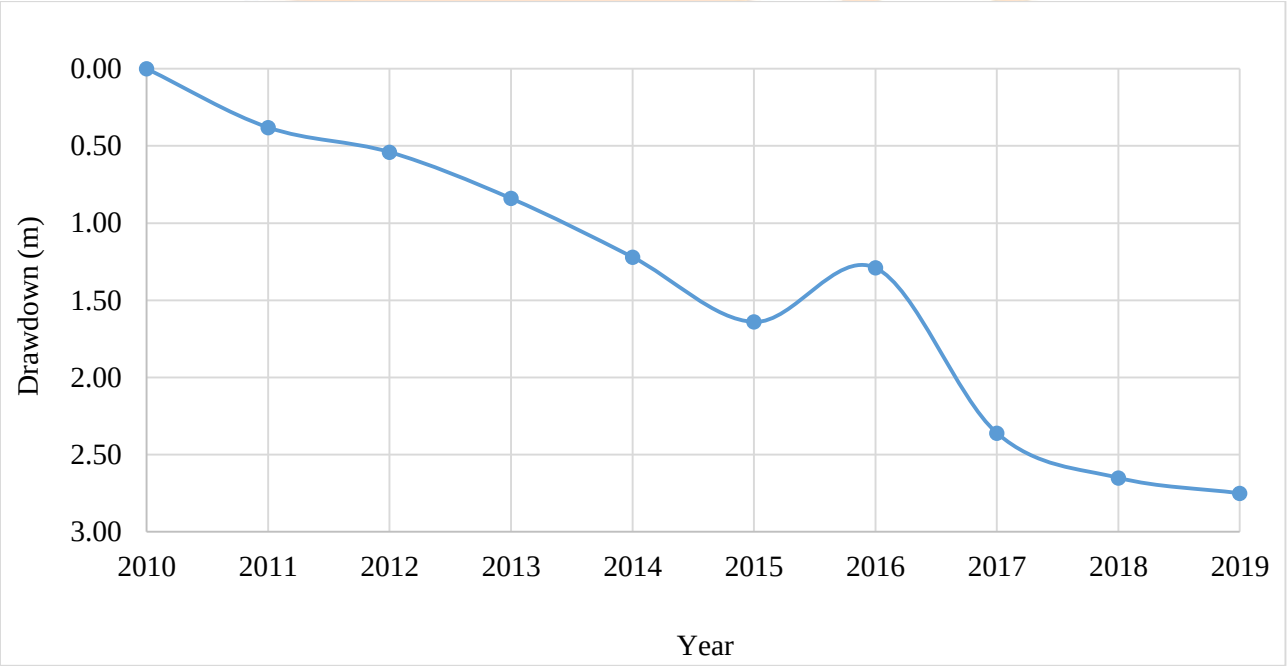

Figure 5.7 Drawdown for observation borehole BH 4768

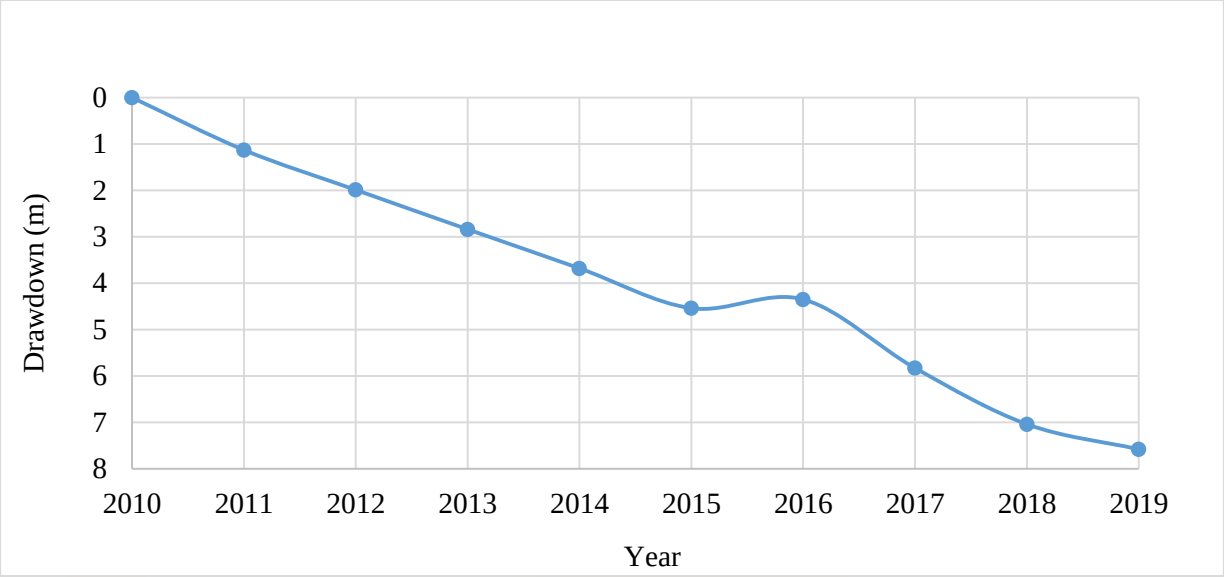

Figure 5.8 Drawdown for observation borehole BH 7521

5.1.6 Linear Trend Analysis

Plots of the annual average water level variation for the boreholes are presented in Appendix I and for illustrative purposes the plot for Observation Borehole BH 7521 is shown in Figure 5.9 together with a trend line with coefficient of determination (R^2). A summary of the results of statistical significance of the trends obtained from the monitoring wells and the production boreholes of the Dukwi Phase II Wellfield based on the recorded water levels (see Table 5.5, Section 5.1.4) are presented in Table 5.6. Figure 5.9 indicates that there was an increase in the annual average water level for Observation Borehole BH 7521 of 0.19 m between 2015 and 2016. This is likely influenced by an increase of the recharge rate of 1 734 136 m^3/year between 2015 and 2016 (see Table 5.1, Section 5.1.1) which caused more water to be added in this borehole, as this borehole is located nearer the zone of high transmissivity (Geotechnical Consulting Services, 1998a).

From Table 5.6, most of the water level slopes determined from the trend model are negative ranging from -3.05 to -0.263 (see Appendix I). A coefficient of determination (R^2) of 80% and above was obtained for most of the results from the trend model, except for monitoring well BH 7546 with coefficient of determination of 63%.

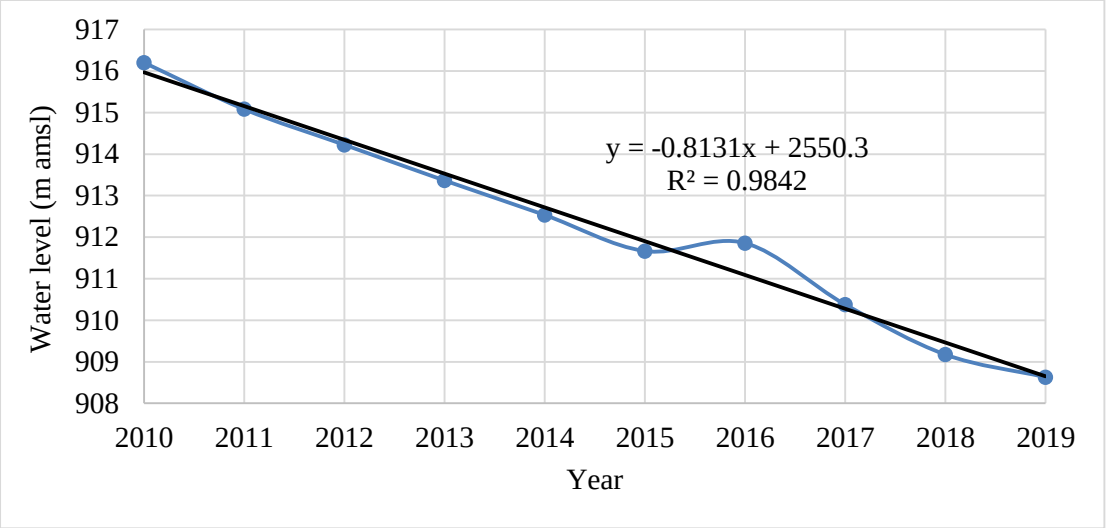

Figure 5.9 Annual average water level fluctuations and statistical significance of trend for Observation Borehole BH 7521

Table 5.6. Summary of the results from linear trend model.

Borehole ID	Location		Slope	R^2
	Longitude (degree: minutes: seconds)	**Latitude** (degree: minutes: seconds)		**(%)**
BH 7516	26° 37' 32.80" E	20° 26' 33.14'' S	-1.09	90
BH 7520	26° 24' 59.36" E	20 ° 27' 08.30" S	-0.816	98
BH 7521	26° 25' 20.05" E	20 ° 27'08.42" S	-0.813	98
BH 7546	26 ° 25' 44.16" E	20 ° 27' 08.47" S	-3.05	63
BH 7639	26°32' 40.32" E	20 °29' 05.61" S	-1.13	80
BH 7641	26° 25' 16.93" E	20° 31' 36.92" S	-0.263	92
BH 7687	26 ° 27' 08.76" E	20 °30' 37.69" S	-0.468	94
BH 7678	26 ° 28' 23.32" E	20 ° 30' 27.73" S	-0.334	95
BH 7674	26 ° 31'24.34" E	20 ° 29'09.19" S	-0.647	88
BH 7675	26 ° 32' 06.00 E	20 ° 29' 08.77" S	-1.11	94

Source for borehole location: Department of Water Affairs (2000)

5.1.7 Correlation Analysis

Correlation analysis based on Pearson Correlation Coefficients (r) (Equation (4.1)) was carried out between groundwater levels of the four production boreholes in m amsl and various hydro-geological variables that include the estimated recharge (see Table 5.1, Section 5.1.1), abstractions (Table 5.4, Section 5.1.3), rainfall (Appendix E) and temperature (Appendix F). The correlations of the drop in water levels with rainfall and temperature of the study area covered the period 2010 to 2019. However, the correlations of the drop of water levels with abstraction rates and recharge rates were from 2013 to 2019 because, records of abstraction rates in the study area started from 2013, as well as the estimated recharge rates. The groundwater levels of the production boreholes used for correlation of the hydro-geological variables are obtained from Table 5.5, Section 5.1.4. Summaries of the correlation analysis are presented in Table 5.7. The correlation coefficients range from -0.357 to 1.000. There is a positive association between abstractions and water levels drop ranging from 0.115 to 0.345. There is also a positive association between the drop of water levels and temperature ranging from 0.050 to 0.518.

The correlation between the water level drop with rainfall is negative ranging from -0.321 to -0.017. There is also a negative correlation between the water level drop and the recharge rates ranging from -0.357 to -0.017.

Table 5.7 Summary of the Pearson correlation coefficients (r) between groundwater level drop and various hydrogeological variables of the study area

Hydro-geological variable	Correlation coefficients (r)			
	Borehole Number			
	BH 7687	BH 7678	BH 7675	BH 7674
Water Level Drop (m amsl)	1.000	1.000	1.000	1.000
Abstractions (mm/year)	0.239	0.345	0.294	0.115
Recharge (mm/year)	-0.234	-0.017	-0.321	-0.357
Temperature (^{o}C)	0.162	0.201	0.050	0.518
Rainfall (mm)	-0.234	-0.017	-0.321	-0.221

5.1.8 Water Chemistry Results

The water chemistry of the study area was analyzed and compared with the Botswana Bureau of Standards (BOS 262:2011) natural water specifications. The Standards specify the chemical requirements of natural water for human consumption. Figures 5.10 to 5.13 represent some of the water chemistry results obtained for water samples from production boreholes and monitoring wells of the study area collected in July and October 2019 together with the Botswana Bureau of Standards (BOS 262:2011) natural water specifications. The water chemistry results for the aforementioned figures were obtained from Appendix A, Tables A1 and A2, which present the parameters that were determined from 10 representative water samples from the study area. The chemical and physical parameters analyzed for include bromine, chloride, fluoride, nitrate, sulphate, carbonate, aluminium, calcium, iron, magnesium, potassium, sodium, manganese, copper, nickel, Total Dissolved Solids (TDS) and Electrical Conductance (EC). Figures 5.10 and 5.12 indicate that most of the water samples, except from Borehole BH 2985 showed higher values of sodium, chloride, TDS and EC than the BOS 262:2011recommended values (also see Appendix A, Tables A1 and A2). In Figures 5.11 and 5.13 however, the concentration of copper in all the water samples exceeded the recommended standards but Boreholes BH 7521 and BH 2985 had fluoride concentrations in excess of the recommended BOS 262:2011specifications.

Water samples that were obtained in July 2019 (see Figure 5.10) indicate EC values that range from 622 µS/cm at Borehole BH 2985 to 3096 µS/cm at Borehole BH 4649. For water samples that were taken in October 2019, the EC values ranged from 544 µS/cm at Borehole BH 2985 to 3097 µS/cm at Borehole BH 4649 (see Figure 5.12). The results indicate that 80% of the water samples obtained from the July 2019 sampling process exceeded the recommended BOS 262:2011 EC value of 1500 µS/cm while 60% of the results of EC of water samples obtained in October 2019 exceeded the recommended Standards.

The chloride concentrations in the wells ranged from 40.1 mg/l at Borehole BH 2985 to 480.4 mg/l at Borehole BH 4649 in July 2019. In October 2019, the chloride concentration ranged from 50.09 mg/l at Borehole BH 2985 to 929 mg/l at Borehole BH 4649. In both months (July and October

2019), 80% of the water samples had chloride concentrations that exceeded the desirable limit of 200 mg/l based on the Botswana Bureau of Standards (2016).

Sodium concentration ranged from 31.72 mg/l at Borehole BH 2985 to 540.5 mg/l at Borehole BH 7521 for water samples obtained in July 2019, while in October 2019 the concentration of sodium ranged from 33.52 mg/l at Borehole BH 2985 to 752.2 mg/l at Borehole BH 4649. In both months (July and October 2019), 90% of the analysed water samples exceeded the recommended sodium concentration of 200 mg/l (Botswana Bureau of Standards, 2016).

The TDS concentration ranged from 95.60 mg/l at Borehole BH 2985 to 2024 mg/l at Borehole BH 4649 in July 2019. For the October 2019 samples, TDS values ranged from 195.23 mg/l at Borehole BH 2985 to 2026 mg/l at Borehole BH 4649. In July 2019, 50% of the analyzed water samples exceeded the recommended TDS amount of 1000 mg/l as specified by the Botswana Bureau of Standards (2016), while in October 2019, 40% of the water samples had higher total dissolved solids than the recommended 1000 mg/l by the Botswana Bureau of Standards (2016).

The concentration of copper ranged from 5.25 mg/l at Borehole BH 7521 to 7.87 mg/l at Borehole BH 7674 in July 2019 (see Figure 5.11), while in October 2019 it ranged from 6.32 mg/l at Borehole BH 7521 to 24.5 mg/l at Borehole BH 7516 (see Figure 5.13). In both months (July and October 2019) all the water samples (100%) analyzed exceeded the recommended Botswana Bureau of Standards (2016) maximum concentration of 2.0 mg/l.

In July 2019 (see Figure 5.11), the fluoride concentrations range from 0.350 mg/l at Borehole BH 7546 to 12.3 mg/l at Borehole BH 7521, while in October 2019 (see Figure 5.13), the range is from 0.37 mg/l at Borehole BH 4649 to 9.7 mg/l at Borehole BH 7521.

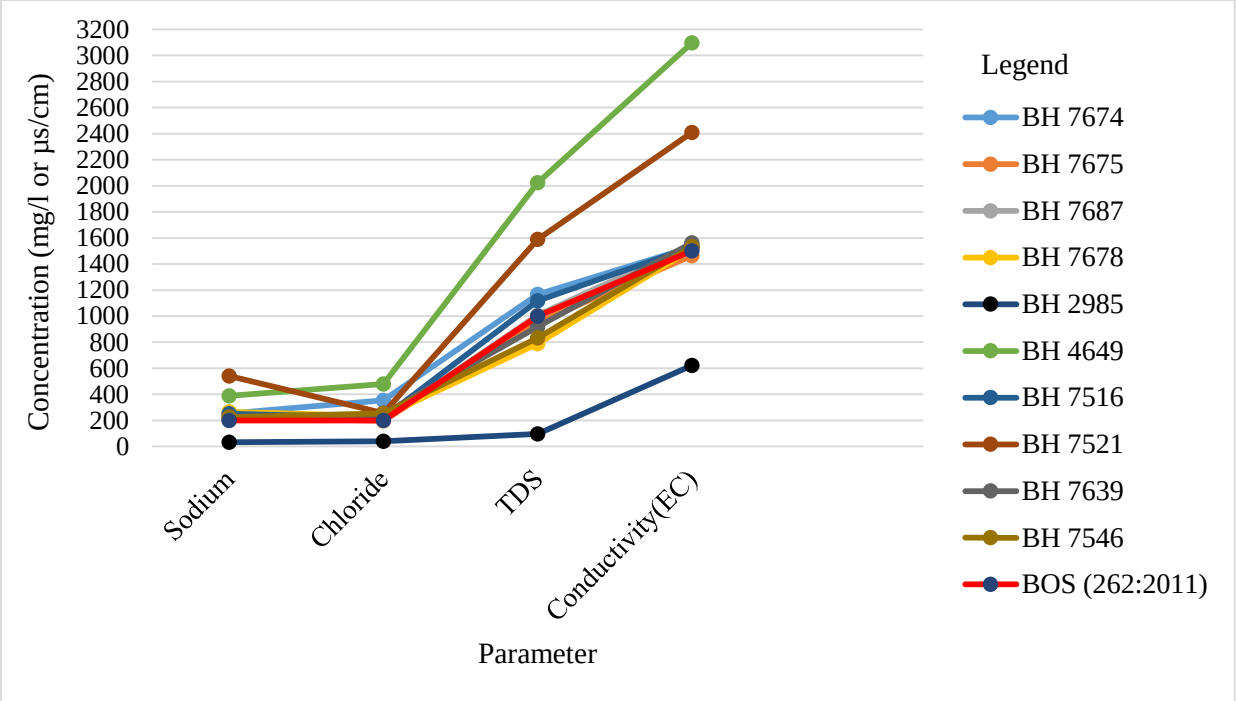

BOS- Botswana Bureau of Standards

Figure 5.10 Water Chemistry Results (July 2019)

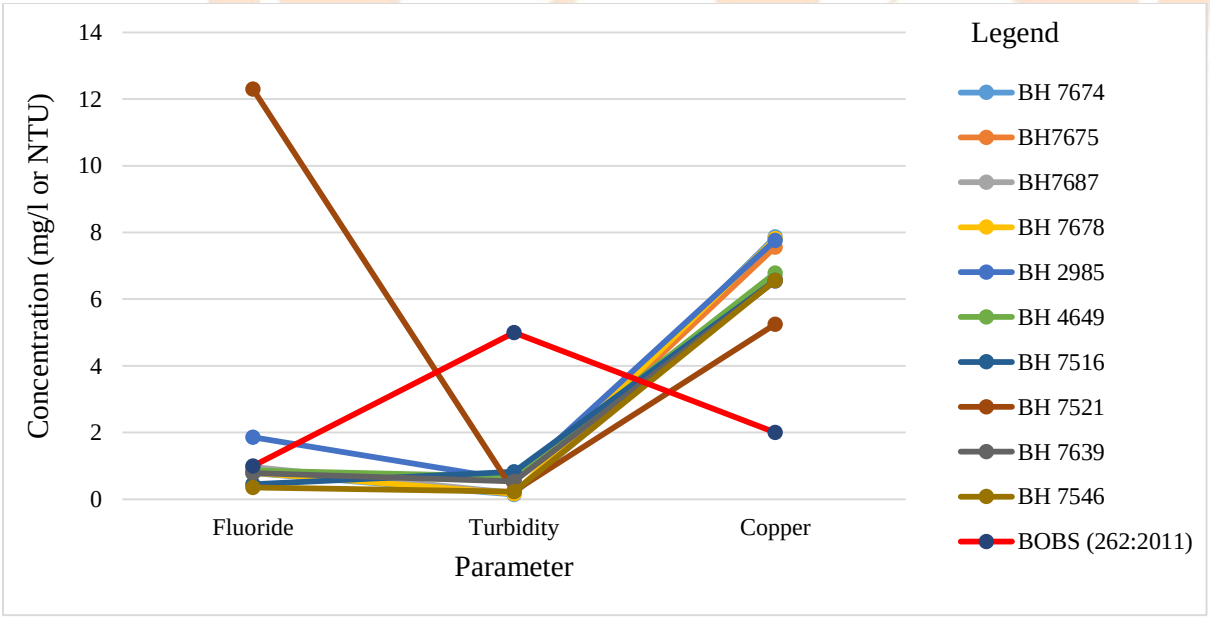

BOS - Botswana Bureau of Standards

Figure 5.11 Dukwi Wellfield Water Chemistry Results (July 2019)

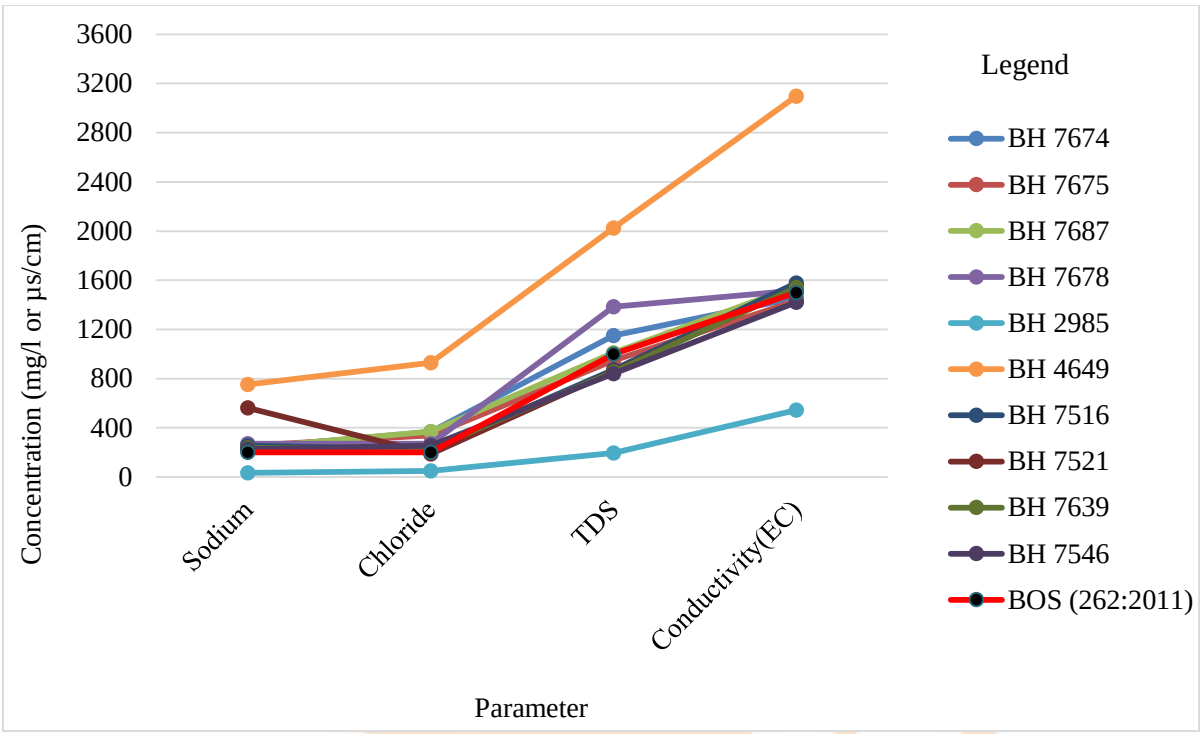

BOS - Botswana Bureau of Standards

Figure 5.12 Dukwi Wellfield Water Chemistry Results (October 2019)

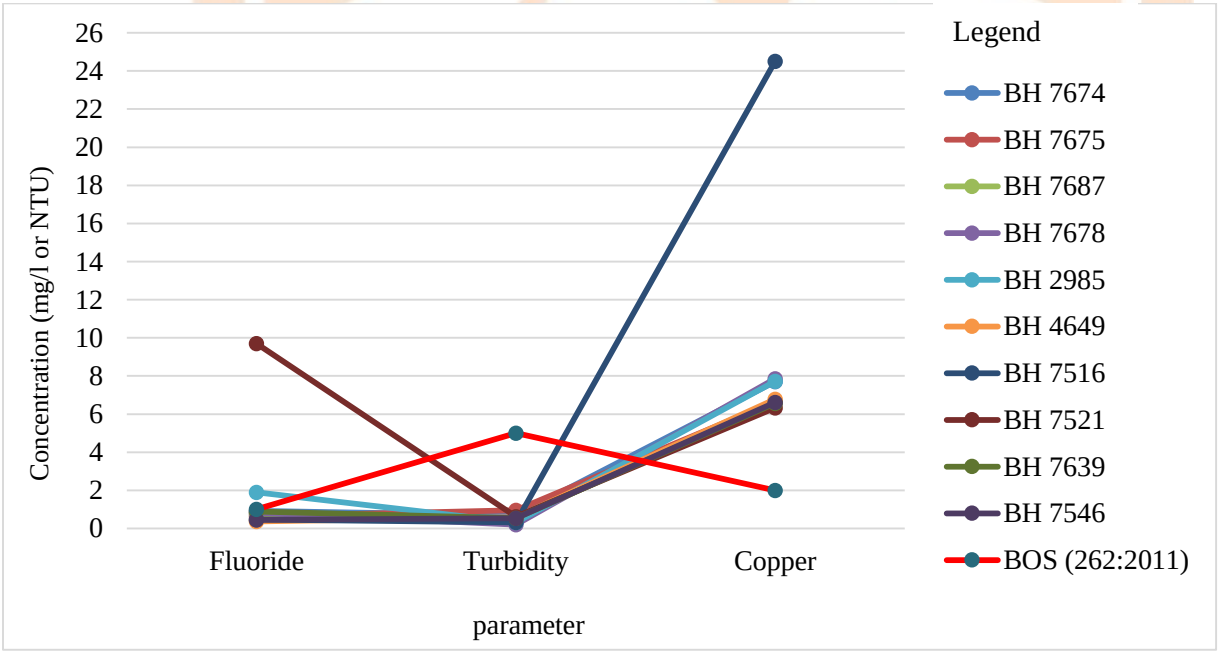

BOS - Botswana Bureau of Standards

Figure 5.13 Dukwi Wellfield Water Chemistry Results (October 2019)

5.1.9 Determination of Groundwater Types

Piper plots (Figures 5.14 and 5.15) were created for the study area using analytical data obtained from hydro-chemical analysis in July and October 2019 (Appendix A Table A1 and A2). A total of 10 water samples were used for the geochemical characterization of groundwater at the wellfield. Generally, the representative water samples from both the production boreholes and monitoring wells of the wellfield can be classified into the sodium chloride type, mixed type, sodium bicarbonate type and the magnesium bicarbonate type from the piper diagrams.

Figure 5.14 shows a piper plot of the water samples collected in July 2019. The figure indicates that in the cation ternary diagram, 9 out of 10 groundwater samples (90%) are of the sodium and potassium type. The sodium and potassium groundwater type results from the Production Boreholes BH 7674, BH 7675, BH 7678 and BH 7687 and the Monitoring Wells BH 4649, BH 7516, BH 7521, BH 7639 and BH 7546. The cation diagram also indicates that 1 out of 10 groundwater samples, (10%) fall within the no dominant type. The no dominant water type is from the Monitoring Well BH 2985.

In the anion diagram (Figure 5.14), 6 out of 10 groundwater samples (60%) are plotted in the bicarbonate field. The bicarbonate water type results from the Monitoring Wells BH 2985, BH 7521, BH 7546 and BH 7639 and the Production Boreholes BH 7675 and BH 7687. The anion diagram indicates that 2 out of 10 groundwater sample (20%) are plotted in the no dominant field. The no dominant water type is from the Monitoring Well BH 7516 and the Production Borehole BH 7678. The anion diagram also indicates that 2 out of 10 groundwater samples (20%) are plotted in the chloride field. The chloride water type is from the Monitoring Well BH 4649 and Production Borehole BH 7674.

In a combination plot of the anions and cations, (Figure 5.14) it is observed that 5 out of 10 groundwater samples (50%) are of the sodium chloride type. The sodium chloride water type results from the Monitoring Wells BH 7516, BH 7546 and BH 7639 and the Production Boreholes BH 7674 and BH 7678. The mixed type is occupied by 3 out of 10 groundwater samples (30%). This water type results from the Production Boreholes BH 7675 and BH 7687 and the Monitoring

Well BH 4649. The sodium bicarbonate and magnesium bicarbonate water types each are occupied by 1 out of 10 groundwater samples (10%). The sodium bicarbonate water type results from the Monitoring Well BH 7521 while the magnesium bicarbonate water type is from the Monitoring Well BH 2985.

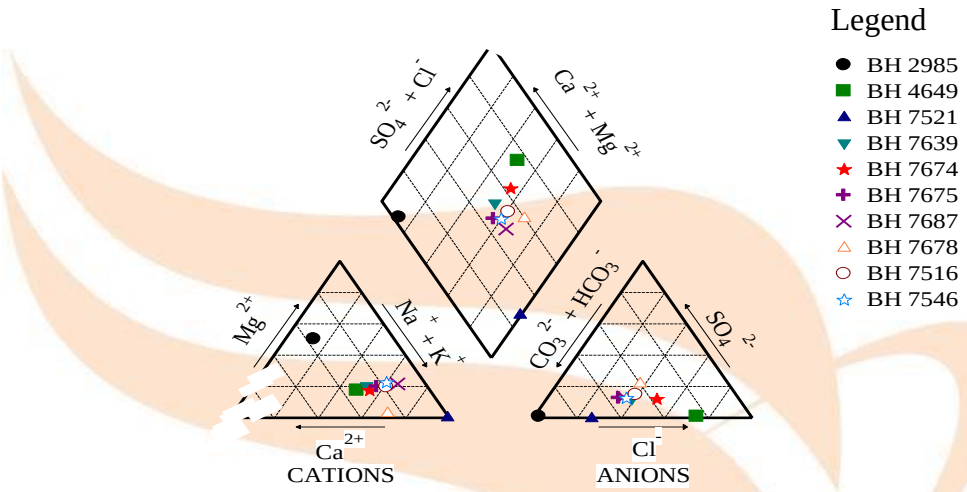

Figure 5.14 Piper plots for the study area (July 2019)

Figure 5.15 shows the piper plot diagram of the water samples collected in October 2019. The cations ternary diagram indicates that 7 out of 10 groundwater samples (70%) are classified as the sodium and potassium type. The sodium and potassium water type results from the Monitoring Wells BH 7516, BH 7521 and BH 7546 and the Production Boreholes BH 7674, BH 7675, BH 7678 and BH 7687. The cations ternary diagram also indicates that 3 out of 10 groundwater samples (30%) belong to the no dominant type. The no dominant water type is from the Monitoring Wells BH 2985, BH 4649 and BH 7639.

The anions diagram (Figure 5.15) indicates that 4 out of 10 groundwater samples (40%) belong to the bicarbonate type. The bicarbonate water type results from the Monitoring Wells BH 2985, BH 7521, BH 7639 and BH 7546. The chloride field is occupied by 1 out of 10 groundwater samples (10%). The chloride water type results from the Monitoring Well BH 4649. The no dominant field is occupied by 5 out of 10 groundwater samples (50%). The no dominant water type is from the

Production Boreholes BH 7678, BH 7674, 7675 and BH 7687 and the Monitoring Well and BH 7516.

The combination of the two ternary diagrams shows that 5 out of 10 groundwater samples (50%) belong to the sodium chloride. The sodium chloride type results from the Monitoring Well BH 7516 and the Production Boreholes BH 7674, BH 7675, BH 7678 and 7687. The combination plot indicates that 2 out of 10 groundwater samples (20%) belong to the mixed type. The mixed water type results from the Monitoring Well BH 4649 and BH 7546. The sodium bicarbonate field is occupied by 1 out of 10 water samples (10%). The sodium bicarbonate water type results from the Monitoring Well BH 7521. The plot also shows that the magnesium bicarbonate field is occupied by 2 out of 10 groundwater samples (20%). This water type is from the Monitoring Wells BH 2985 and BH 7639.

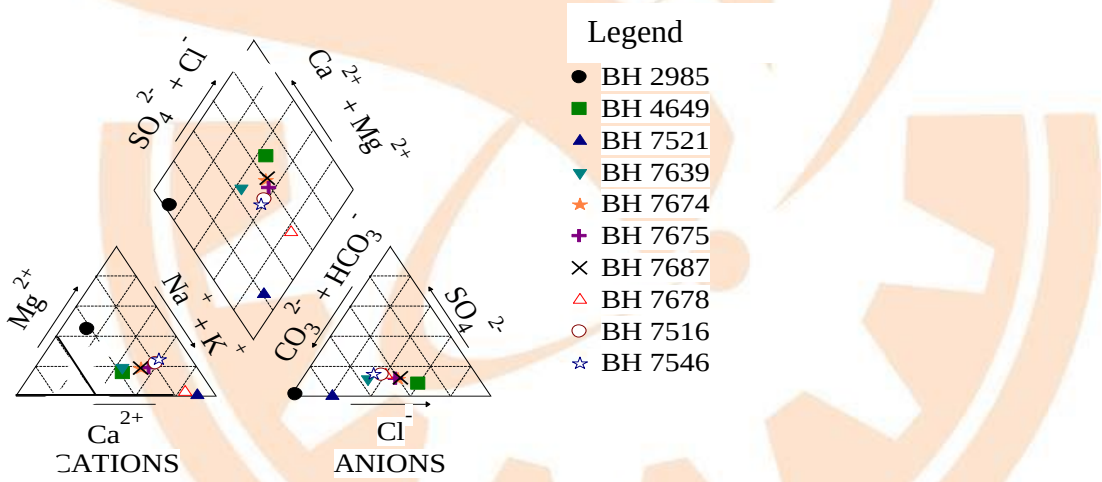

Figure 5.15 Piper plot of the study area (October 2019)

5.1.10 Simulated Land Subsidence

Figure 5.16 shows the plan view of the simulated vertical displacement of the ground surface in the study area due to pumping from 2013-2019 from MODFLOW SUB and ModelMuse analysis. The contours in the figure which are at 0.001 m intervals represent the vertical displacement of the earth surface due to pumping, while the various colors (blue to red) show the hydraulic heads influenced by pumping. Land subsidence was simulated using the mean abstraction rates of the Pumping Boreholes BH 7674, BH 7675, BH 7678 and BH 7687 that ranged from 261 368 m^3/year to 355 392 m^3/year (see Table 5.4, Section 5.1.3).

The results as obtained from MODFLOW SUB and ModelMuse show that the displacement of the surface increased towards the pumping boreholes. The displacement contours around the production boreholes ranged from 0.008 m to 0.022 m. The highest land subsidence of 0.022 m occurred around Borehole BH 7675, while the least subsidence of 0.008 m occurred around Borehole BH 7687. The hydraulic heads experienced around the boreholes from the color coding in Figure 5.16 ranged from 966.819 meters above mean sea level (m amsl) to 978.5401 m amsl following the pumping of groundwater out of the aquifer system. The least hydraulic head of 966.819 m amsl occurred at Borehole BH 7675 while the highest hydraulic head of 978.5401 m amsl occurred around Borehole BH 7687. The hydraulic heads declined below the reference datum of 1000 m amsl which was used in the modeling exercise as stated in Section 4.1.3.10.

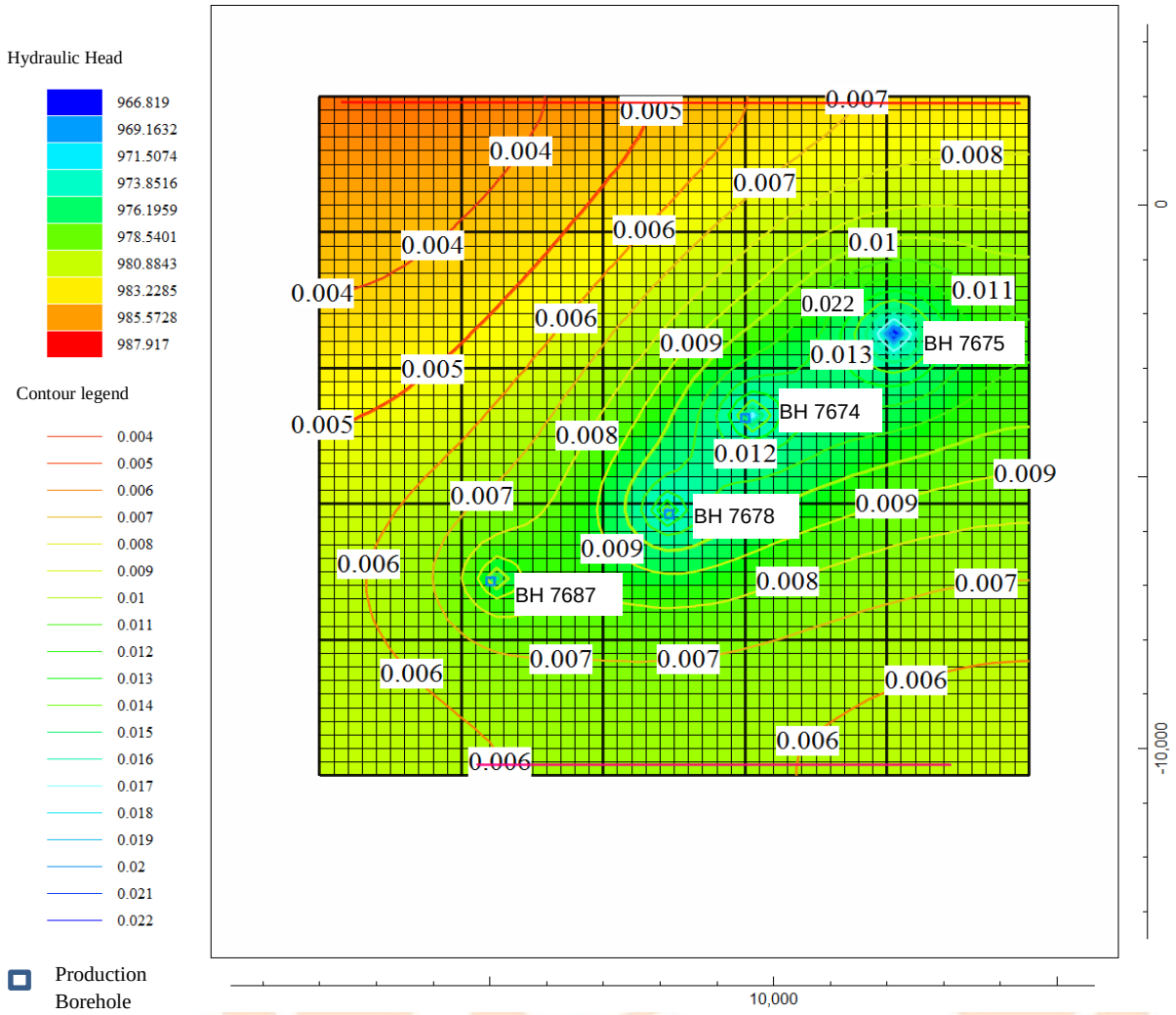

Figure 5.16 Simulated Land subsidence (in meters) of the study area (2013-2019)

Figure 5.17 shows the plan view of the simulated projected vertical displacement of the ground surface at the study area due to future groundwater exploitation from 2019 to 2031. The figure (with contour intervals of 0.001 m), indicates that the magnitude of land subsidence around the production boreholes will range from 0.015 m to 0.031 m. The displacement of the ground surface will increase towards the pumping boreholes hence areas around these boreholes will be more affected by land subsidence. The highest displacement of 0.031 m will occur around Borehole BH 7675 and the least displacement of 0.015 m will occur around Borehole BH 7687. There will be more reduction of the hydraulic heads around the pumping boreholes ranging from 789.695 m

amsl to 791.7693 m amsl with the highest hydraulic head of 791.7693 m amsl occurring around Borehole BH 7687 and the least hydraulic head of 789.695 m amsl occurring at Borehole BH 7675.

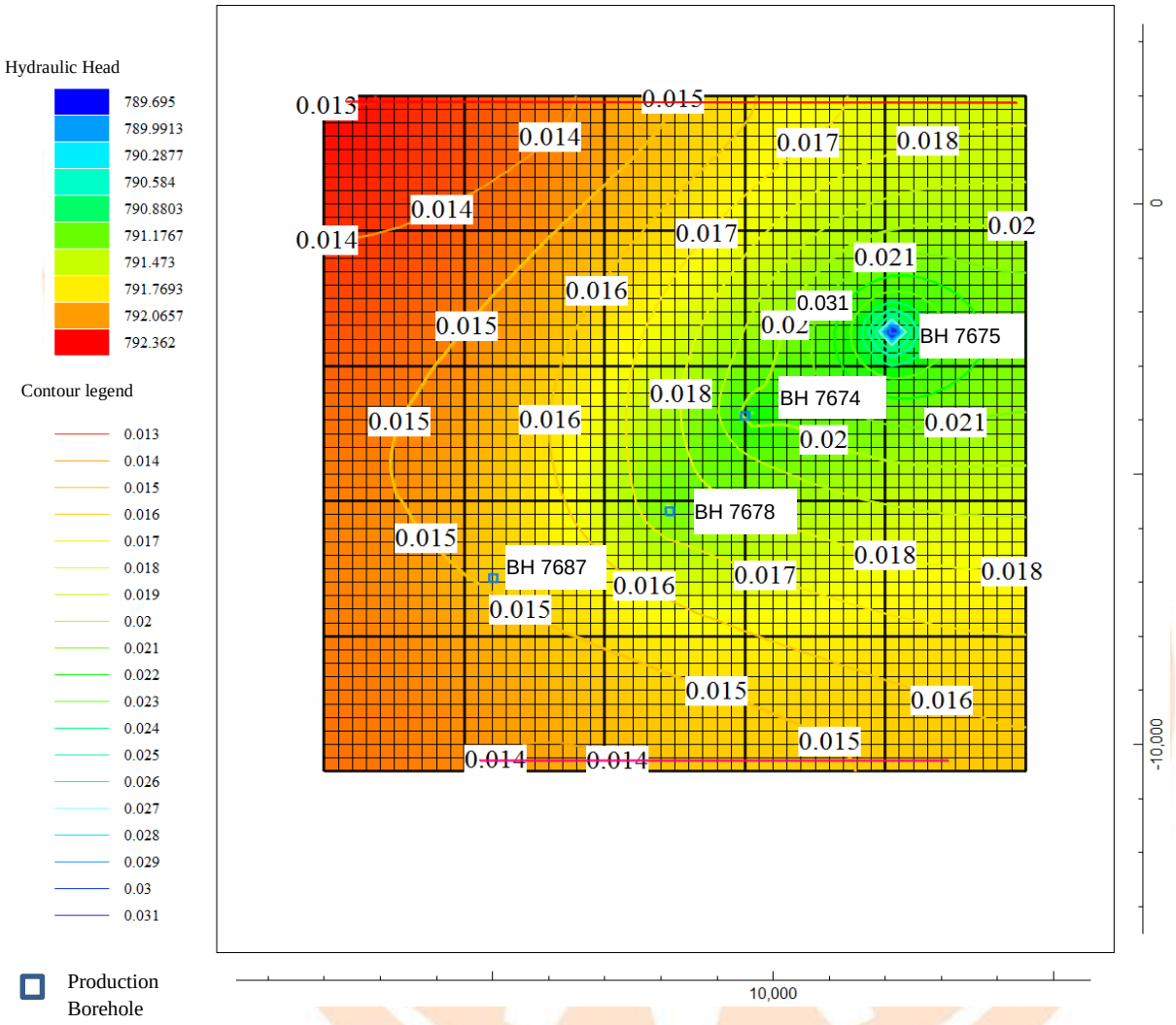

Figure 5.17 Projected simulated land subsidence (in meters) of the study area (2019-2031)

5.1.11 Estimated Land Subsidence

Table 5.8 presents the specific storage, hydraulic head variations, the boreholes thicknesses and amount of land subsidence due to pumping in the production boreholes (BH 7674, 7675, BH 7678 and BH 7687) determined from Equation (4.10). The specific storage of the production boreholes ranges from 0.0000154 to 0.0000436, with Borehole BH 7687 having the highest specific storage, while Borehole BH 7675 has the least specific storage. Borehole BH 7675 has the highest hydraulic head variation of 5.51 m amsl, while Borehole BH 7687 has the least hydraulic head variation of 1.36 m amsl. The aquifer thickness ranges from 125 m to 198 m, with the highest thickness of 198 m occurring at Borehole BH 7675, and the least borehole thickness of 125 m occurring at Borehole BH 7678. As indicated in Table 5.8, the estimated land subsidence around the production boreholes from 2013 to 2019 ranges from 0.008598 m to 0.0168 m. This range falls within the range of results of land subsidence (0.008 m to 0.022 m) obtained from MODFLOW and ModelMuse.

Table 5.8 Land subsidence due to pumping from the production boreholes (2013-2019)

Borehole Number	Specific Storage	Hydraulic head change (m amsl)	Thickness (m)	Land subsidence (m)
BH 7674	0.0000221	3.40	197	0.0148
BH 7675	0.0000154	5.51	198	0.0168
BH 7678	0.0000219	4.10	125	0.0112
BH 7687	0.0000436	1.36	145	0.008598

5.2 Discussions

5.2.1 Estimated Recharge

The mean annual recharge of the study area from 2013 to 2019 is 1 149 691 m^3/year (see Table 5.1, Section 5.1.1). The recharge is dependent on factors such as the aquifer's hydraulic conductivity, annual rainfall and minimum and maximum average temperatures. The recharge is episodic as it is directly related to the mean annual rainfall of 206.2 mm.

The aquifer hydraulic conductivity ranged from 0.000109 m/min to 0.0413 m/min (see Table 5.3, Section 5.1.2) suggesting that the aquifer is heterogeneous. Consequently, this might have resulted in less recharge of the aquifer by interference with the distribution and movement of groundwater within the subsurface.

The maximum average temperature recorded at the study area is 30.84 ^oC while the minimum average temperature is 15.14 ^oC (see Appendix F) thus, indicating a difference of 15.70 ^oC between the minimum and maximum average temperatures. This significant rise in temperature could result in higher evapotranspiration rates of groundwater at adjacent recharge areas such as along the Mosetse River, (located at about 3 km from the wellfield area) resulting in less recharge of the aquifer. Condon *et al.* (2020) established that temperature increase of around 1.5 ^oC can reduce the potential recharge of groundwater by 12-15% in arid regions and reduce the surface storage by more than 100 000 million cubic meters. Therefore, 15 ^oC increase in temperature which is a ten-fold increase could result in similar proportions of reduction in potential groundwater recharge and surface storage in the study area.

5.2.2 The Hydraulic Properties

Borehole BH 7675 has the highest transmissivity estimate of 8.171 m^2/min while Borehole BH 7687 has the least transmissivity estimate of 0.01587 m^2/min. The highest transmissivity of 8.171 m^2/min at Borehole BH 7675 likely led to more extraction of groundwater resources with mean abstraction rate of 355 392 m^3/year. This is because the aquifer was able to transmit more water

throughout its saturated thickness at Borehole BH 7675 as compared to Borehole BH 7687, thus leading to more depletion of groundwater resources.

The hydraulic conductivities determined from the production boreholes (BH 7674, BH 7675, BH 7678 and BH 7687) range from 0.000109 m/min to 0.0413 m/min, with Borehole BH 7675 having the highest hydraulic conductivity, while Borehole BH 7687 has the least hydraulic conductivity. Therefore, the rate of groundwater flow through the aquifer at Borehole BH 7675 is higher as compared to flow at Borehole BH 7687, resulting in the extraction of more water at Borehole BH 7675, causing an overall increase in decline of groundwater at the study area.

Borehole BH 7675 has the highest estimated storativity of 0.0003299, while Borehole BH 7678 has the least estimated storativity of 0.0002126. Therefore, the aquifer has the ability to release more volume of water from storage at Borehole BH 7675 as compared to Borehole BH 7678, thus leading to increased depletion of groundwater resources.

Borehole BH 7675 has the highest transmissivity estimate of 8.171 m^2/min and radius of influence of 2 583.6 m, while Borehole BH 7687 has the least transmissivity estimate of 0.01587 m^2/min and radius of influence of 135.16 m. This is because the radii of influence are directly related to the aquifer transmissivities. The highest transmissivity of 8.171 m^2/min at Borehole BH 7675 resulted in a higher mean abstraction rate of 355 392 m^3/year which is likely to have caused the cone of depression around Borehole BH 7675 to expand further and hence resulting in an increase in the radius of influence around the well, as compared to Borehole BH 7687.

The average radius of influence of the production boreholes of 1 001.0 m can result in more adverse effects on the environment at the study area such as increased land subsidence with time. This is similar with the results obtained by Yihdego (2018) that a higher radius of influence than the recommended average radius of influence of 963 m can result in water related problems such as land subsidence, which can result to high economic losses such as damage to infrastructure.

5.2.3 Abstraction Rates

The mean annual total abstraction rate of the production boreholes from 2013 to 2019 is 1 253 546 m^3/year as indicated in Table 5.4, Section 5.1.3. This exceeds the mean annual recharge rate of 1 149 691 m^3/year. A higher mean annual abstraction rate than the mean annual recharge rate leads to the depletion of groundwater resources at the study area.

Abstraction rates were influenced by different factors such as the high aquifer transmissivity of 8.171 m^2/min. High transmissivity rates lead to more extraction of groundwater resources as indicated by Maurice *et al.*, (2019) at five sites (Seeta, Mubende, Rukungiri, Makutapora and Singida) in Uganda, where the transmissivity rates ranged from 0.0069 m^2/min to 0.069 m^2/min. High abstraction rates that are influenced by higher transmissivity rates can lead to further depletion of the groundwater resources

5.2.4 Recorded Water Levels

In 2019, the Production Borehole BH 7675 had a higher hydraulic head variation of 11.93 m amsl while Borehole BH 7687 had the least hydraulic head variation of 2.39 m amsl in comparison to other production boreholes, as presented in Table 5.5, Section 5.1.4. A higher head variation in Borehole BH 7675 is a consequence of a high mean abstraction rate of 355 392 m^3/year while the least head variation in Borehole BH 7687 is due to less mean abstraction rate of 261 368 m^3/year (see Table 5.4, Section 5.1.3).

The decline of the water levels at the study area may have been influenced by higher manganese concentrations of 109 µg/l and 109.4 µg/l recorded in July 2019 and October 2019 respectively, as presented in the water chemistry results tables (Appendix A, Tables A1 and A2). These concentrations are higher than the recommended manganese concentration of 100.0 µg/l based on the Botswana Bureau of Standards (2016). The presence of manganese in groundwater likely occurred due to the dissolution of manganese-bearing minerals such as psilomelane and pyrolusite which are commonly found in sedimentary rocks such as black shales. In October 2019, the manganese concentration of 109.4 µg/l is relatively high as compared to the manganese concentration of 109 µg/l recorded in July 2019. This is likely due to an increase of the average

monthly rainfall amount of 4.2 mm from July to October 2019 (see Appendix E), which caused more water to be added in the aquifer system, and hence increased the dissolution of manganese-bearing minerals.

The presence of manganese in the aquifer of the study area (Mea Arkose Aquifer) may have restricted groundwater flow by clogging the aquifer system as reported by Shand *et al.* (2007); Berlin and Kumar (2014) and Warren *et al.* (2015) who have indicated that the presence of chemical parameters such as iron and manganese in groundwater can form chemical precipitation that can reduce the aquifer's hydraulic conductivity and thus reduce the recharge rate at groundwater temperatures above or below 25 ^{o}C and pH values below 8. This can result in lower levels of groundwater.

5.2.5 Drawdown Curves

The drawdowns of the production boreholes and the monitoring wells from 2010 to 2019 range from 0.00 m to 7.58 m and increase with time. The drawdown curves indicate some decrease in drawdowns for the Production Borehole BH 7687 and the Monitoring Wells BH 4768 and BH 7521 of 0.05 m, 0.35 m and 0.19 m respectively between 2015 and 2016. Lesser drawdowns experienced at the study area during this period may be due to an increase in recharge rate of 1 734 136 m^3/year between 2015 and 2016 (see Table 5.1, Section 5.1.1).

The Production Borehole BH 7678 experienced a drawdown decrease of 0.090 m between 2017 and 2018 which may have resulted from a 0.075% decrease in abstraction rate for this borehole within the period (see Table 5.4, Section 5.1.3). This borehole also experienced a higher drawdown increase of 2.56 m, between 2018 and 2019, which was likely due to a 7.61% increase in abstraction rates.

Borehole BH 7687 experienced a drawdown decrease of 0.05 m between 2015 and 2016. This is likely due to a 1.88% decrease in abstraction rates from 2015 to 2016. This borehole also experienced a drawdown increase of 0.1 m between 2018 and 2019. This may have been influenced by a 6.3% increase in abstraction rates between 2018 and 2019 (see Table 5.4, Section 5.1.3).

There was an increase of drawdown of 0.1 m between 2018 and 2019 for Observation Well BH 4768. This may be influenced by a 0.60% increase in recharge rates between 2018 and 2019 (see Table 5.1, Section 5.1.1).

5.2.6 Linear Trend Analysis

Most of the slopes from the trend model ranging from -3.05 to -0.263 are negative, hence indicating that they are statistically significant. The negative slopes show that there is a decrease in the water levels of the monitoring and production boreholes with time in years. A very high coefficient of determination of more than 80% was found in most of the results from the trend model. This together with the negative slopes obtained from the linear trend model make it an appropriate model to represent the fluctuations of the levels of groundwater in the wellfield area.

5.2.7 Correlation Analysis

There is a positive correlation that ranges from 0.115 to 0.345 between abstraction rates and the drop of water levels in the production boreholes from 2013 to 2019. The positive association indicates that increase in abstraction rates at the wellfield area result in further drop of water levels. The increase in abstraction rates may have been influenced by the location of the boreholes along the zone of higher transmissivity rates that ranged from from 0.01587 m^2/min to 8.171 m^2/min as presented in Table 5.3, Section 5.1.2. A zone of higher transmissivity rates likely indicates a highly fractured zone due to major faults found at the wellfield area such as the Chidumela Fault and the Red Beds Faults (see Figure 2.7, Section 2.7.3).

A positive association that ranges from 0.050 to 0.518 occurs between the drop of water levels and recorded temperatures. Thus, the high temperatures experienced at the wellfield area, with a mean annual maximum temperature of 30.84 ^{o}C (see Appendix F) has influence on the drop of water levels at the study area.

5.2.8 Water Chemistry Results

Figures 5.10 to 5.13 represent some of the water chemistry results from water samples collected from the study area in July and October 2019 together with the BOS 262:2011 natural water specifications. The results were used as provided by the different laboratories where the samples were tested, devoid of any uncertainties, taking cognisance of the fact that all the laboratories were guided by and adhered to the BOS 262 2011 specifications for water quality analysis as stated in Section 4.1.22 though there could be some human factors affecting the results generated.

The chloride concentration at the wellfield area ranged from 40.1 mg/l at Borehole BH 2985 to 480.4 mg/l at Borehole BH 4649 in July 2019 and from 50.09 mg/l at Borehole BH 2985 to 929mg/l at Borehole BH 4649 in October 2019. High chloride concentration in Borehole BH 4649 could probably be attributed to the dissolution of biotite and hornblende minerals in basalt rocks. The hydroxyl ions in these minerals are likely to be substituted by the chloride ions from the rainwater that recharges the Mea Arkose Aquifer. This ionic substitution is likely influenced by the ionic radii difference of approximately 0.128 nanometres that exist between the chloride and the hydroxyl ions. The chloride ions in rainwater are likely due to the movement of chloride ions from the soil which usually consists of sodium chloride by the air masses which usually carry these ions from the soil to the atmosphere.

In October 2019 the chloride concentration of 929 mg/l is high in Borehole BH 4649 as compared to the chloride concentration of 480.4 mg/l obtained in July 2019. This is probably influenced by an increase of the average monthly rainfall amount of 4.2 mm from July 2019 to October 2019 (see Appendix E) and high groundwater temperature of 26.3 ^{o}C experienced in this borehole in October 2019 (see Appendix A, Table A2), which must have led to an increase in the dissolution of biotite and hornblende minerals in basalt rocks.

In both months (July and October 2019), 80% of the water samples had chloride concentrations that were higher than the desirable limit of 200 mg/l based on the Botswana Bureau of Standards (2016). This is probably influenced by the dissolution of apatite, biotite and hornblende minerals in basalts and dolerites that are some of the lithological units in the area.

The sodium concentrations ranged from 31.72 mg/l at Borehole BH 2985 to 540.5 mg/l at Borehole BH 7521 in the water samples collected in July 2019, while in October 2019, the range was from 33.52 mg/l at Borehole BH 2985 to 752.2 mg/l at Borehole BH 4649. In July 2019, the high sodium concentration of 540.5 mg/l in Borehole BH 7521 is probably due to the dissolution of montmorillonite in black shales which are the main sedimentary rocks in this borehole (occupying borehole depth of about 103 m, Appendix B). The sodium concentration of 752.2 mg/l obtained in Borehole BH 4649 in October 2019 is likely due to the dissolution of montmorillonite found in clay and shale and plagioclase (labradorite) in basalt. In October 2019, this concentration is high in Borehole BH 4649 probably due to high groundwater temperature of 26.3 ^{o}C experienced in the borehole (see Appendix A, Table A2) which influenced more dissolution of sodium-bearing minerals.

The TDS concentrations range from 95.60 mg/l at Borehole BH 2985 to 2024 mg/l at Borehole BH 4649 in July 2019, while in October 2019 it ranges from 195.23 mg/l at Borehole BH 2985 to 2026 mg/l at Borehole BH 4649. The TDS concentrations at the study area may be influenced by the dissolution of the calcite mineral found in the calcite cement which commonly join together the grains of rocks such as sandstones. The TDS concentrations that range from 195.23 mg/l to 2026 mg/l in October 2019 are high as compared to the concentrations that range from 95.60 mg/l to 2024 mg/l which are obtained in July 2019. This is probably due to high groundwater temperatures that range between 23.2 ^{o}C and 27.3 ^{o}C and an increase of the average monthly rainfall amount of 4.2 mm from July 2019 to October 2019 which led to more dissolutions of the calcite mineral.

High TDS concentrations at Borehole BH 4649 are probably influenced by more sodium concentrations that range from 388.1 mg/l to 752.2 mg/l and chloride concentrations that range from 480.4 mg/l to 929 mg/l in July and October 2019 as presented in the water chemistry results (Appendix A, Table A1 and A2). Less TDS concentrations at Borehole BH 2985 are probably due to low sodium concentrations that range from 31.72 mg/l to 33.52 mg/l and chloride concentrations that range from 40.1 mg/l to 50.09 mg/l.

The EC of the study area ranges from 622.0 µS/cm at Borehole BH 2985 to 3096 µS/cm at Borehole BH 4649 in July 2019 while in October 2019 it ranges from 544.0 µS/cm at Borehole BH 2985 to 3097 µS/cm at Borehole BH 4649. High EC concentrations obtained for Borehole BH 4649 in July and October 2019 are influenced by increase in TDS concentrations that ranges from 2024 mg/l to 2026 mg/l in this borehole, while less EC concentrations determined at Borehole BH 2985 are influenced by less TDS concentrations that range from 95.60 mg/l to 195.23 mg/l.

In July 2019, 8 out of 10 (80%) of the results of EC of the water samples exceeded the recommended Botswana Bureau of Standards, (2016) value of EC of 1500 µS/cm while in October 2019, 6 out of 10 (60%) of the results of EC of the water samples exceeded the recommended EC value. This indicates that most of the groundwater at the study area is not suitable for human consumption. High EC concentrations at the study area are probably influenced by high concentration of parameters, such as sodium and chloride. The sodium concentrations are as high as 540.5 mg/l in July 2019 and 752.2 mg/l in October 2019 (see Appendix A, Tables A1 and A2) while the chloride concentrations are as high as 480.4 mg/l in July 2019 and 929 mg/l in October 2019.

Less EC concentration in October 2019 is caused by a 1.46% and 6.84% decrease in TDS concentrations for Boreholes BH 7674 and BH 7639 respectively that occurred from July 2019 to October 2019 as shown in the water chemistry results (Appendix A, Tables A1 and A2).

The copper concentrations range from 5.25 mg/l in Borehole BH 7521 to 7.87 mg/l in Borehole BH 7674 in July 2019 while in October 2019 the range is from 6.32 mg/l in Borehole BH 7521 to 24.5 mg/l in Borehole BH 7516. It is most likely that high copper concentration in the Production Borehole BH 7674 is due to the weathering of mainly dark brownish grey to black mudstones, dark grey siltstone, pale grey arkose and dark grey-black shales with organic matter. These rocks are mainly found in this borehole (occupying borehole depth of about 110 m).

The copper concentrations that range from 6.32 mg/l to 24.5 mg/l are higher in October 2019 as compared to the concentrations that range from 5.25 mg/l to 7.87 mg/l in July 2019. This is

probably due to an increase of the average monthly rainfall amount of 4.2 mm and groundwater temperatures as high as 27.3 ^{o}C experienced in October 2019 which enhanced the weathering of copper-bearing rocks such as black shales.

The copper concentration in boreholes of the study area may also be influenced by the presence of hydrogen ions in groundwater due to the pH of groundwater with range in values between 7.12 and 8.69 in July 2019 and between 7.14 and 8.51 in October 2019 (Appendix A, Table A1 and A2). This may have resulted in causing more cooper metal to be in a soluble phase, as the hydrogen ions attracted many negatively charged surfaces in sediments such as clays.

The fluoride concentrations range from 0.350 mg/l at Borehole BH 7546 to 12.3 mg/l at Borehole BH 7521 in July 2019 (see Figure 5.11), while in October 2019 (see Figure 5.13), the range is from 0.37 mg/l at Borehole BH 4649 to 9.7 mg/l at Borehole BH 7521. High fluoride concentrations experienced in Borehole BH 7521 that range from 9.7 mg/l to 12.3 mg/l are likely due to the dissolution of fluoride-bearing minerals, such as biotite and hornblende. The fluoride exists in these minerals as an isomorphous replacement in the hydroxyl ions, as the ionic radius of fluoride (133 pm) is similar to that of the hydroxyl ions (140 pm).

A lower mean annual groundwater recharge of 1 149 691 m^3/year than the mean annual total abstraction rate of 1 253 546 m^3/year may have resulted in less fresh water entering the aquifer system, which caused the groundwater components such as TDS, copper, sodium and chloride to be enriched. Low groundwater recharge than abstraction rates lead to a high concentrations of ions in groundwater, following dissolution from the mineral surfaces within the aquifer, hence increasing groundwater salinity.

5.2.9 Groundwater Types

The cation ternary diagrams for July 2019 indicates that that the sodium and potassium field is occupied by 9 out of 10 groundwater samples (90%) from the Production Boreholes BH 7674, BH 7675, BH 7678 and BH 7687 and the Monitoring Wells BH 4649, BH 7516, BH 7521, BH 7639 and BH 7546, while in October 2019 is occupied by 7 out of 10 groundwater samples (70%) from

the Monitoring Wells BH 7516, BH 7521 and BH 7546 and the Production Boreholes BH 7674, BH 7675, BH 7678 and BH 7687. The sodium and potassium water type at the study area may be a result of the dissolution of potassium-bearing minerals (e.g. illite and muscovite) and sodium-bearing minerals such as montmorillonite in clay and sedimentary rocks like shales that occur in the area.

In July 2019, the sodium and potassium field is occupied by 9 out of 10 groundwater samples (90%) while in October 2019 it is occupied by 7 out of 10 groundwater samples (70%). The 20% difference in the number of groundwater samples collected for the sodium and potassium water type between July 2019 and October 2019 is influenced by changes of the water types for Boreholes BH 4649 and BH 7639 from the sodium and potassium water type in July 2019 to the no dominant water type in October 2019 (see Figures 5.14 and 5.15, Section 5.1.9).

The no dominant groundwater type for Borehole BH 7639 obtained in October 2019 is probably caused by the mixing of chemically different water types, such as the sodium and potassium water type from the dissolution of sodium-bearing minerals e.g., montmorillonite and potassium-bearing minerals e.g., illite and muscovite in rocks like shale and the calcium water type from the dissolution of calcite in calcrete. In Borehole BH 4649 the no dominant water type is likely due to the combination of the magnesium water type from the dissolution of magnesium-bearing minerals (e.g., olivine) in basalt and the sodium and potassium water type from the dissolution of montmorillonite, illite and muscovite in shale. An increase in the average monthly rainfall of 4.2 mm between July 2019 and October 2019 probably attributed to an increase in the dissolution of these minerals. The mixing of chemically different water types in these boreholes also probably led to the occurrence of the no dominant water type without any cation exceeding 50% of the total ionic charge of the water samples.

The cation diagrams also shows that no dominant field is occupied by 10% of the water samples from Monitoring Well BH 2985 in July 2019, and 30% of water samples from Monitoring Wells BH 2985, BH 4649 and BH 7639 in October 2019. The no dominant water type in the Monitoring Well BH 2985 is probably caused by the combination of different water types, such as the calcium

water type from the dissolution of calcite in calcrete with the sodium and potassium water type from the dissolution of illite, muscovite and montmorillonite found in clay. The no dominant water type in the Monitoring Well BH 4649 is probably influenced by the combination of various water types including the sodium and potassium water types from the dissolution of illite, muscovite and montmorillonite in shales and the magnesium water type from the dissolution of olivine in basalt. The no dominant water type in the Monitoring Well BH 7639 is likely due to the mixing of different water types, such as the sulphate water type from the dissolutions of pyrite in carbonaceous shale with the sodium and potassium water type from the dissolution of illite, muscovite and montmorillonite in shales.

The anion ternary diagram for July show that the bicarbonate field is occupied by 6 out of 10 groundwater samples (60%) from the Monitoring Wells BH 2985, BH 7521, BH 7546 and BH 7639 and the Production Boreholes BH 7675 and BH 7687, while in October 2019 it is occupied by 4 out of 10 groundwater samples (40%) from the Monitoring Wells BH 2985, BH 7521, BH 7639 and BH 7546. The bicarbonate concentrations at the wellfield area may be influenced by the dissolution of carbon dioxide that results from the oxidation of carbon in organic matter found in rocks such as black shales and coals and from the rainfall that recharge the Mea Arkose Aquifer within the study area. This likely resulted in the occurrence of carbonic acid in groundwater, which dissolved the silicate minerals found in sedimentary rocks that underlie the study area such as sandstones, mudstones and shales and the calcite mineral found in the calcite cement which commonly binds together the grains of sedimentary rocks such as sandstones and shales. The dissolution of the silicate and calcite minerals in groundwater likely led to the formation of the bicarbonate ions in groundwater.

In October 2019, the bicarbonate field is occupied by 4 out of 10 groundwater samples (40%) while in July 2019 it is occupied by 6 out of 10 groundwater samples (60%). The 20% difference in the number of groundwater samples collected in July and October 2019 for the bicarbonate water type is caused by changes of the water types for Boreholes BH 7675 and BH 7687 from the bicarbonate water types in July 2019, to the no dominant water types in October 2019.

In Borehole BH 7675, the no dominant water type experienced in October 2019 may probably be due to the combination of the sodium and potassium water type from the dissolution of illite, muscovite and montmorillonite in shales with the bicarbonate water type from the dissolution of the silicate minerals found in rocks such as sandstone and mudstones and the calcite mineral found in the calcite cement which commonly join together the grains of rocks such as sandstones.

The no dominant water type experienced in Borehole BH 7687 in October 2019 is probably caused by the mixing of different groundwater types such as the sulphate water type from the dissolution and oxidation of marcasite and pyrite minerals which commonly occur in black shales with the chloride water type from the dissolution of chlorite mineral found in schists and metadolerite.

The dissolution of the marcasite, pyrite and chlorite minerals in Borehole BH 7687 as well as the montmorillonite, muscovite, silicate and calcite minerals in Borehole BH 7675 was likely high in October 2019 due to a high average monthly rainfall amount of 4.2 mm and high groundwater temperatures of 25.2 ^{o}C and 25.7 ^{o}C which were experienced in Boreholes BH 7675 and BH 7687 respectively. The combination of these water types probably led to the occurrence of the no dominant water type, without any anion exceeding 50%.

The combination plots for the cation and anion ternary diagrams for July and October 2019 indicate that the sodium chloride field is occupied by 5 out 10 (50%) each of the representative water samples. In July 2019, this water type results from the Monitoring Wells BH 7516, BH 7546 and BH 7639 and the Production Boreholes BH 7674 and BH 7678, while in October 2019 it is from the Monitoring Well BH 7516 and the Production Boreholes BH 7674, BH 7675, BH 7678 and BH 7687. The sodium chloride concentration in groundwater is probably caused by the reaction of the sodium ions from the sodium and potassium water type that is occupied by 90% and 70% of the representative water samples in July and October 2019 with the chloride ions from the chloride water type that is represented by 20% and 10% of the water samples collected in July and October 2019.

The piper plots for the combination of the anions and cations in July and October 2019 indicate that the sodium bicarbonate field is occupied by 1 out of 10 (10%) each of the representative water samples. In both months, the sodium bicarbonate water type is from the Monitoring Well BH 7521. The occurrence of the sodium bicarbonate water type is likely caused by the cation exchange of calcium ions from the no dominant water type for sodium ions as groundwater passes through the clay layers found in the study area. The sodium bicarbonate water type may also be due to the reaction of the sodium ions from the sodium and potassium water type with the bicarbonate ions from the bicarbonate water type.

The piper plot for the July 2019 water samples indicates that the magnesium bicarbonate field is occupied by 1 out of 10 groundwater samples (10%) from the Monitoring Well BH 2985 while for the October 2019 samples, shows that the magnesium bicarbonate field is occupied by 2 out of 10 groundwater samples (20%) from Monitoring Wells BH 2989 and BH 7639. The occurrence of the magnesium bicarbonate water type in these boreholes may be influenced by the reaction of the magnesium ions that are formed from the dissolutions of magnesium carbonate commonly found in carbonate rocks such as calcrete with the bicarbonate ions from the bicarbonate water type.

In July 2019 the magnesium bicarbonate field is occupied by 1 out of 10 groundwater samples (10%) while in October 2019 it is occupied by 2 out of 10 groundwater samples (20%). The 10% difference in the number of groundwater samples obtained for the magnesium bicarbonate water type between July and October 2019 is influenced by the changes of water type for Borehole BH 7639 from the sodium chloride type in July 2019, to the magnesium bicarbonate water type in October 2019 as presented in Figures 5.14 and 5.15, Section 5.1.9.

The magnesium bicarbonate groundwater type found in Borehole BH 7639 in October 2019 is probably caused by an increase in the dissolution of magnesium carbonate in calcrete and bicarbonate-bearing minerals including calcite which is commonly found in cement of rocks such as black shales and sandstones. The dissolution of magnesium carbonate and calcite was probably high in October 2019 due to a higher average monthly rainfall amount of 4.2 mm experienced during this month.

The piper plots for July and October 2019 show that the mixed water type is represented by 3 out of 10 groundwater samples (30%) and 2 out of 10 groundwater samples (20%) respectively from the wellfield area. The mixed water type may be influenced by the combination of two chemically different groundwater types, such as the magnesium bicarbonate and sodium bicarbonate groundwater types found at the study area.

5.2.10 Simulated Land Subsidence

Based on estimates from MODFLOW SUB and ModelMuse, the simulated land subsidence of the study area from 2013 to 2019 indicates the possible occurrence of land subsidence of 0.008 m at Borehole BH 7687 to 0.022 m at Borehole BH 7675 due to pumping of water from the boreholes. This is consistent with the results of land subsidence calculated based on the specific storage and hydraulic head variations that ranges from 0.008598 m to 0.0168 m (see Table 5.8, Section 5.1.11).

Land subsidence is strongly related and directly proportional to the pumping rate. The Production Borehole BH 7675 has higher land subsidence of 0.022 m and average pumping rate of 355 392 m^3/year while the Production Borehole BH 7687 has the least land subsidence of 0.008 m and pumping rate of 261 368 m^3/year. In order to find out the cause of a higher pumping rate of 355 392 m^3/year that leads to a higher subsidence of 0.22 m at Borehole BH 7675 as compared to Borehole BH 7687, the map that illustrates the location of the monitoring wells and production boreholes of the wellfield area (see Figure 2.1, Section 2.1) was superimposed over the map of the geological structures at the study area (see Figure 2.7, Section 2.7.3). A higher land subsidence of 0.022 m experienced at Borehole BH 7675 is likely due to the location of this borehole along the Bushman lineament and nearer the Chidumela Fault and the Basement contact, (see Figure 5.18) , which are probably highly fractured and permeable. This led to a higher pumping rate at Borehole BH 7675 as compared to Borehole BH 7687. Figure 5.18 shows the location of the boreholes and the major and minor lineaments and structures that influence the hydrogeology of the study area.

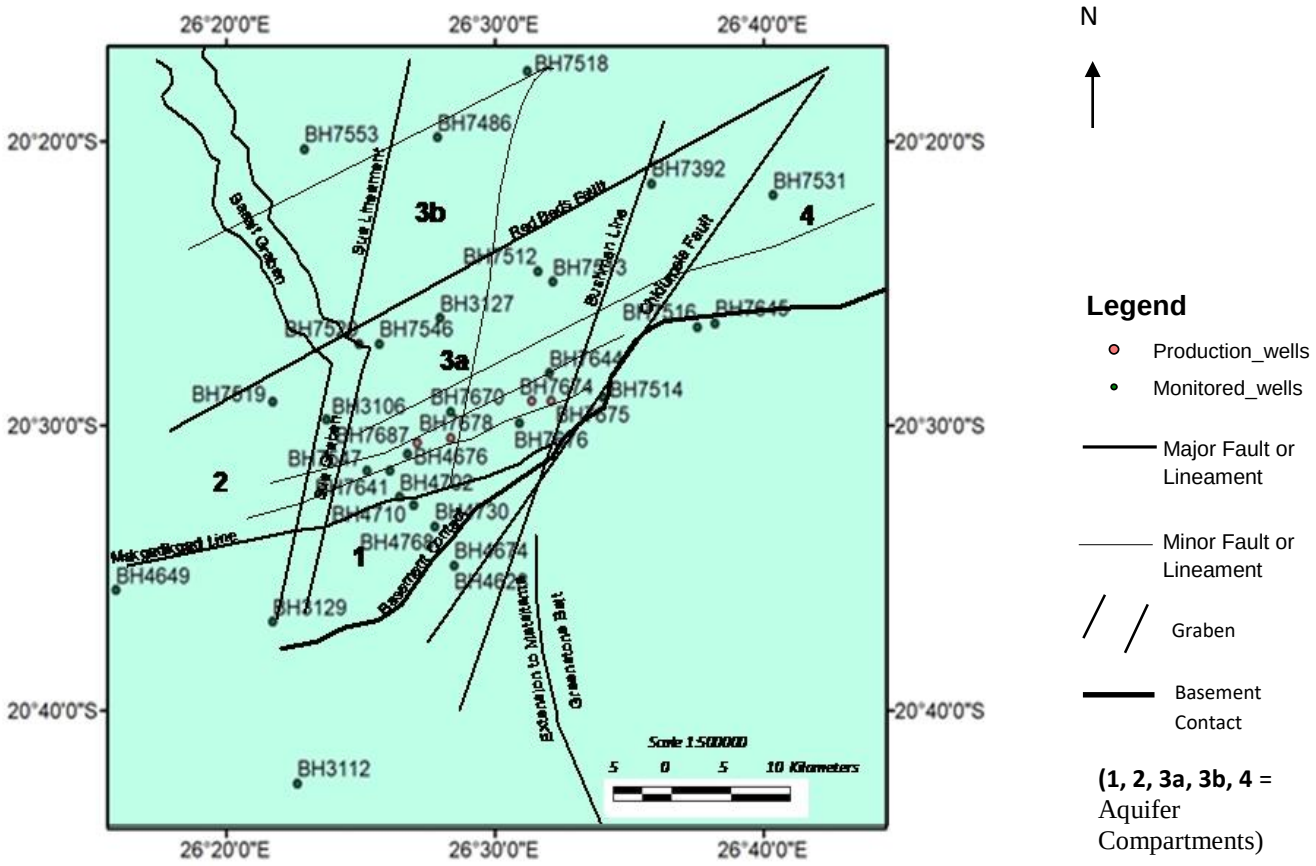

Figure 5.18. The location of boreholes and geological structures that influence the hydrogeology of the study area.

The Production Borehole BH 7675 has higher land subsidence of 0.022 m and the least hydraulic head of 966.819 m amsl, while Borehole BH 7687 has the least subsidence of 0.008 m and higher hydraulic head of 978.5401 m amsl. This is because land subsidence is inversely proportional to the hydraulic heads. The least hydraulic head of 966.819 m amsl experienced in Borehole BH 7675 likely resulted in a higher increase in the effective stress on the Mea Arkose Aquifer skeleton and a further decrease in the pore fluid pressure around this borehole, as compared to Borehole BH 7687. This likely resulted in higher compression of the aquifer's skeleton around Borehole BH 7675.

Borehole BH 7687 has the highest specific storage of 0.0000436 and the least subsidence of 0.008 m, while Borehole BH 7675 has the least specific storage of 0.0000154 and the highest subsidence of 0.022 m. This is contrary to the findings of Maurice *et al*. (2019) and Smith and Majumdar (2020) where land subsidence increased with the increasing specific storage of the aquifer. The highest calculated subsidence in Borehole BH 7675 may be influenced by a high layer thickness of 198 m determined from this borehole, while the least calculated subsidence for Borehole BH 7687 may be influenced by the least layer thickness of 145 m as presented in Table 5.8, Section 5.1.11. This is because land subsidence normally increases with the thickness of the aquifer, likely due a higher compressibility of fine grained sediments such as clay and silt found in rocks such as siltstone and mudstone.

Further displacement of the ground surface around the pumping wells ranging from 0.015 m to 0.031 m will occur due to future groundwater exploitation from 2019 to 2031. This is probably because land subsidence is cumulative and will include prior land subsidence to this time frame. The margin of land subsidence of 0.015 m to 0.031 m that will occur around the production boreholes from 2019 to 2031 will be high as compared to the margin of land subsidence of 0.008 m to 0.022 m which occurred from 2013 to 2019. This is because the mean annual total abstraction rate of 1,253,546 m^3/year that was experienced from 2013 to 2019 is likely to double and increase further than the mean annual recharge rate as the area is experiencing a continuous population growth as stated in section 5.1.3. This will lead to increased land subsidence from 2019 to 2031 as compared to subsidence that occurred from 2013 to 2019.

CHAPTER 6

CONCLUSIONS AND RECOMMENDATIONS

6.1 Conclusions

From the foregoing, the following conclusions are drawn:

- The statistical trends show a declining water table with the coefficient of determination that ranged from 63% to 98%.
- There is a positive correlation ranging from 0.115 to 0.345, of the water level drop with abstraction rates.
- The correlation between the water level drop and temperatures is positive and ranges from 0.050 to 0.518.
- There is a negative correlation ranging from -0.321 to -0.017, of the water level drop with rainfall hence indicating that rainfall that is experienced at the wellfield area does not contribute to the drop of the water levels as water will be added in the aquifer system.
- The correlation between the water level drop and the recharge rates is negative ranging from -0.357 to -0.017.
- A higher mean annual total abstraction rate of 1 253 546 m^3/year than the mean annual recharge rate of 1 149 691 m^3/year led to the depletion of groundwater resources at the Dukwi Wellfield from 2013 to 2019.
- The transmissivity estimates determined from the study area are high as 8.171 m^2/min. This higher transmissivity rates contributed to the decline of groundwater levels by influencing more extraction of groundwater resources and abstraction rates as high as 355 392 m^3/year.
- The hydraulic conductivities determined from the wellfield area range from 0.000109 m/min to 0.0413 m/min. A higher hydraulic conductivity of 0.0413 m/min contributed to the decline of groundwater levels by leading to a higher rate of groundwater flow through the aquifer system.

- The storativity estimates from the study area range from 0.0002126 to 0.0003299. A higher storativity estimate of 0.0003299 led to more depletion of groundwater resources as more volume of water was released from the aquifer storage.
- The decline of the water levels contributed to a high concentration of parameters such as chloride, sodium, TDS, EC and copper in the monitoring wells and production boreholes of the study area such as in the Monitoring Well BH 4649 and the Production Borehole BH 7687.
- The mean abstraction rates of the production boreholes range from 261 368 m^3/year to 355 392 m^3/year. This led to land subsidence with ranges from 0.008 m to 0.022 m and hydraulic heads that ranged from 966.819 m amsl to 978.5401 m amsl from 2013 to 2019.
- It is projected that an increase in land subsidence ranging from 0.015 m to 0.031 m will occur due to future groundwater exploitations from 2019 to 2031.

6.2 Recommendations

This study has shown that groundwater depletion at the Dukwi wellfield area is attributed to low replenishment rates than abstraction rates. In order to improve the recharge rates of the aquifer at the study area and to mitigate the effects of groundwater depletion, the following recommendations are made:

1. In order to mitigate the detrimental effects that can result from land subsidence at the study area, such as damage to infrastructure, a maximum land subsidence threshold of say 5 mm per year as recommended by Nicholls *et al*. (2021) should be established by the Tutume Sub district Council which governs the wellfield area. This can be done by measuring land subsidence on a yearly basis by the monitoring teams of the wellfield area that include the Department of Water Affairs and the Water Utilities Corporation, by means of a variety of technologies that include Geographic Information System and the Global Positioning System. These technologies will help to automatically measure land subsidence hence assisting in monitoring land subsidence to be below the established threshold. This should be done by reducing the groundwater extraction rates if the measured land subsidence at the wellfield area exceeds the recommended threshold of 5 mm per year.

2. Different methods that are less energy consuming such as the Specific Conductance and the Electromagnetic methods should be implemented and used by the monitoring teams of the wellfield area (Department of Water Affairs and the Water Utilities Corporation) to measure and monitor the TDS and EC concentrations at the study area. This will help to determine whether the water quality at the study area is suitable for human consumption based on the recommended Botswana Bureau of Standards.

REFERENCES

Anjomshoaa, A. (2019), 'Filling missing meteorological data in heating and cooling seasons separately', (June 2017), pp. 701-710. doi: 10.1002/joc.5836.

Anon., (2006), "Porosities and Hydraulic Conductivities for various rocks and sediments", *https://www.open.edu/openlearn/ocw/pluginfile.php/625504/mod_resource/content/2/s278_3_table1.pdf*. Accessed: May 14, 2020.

Anon. (2020a), "Hwr 431/531 hydrogeology lab section laboratory 5", *http://quebec.hwr.arizona.edu/classes/hwr431/Lab5_Pumping. pdf*. Accessed: January 2, 2020.

Anon. (2020b), "What is a piper plot", Available at: *www.cloudfront.net/webinar/Webinar%20Data/PiperPlotInstructions.pdf*. Accessed: November 10, 2020.

Baltazar, J. C. and Claridge, D. E. (2002), 'Restoration of Short Periods of Missing Energy Use and Weather Data Using Cubic Spline and Fourier Series Approaches : Qualitative Analysis'.

Barlow P. M. and Leake. S. A. (2012), Streamflow Depletion by Wells - Understanding and Managing the Effects of Groundwater Pumping on Streamflow. US Geol Surv Circular 1376. Available at *https://pubs.usgs.gov/circ/1376/pdf/circ1376_barlow_report_508.pdf*. Accessed: November 23, 2019.

Barrett, P. J., Froggatt, P. C. and Land, V. (2012), 'Densities, porosities, and seismic velocities of some rocks from Victoria Land, Antarctica Densities, porosities and seismic velocities of some rocks from', 8306. doi: 10.1080/00288306.1978.10424049.

Bartolino, J. R. and Cunningham, W. L. (2003), 'Ground-Water Depletion Across the Nation', U.S Geological Survey Fact Sheet 103-03, (November), p. 4. Available at: *https://pubs.usgs.gov/fs/fs-103-03/JBartolinoFS(2.13.04).pdf*. Accessed: November 3, 2019.

Benett. J. D. (1970), *Geological Map of the Mosetse-Matsitama Area (QDS 2026D & 2126B) with Brief Description* , Geological Survey Department, Lobatse, pp. 113-123.

Berlin, K. W. and Kumar, P. J. S. (2014), 'Introduction to Managed Aquifer Recharge (MAR) - Overview of schemes and settings worldwide Introduction to Managed Aquifer Recharge (MAR) - Overview of schemes and settings world wide'.

Bierkens, M. F. P. (2019), 'Non-renewable groundwater use and groundwater depletion : a review', IOP Publishing.

Botswana Bureau of Standards (2016), 'BOS 262:2011', 23pp.

Botswana Meteorological Services (2019a), *Nata and Sowa Town Monthly and Daily Rainfall*, 2pp.

Botswana Meteorological Services (2019b), *Sua Pan Max-Min Temperatures*, 211pp.

Brikowski, T. (2013), 'GEOS 4430 Lecture Notes : Well Testing', 41pp.

Brunner, P. and Kinzelbach, W. (2008), 'Sustainable Groundwater Management', *Encyclopedia of Hydrological Sciences*, pp. 1-10. doi: 10.1002/0470848944.hsa164.

Buchanan, R. and Buddemeir R. W. (1993), Kansas Groundwater. Kansas Geological Survey, Available at: *http://www.kgs.ku.edu/Publications/Bulletins/ED10/06_wells.html*. Accessed: May 13, 2020.

Butler, J. J. (1991), 'A Stochastic Analysis of Pumping Tests in Laterally Nonuniform Media', *Water Resources Research*, 27(9), pp. 2401–2414. doi: 10.1029/91WR01371.

California Department of Water Resources (2003), 'Basic Groundwater Concepts', *Bulletin 118*, pp. 79-104. Available at: *http://www.water.ca.gov/pubs/groundwater/bulletin_118/california's_groundwater-bulletin_118_-_update_2003_/bulletin118-chapter6.pdf*. Accessed: February 21, 2019.

Central Pollution Control Board (2007), 'Guidelines for Water Quality Monitoring, Parivesh Bhawan, Delhi, India

Central Statistics Office (2009), 'Botswana Water Statistics', Available at: *www.l.eis.gov.bw/EIS/Reports/Botswana%20water-statistics%20report.pdf*. Accessed: October 26, 2018.

Chaoka, R. T., Alemaw, B. F., Molwalelfhe, L. and Moreomongwe, M. (2006) 'Investigating the causes of water-well failure in the Gaotlhobogwe wellfield in southeast Botswana'.

Chee, J. D. and Queen, T. (2016) 'Pearson's Product-Moment Correlation : Sample Analysis Jennifer Chee University of Hawaii at M ā noa School of Nursing', (May 2015). doi: 10.13140/RG.2.1.1856.2726.

Chen, H. and Claridge, D. E. (2000), 'Procedures for filling short gaps in energy use and weather data', *Twelfth Symposium on Improving Building Systems in Hot and Humid Climates*, (iii), pp.

314-326.

Chen, C., Pei, S. and Jimmy, J. (2003), 'Land subsidence caused by groundwater exploitation in Suzhou City, China', (41372261). doi: 10.1007/s10040-002-0225-5.

Chilton, J. (1996), 'Chapter 9 - Groundwater', *Water quality assessments-A Guide to use of Biota, sediments and water in Environmental Monitoring*, 5, p. 88. doi: https://doi.org/10.1016/B978-0-408-01409-0.50011-8.

Condon, L. E., Atchley, A. L. and Maxwell, R. M. (2020), 'Evapotranspiration depletes groundwater under warming over the contiguous United States', *Nature Communications*. Springer US, 11(1). doi: 10.1038/s41467-020-14688-0.

Cui, Y., Su, C., Shao, J., Wang, Y. and Cao, X. (2014), 'Development and Application of a Regional Land Subsidence Model for the Plain of Tianjin', 25(3), pp. 550-562. doi: 10.1007/s12583-014-0447-1.

Delleur, J. W. (2006), *The handbook of Groundwater Hydrology*, 2nd ed, CRC Press Taylor and Francis Group, New York, 37pp.

De Louw, P. G. B. (2013), *Saline seepage in deltaic areas.*

Deng, X., Li, F., Zhao, Y. and Li, S. (2018), 'Regulation of deep groundwater based on MODFLOW in the water intake area of the South-to-North Water Transfer Project in Tianjin, China', *Journal of Hydroinformatics*, 20(4), pp. 989-1007. doi: 10.2166/hydro.2018.126.

Department of Environmental Affairs (2006), 'Water accounts of Botswana (1992-2003)', Available at: *https://unstats.un.org/unsd/envaccounting/ceea/archive/Water/Botswana_WaterAcc_2006.pd*. Accessed: October 26, 2018).

Department of Water Affairs (1976), *Sua Project, Dukwe New Town ground Water Study*, SWECO Swedish Consulting Group, Sweden, 57pp.

Department of Water Affairs (1995a), *Dukwi Wellfield Extension and Resource Evaluation Main Report*, Water Surveys Botswana, Gaborone, 174pp.

Department of Water Affairs (1995b), *Dukwi Wellfield Extension and Resource Evaluation: Water Demand Study*, Water Surveys Botswana, Gaborone, 34pp.

Department of Water Affairs (2000), *Dukwi Old Modeling Report*, 186pp.

Department of Water Affairs (2019a), *Wellfield GIS Data*, 30pp.

Department of Water Affairs (2019b). *Dukwi Production and Observation Data*, 58pp.

Department of Water Affairs (2019c), *Dukwi Wellfield Chemistry Results*, 4pp.

Dinu, C., Drobot, R., Ionut, C. P. and Blidaru, T. V. (2017), 'Flash-Flood Modelling With Artificial Neural', *Mathematical Modelling in Civil Engineering*, 13(3), pp. 10–20. doi: 10.1515/mmce.

Doll, P. (2002), 'Impact of climate change and variability on irrigation requirements: A global perspective', *Climatic Change*, 54(3), pp. 269–293. doi: 10.1097/00010694-197402000-00005.

Dragoni, W. (1998), 'Some considerations regarding the radius of influence of a pumping well', *Hydrogeologie*, 3(1), pp. 21–25. Available at: *http://scholar.google.com/scholar?hl=en&btnG=Search&q=intitle:Some+considerations+regarding+the+radius+of+influence+of+a+pumping+well#0*. Accessed: November 25, 2019.

Duffield G. M. (2020), Aquifer Testing 101: Hydraulic Properties. Available at *hydrosolve@aqtesolv.com/aquifer-tests/aquifer-tests/aquifer-properties.htm* Accessed: September 20, 2019.

Du Plessis, A. J. E. and Rowntree, K. M. (2003), 'Water resources in Botswana with particular reference to the savanna regions', *South African Geographical Journal*, 85(1), pp. 42-49. doi: 10.1080/03736245.2003.9713783.

Erickson, T. O. and Stefan, H. G. (2009), 'Natural Groundwater Recharge Response to Urbanization: Vermillion River Watershed, Minnesota', *Journal of Water Resources Planning and Management*, 135(6), pp. 512-520. doi: 10.1061/(asce)0733-9496(2009)135:6(512).

Fanta, B., Zaake, B. T. and Kachroo, R. K. (2002), 'A study of variability of annual river flow of the southern African region', 46(February), pp. 513-524.

Fitch, P., Brodanic, B., Stenson, M. and Booth, N (2016), *Integrated Groundwater Management: Concepts, Approaches and Challenges*. doi: 10.1007/978-3-319-23576-9_26.

Fitts, C. R. (2013) Groundwater: *The big picture, Groundwater Science*. doi: 10.1016/B978-0-12-384705-8.00001-7.

Freeze, R. A. and Cherry, J. A. (1979), *Groundwater*, Prentice Hall, Inc., Englewood Cliffs, New Jersey, 604 pp.

Galloway, D. L., Erkens, G., Kuniansky, E. L. and Rowland, J. C. (2016), Preface: Land subsidence processes. *Hydrogeology Journal*, *24*(3), 547-550. https://doi.org/10.1007/s10040-016-1386-y.

Geotechnical Consulting Services (1998a), “Review of Monitoring Performed by DWA and DGS: Assessment of Water Resource and Improvement of Techniques”, *Dukwi Wellfield Report*, Gaborone, 68pp.

Geotechnical Consulting Services (1998b), “Review of Monitoring Performed by DWA and DGS: Assessment of Water Resource and Improvement of Techniques”, *Dukwi Wellfield Modelling Report*, Gaborone, 50pp.

Ghazavi, R. and Ebrahimi, H. (2018), ‘Hydrological Impacts of Large Reservoir Dam and Land Subsidence on Downstream Groundwater Resources using Mathematical Modeling’, 7, pp. 51–60. doi: 10.22052/jdee.2017.63257.

Gingrich, P. (2004), ‘Chapter 11 Association Between Variables’, *Introductory Statistics for the Social Sciences - http://uregina.ca/~gingrich/text.htm*, pp. 794-835. Available at: *http://uregina.ca/~gingrich/text.htm*. Accessed: January 4, 2019.

Giordano, M. (2010), ‘Global Groundwater? Issues and Solutions’, *Ssrn*, (November 2009). doi: 10.1146/annurev.environ.030308.100251.

Green. D. (1966), *The Karroo System in Bechuanaland*, Geological Survey Department, Lobatse, 74p.

Green, T. R., Taniguchi, M., Kooi, H., Gurdak, J., Allen, D. M., Hiscock, K. M., Treidel, H. and Aureli, A (2011), ‘Beneath the surface of global change: Impacts of climate change on groundwater’, *Journal of Hydrology*, 405(3–4), pp. 532-560. doi: 10.1016/j.jhydrol.2011.05.002.

Green, T. R. (2016), *Linking Climate Change and Groundwater*. doi: 10.1007/978-3-319-23576-9.

Harter (2003), "Basic Concepts of Groundwater Hydrology", University of California webpage, Available at: *www.groundwater.ucdavis.edu/files/156562.pdf*. Accessed: July 15, 2019.

Heath, R. C. (2009), ‘Groundwater Hydrology PART 1 : Basic Groundwater Hydrology’, 11pp.

Hoffmann, J., Leake, S. A., Galloway, D. L. and Wilson, A. M. (2000), ‘MODFLOW-2000 Ground-Water Model - User Guide to the Subsidence and Aquifer-System Compaction (SUB) Package’.

Holzer, T. L and Johnson, A. I. (1985), "Land Subsidence Caused by Ground Water Withdrawal in Urban Areas" (T. L. Holzer and A. I. Johnson, sen. editors), *GeoJournal, Vol. 11, No. 3,*

Water in the Urban Environment Published by: Springer Stable URL: https://www.jstor.org/stable/41143552, pp. 245-255.

Howard, J. P. (2018), 'Interpolation and Extrapolation', *Computational Methods for Numerical Analysis with R*, (February), pp. 95–132. doi: 10.1201/9781315120195-4.

Intergovernment Panel on Climate Change (2007a), 'The Scientific Basis' Climate Change 2001: Working Group II Contribution to the Fourth Assessment Report of the Intergovernmental Panel on Climate Change, Available at: *https://archive.ipcc.ch/ipccreports/tar/vol4/index.php?idp=76*. Accessed: July 21, 2019.

Intergovernment Panel on Climate Change (2007b), 'Climate Change Impacts, Adaptation and Vulnerability', Climate Change 2007: Working Group II Contribution to the Fourth Assessment Report of the Intergovernmental Panel on Climate Change, Available at: *https://archive.ipcc.ch/publications_and_data/ar4/wg2/en/ch3s3-4-2.*html. Accessed: January 30, 2021.

Iqbal, S. (2015), What are the groundwater zones, Aeration, Phreatic zone and Vadose zone. Civil engineering webpage, Available at: www.iamcivilengineer.com/what-are-groundwater-zones-aeration. Accessed: July 12, 2019.

Jacob, C. E. (1946), 'Drawdown Test to Determine Effective Radius of Artesian Well', *Hydraulic Engineering Journal*, 112 (1), pp. 1047-1070.

Jones, A. M. (2006), 'Environmental biology', *Environmental Biology*, pp. 1-197. doi: 10.4324/9780203137574.

Kelbe, B. E., Taylor, R. H. and Haldorsen, S. (2011), 'Groundwater hydrology', *Ecology and Conservation of Estuarine Ecosystems: Lake St Lucia as a Global Model*, pp. 151-168. doi: 10.1017/CBO9781139095723.010.

Konikow, L. F. and Kendy, E. (2005), 'Groundwater depletion: A global problem', *Hydrogeology Journal*, 13(1), pp. 317–320. doi: 10.1007/s10040-004-0411-8.

Krinner, G., Arblaster, J., Dufresne, J., Fichefet, T., Friedlingstein, P., Gao, X., Gutowski, W. J., Jonh, T., Shongwe, M., Tebaldi, C., Weaver , A., J. and Wehner, M (2013), 'Long-term climate change: Projections, commitments and irreversibility', *Climate Change 2013 the Physical Science Basis: Working Group I Contribution to the Fifth Assessment Report of the Intergovernmental Panel on Climate Change*, 9781107057, pp. 1029-1136. doi:

10.1017/CBO9781107415324.024.

Kumar, C. P. (2012), 'Climate Change and Its Impact on Groundwater Resources', *International Journal of Engineering and Science*, 1(5), pp. 43-60. Available at: *http://www.researchinventy.com/papers/v1i5/F015043060.pdf*. Accessed: February 5, 2020.

Kumar, C. P. and Singh, S. (2016) 'Climate Change Effects on Groundwater Resources', (February).

Legadiko, O. D. (2015), "Characterisation and groundwater flow modeling, Dukwi Wellfield Phase II North-Eastern Sub-District Botswana", *unpublished Master's Thesis*, University of Botswana, Gaborone, 105pp.

Manger, E. (1963), 'Porosity and Bulk Density of Sedimentary Rocks', US Geol Survey Cir 1144, *https://pubs.usgs.gov/bul/1144e/report.pdf. Accessed May, 14 2020.*

Manoj, K., Ghosh, S. and Padhy, P. K. (2013), 'Characterization and Classification of Hydrochemistry using Multivariate Graphical and Hydrostatistical Techniques', 3(5), pp. 32–42.

Mason, R. (1998), "Tectonic Setting of the Kalahari Suture Zone - Botswana", *The International Conference on the Role of a National Geological Survey in Sustainable Development*, Geological Survey Department, Lobatse, pp. 51-54.

Mastrocicco, M., Busico, G. and Colombani, N. (2018), 'Groundwater Temperature Trend as a Proxy for Climate Variability', *Proceedings*, 2(11), p. 630. doi: 10.3390/proceedings2110630.

Maurice, L., Taylor, R. G., Tindimugaya, C., MacDonald, A. M., Johnson, P., Kaponda, A., Owor, M., Sanga, H., Bonsor, H. C., Darling, W. G. and Gooddy, D. (2019) 'Characteristics of high-intensity groundwater abstractions from weathered crystalline bedrock aquifers in East Africa', *Hydrogeology Journal*, 27(2), pp. 459-474. doi: 10.1007/s10040-018-1836-9.

McCulloch, G. P., Irvine, K., Eckardt, F. D. and Bryant, R. (2008), Hydrochemical fluctuations and crustacean community composition in an ephemeral saline lake (Sua Pan, Makgadikgadi Botswana). *Hydrobiologia*, *596*(1), 31-46. https://doi.org/10.1007/s10750-007-9055-8.

Meier, P. M., Carrera, J. and Sánchez-Vila, X. (1998), 'An evaluation of Jacob's method for the interpretation of pumping tests in heterogeneous formations', *Water Resources Research*, 34(5), pp. 1011-1025. doi: 10.1029/98WR00008.

Mills, Z., Dickenson, K., Dudley, D., Seger, D., Yoder, K., Carstairs, J., Bodane, B., McCotter,

G., Michels, A. and Williams, C. (2019), *What is a piper plot (trilinear diagram*), Available at: *https://support.goldensoftware.com/hc/en-us/articles/115003101648-What-is-a-piper-plot-trilinear-diagram*. Accessed: May 24, 2020.

Minderhoud, P. S. J; Erkens, G; Pham, V. H, Bui, V. T, Erban, L; Kooi, H and Stouthamer, E. (2017), 'Impacts of 25 years of groundwater extraction on subsidence in the Mekong delta , Vietnam' *Environmental Research Letters*, 12 (2017), 14 pp.

Montoya, S. and Carita, G. (2018), *What is a Piper plot diagram for water chemistry analysis and how to create one*, Available at: *www.hatarilabs.com/ih-en/what-is-a-piper-diagram-and-how-to-create-one*. Accessed: June 4, 2020.

Moore, R. B., Schwarz, G. E., Clark, S. F., Walsh, G. J and Degnan, J. R (2002), *Factors Related to Well Yield in the Fractured-Bedrock Aquifer of New Hampshire, U.S. Geological Survey Professional Paper*.

Motevalli, A., Pourghasemi, H. R., Hashemi, H. and Gholami, V. (2019), *Assessing the Vulnerability of Groundwater to Salinization Using GIS-Based Data-Mining Techniques in a Coastal Aquifer, Spatial Modeling in GIS and R for Earth and Environmental Sciences*. Elsevier Inc. doi: 10.1016/b978-0-12-815226-3.00025-9.

Mustafa, S. M. T., Abdollah, K., Verbeiren, B. and Huysmans, M. (2017), 'Identification of the influencing factors on groundwater drought and depletion in north-western Bangladesh', *Hydrogeology Journal*, 25(5), pp. 1357–1375. doi: 10.1007/s10040-017-1547-7.

Nagar, E. A. (2007), 'Guidelines for Water Quality Monitoring Central Pollution Control Board Parivesh Bhawan Foreword'.

Nelson, S. A. (2015), 'Groundwater', pp. 1-11.

Neuman, S. P., Blattstein, A., Riwa, M., Tartakovsky, D. M., Guadagnini, A. and Ptak, T. (2007) 'Type curve interpretation of late-time pumping test data in randomly heterogeneous aquifers', 43, pp. 1-15. doi: 10.1029/2007WR005871.

New Hampshire Fish and Game Department (2013), "Coldwater Streams Climate Assessment" Available at: *https://extension.unh.edu/resources/files/Resource004598_Rep6559.pdf*. Accessed: August 7, 2019.

Nimmo, J. R., Healy, R. W. and Stonestrom, D. A. (2005) 'Aquifer Recharge', *Encyclopedia of Hydrological Sciences*, pp. 2229-2246. doi: 10.1002/0470848944.hsa161a.

Noor, N. M., Yahaya, A. S. and Ramli, N. O. R. A. (2004), 'Using the linear interpolation technique to estimate missing values for air pollution data.

North, R. P. (2012), 'The In uence of Climate Change on the Occurrence of Hypoxia in Swiss Lakes The influence of climate change on the occurrence of hypoxia in Swiss lakes', (20802).

Oosterbaan, R. and Nijland, H. (1986), 'Determining the Saturated Hydraulic Conductivity', *Drainage Principles and Applications*, (April), p. 37. Available at: *http://www.waterlog.info/pdf/chap12.pdf*. Accessed: February 18, 2020.

Oregon State University (2020), Groundwater and Wells: Understanding Groundwater, Available at: *www.wellwater.oregonstate.edu/groundwater-and-wells*. Accessed: June 24, 2020.

Orica (2014), Hydraulic Capture, Available at: *www.orica.com/ArticleDocuments/991/HydraulicContainmentExplanation.pdf.aspx.* Accessed: February 13, 2019.

Patil, M., Saha, A., Karwariya, S., Pingale, S. M., Goyal, V. C., Rathore, D. S. and Behera, N. (2019), 'Assessment of rainfall recharge using rainfall infiltration factor method and empirical equation, *Dicover Nature*, Vol. 13, 2019, pp. 1-8.

Population Action International (2011), 'Pai-1293-Water-4Pg', *Population Action International*.

Purushotham, D., Prakash, M. R. and Rao, A. N. (2011), 'Groundwater depletion and quality deterioration due to environmental impacts in Maheshwaram watershed of R. R. district, AP India ', pp. 1707-1721. doi: 10.1007/s12665-010-0666-4.

Qureshi, A. S., McCornick, P. G., Sarwar, A. and Sharma, B. R. (2010), 'Challenges and Prospects of Sustainable Groundwater Management in the Indus Basin, Pakistan', *Water Resources Management*, 24(8), pp. 1551–1569. doi: 10.1007/s11269-009-9513-3.

Rahmani, S. E. A., Chibane, B. and Boucefie, A. (2017), 'Groundwater recharge estimation in semi-arid zone : a study case from the region of Djelfa (Algeria)', pp. 2255-2265. doi: 10.1007/s13201-016-0399-y.

Remy, L. L., Clay, T. and Oliva, G. (2005), 'Do We Have a Linear Trend ?'

Reeves,. C.V. (1978), *Reconnaissance Aeromagnetic Survey of Botswana 1975-1977*, Terra Surveys Ltd, Edinburgh, 199pp.

Moore, R. B., Schwarz, G. E., Clark, S. F., Walsh, G. J and Degnan, J. R (2002), *Factors Related to Well Yield in the Fractured-Bedrock Aquifer of New Hampshire, U.S. Geological Survey*

Professional Paper.

Nicholls, R.J., Lincke, D., Hinkel, J., Brown, S., Vafeids, A. T., Meyssignac, B., Hanson, S. E., Merkens, J. L. and Fag, J. (2021), 'A global analysis of subsidence, relative sea-level change and coastal flood exposure', *Nature Climate Change* 11(4), pp. 338–342. doi.org/10.1038/s41558-021-00993-z

Sadashivaiah, C., Ramakrishnaiah, C. R. and Ranganna, G. (2008), 'Hydrochemical Analysis and Evaluation of Groundwater Quality in Tumkur Taluk , Karnataka State , India', 5(3), pp. 158-164.

Schad, H. and Teutsch, G. (1994), 'Effects of the investigation scale on pumping test results in heterogeneous porous aquifers', *Journal of Hydrology*. Elsevier, 159(1-4), pp. 61-77. doi: 10.1016/0022-1694(94)90249-6.

Sfinchez-vila, X., Meier, P. M. and Carrera, J. (1999), 'Pumping tests in heterogeneous aquifers: An analytical study of what can be obtained from their interpretation using Jacob's method, 35(4), pp. 943-952.

Shand, P., Edmunds, W. M., Lawrence, A. R., Smedley, P. L and Burke, S. (2007), 'The natural (baseline) quality of groundwater in England and Wales', *BGS Research Report RR/07/06*, 72pp.

Singhal, B. B. S. and Gupta, R. P. (2010), *Applied Hydrogeology of Fractured Rocks*, Kluwer Academic Publishers, Indian, 2nd edition, 408pp.

Siva Prasad, Y. and Venkateswara Rao, B. (2018) 'Groundwater recharge estimation studies in a khondalitic terrain of India', *Applied Water Science*. Springer Berlin Heidelberg, 8(4), pp. 1-9. doi: 10.1007/s13201-018-0738-2.

Smith, R.A. (1984), "The lithostratigraphy of the Karoo Supergroup in Botswana", *Bulletin of Botswana Geological Survey*, 26, 239pp.

Smith, R. G. and Majumdar, S. (2020), 'Groundwater Storage Loss Associated With Land Subsidence in Western United States Mapped Using Machine Learning', *Water Resources Research*, 56(7), pp. 1-14. doi: 10.1029/2019WR026621.

Stansfield. G. (1973), *The Geology of the Area around Dukwe and Tlalamabele, Central District, Botswana: Geological Survey District Memoir 1*, Geological Survey Department, Lobatse, 74pp.

Statistic Botswana (2015), *Tutume Sub District: Population and Housing Census Selected Indicators 2011*, Statictics Botswana Publishers, Gaborone, *www.statsbots.org.bw/sites/default/files/publications/central%20Tutume.pdf*. Accessed: February 13, 2019.

Taoukis, P. S., Tsironi, T. N. and Giannakourou, M. C. (2014), *'Reaction kinetics', Food Engineering Handbook: Food Engineering Fundamentals*, pp. 529-569. doi: 10.1201/b17843.

Taylor, R. G., Scanion, B. R., Doell, P. and Rodell, M. (2013) 'Ground water and climate change', (April). doi: 10.1038/nclimate1744.

Terzaghi, K. (1925), *Erdbaumechanik auf bodenphysikalisher Grundlage*, Deuticke, Wien, Austria, 399pp.

Todd, D. and Mays, L. (2005), *Groundwater Hydrology*, 3rd Edition, John Wiley and Sons, Inc., Hoboken, 652pp.

Tomlinson, P., Knapp, M., Sutherland, A and Campbell, A. (2016), 'What Is the Difference between Weather and Climate?', *Western Folklore*, 15(1), 62pp. doi: 10.2307/1496415.

Trading Economics (2019), *Botswana Population*, *https://tradingeconomics.com/botswana/population*. Accessed: November 12, 2019.

Vissers, M. J. M. (2004), *Patterns of groundwater quality*.

Wada, Y., Van Beek, L. P. H., Van Kempen, C. M., Reckman, J. W. T. M., Vasak, S and Bierkens, M. F. P (2010), 'Global depletion of groundwater resources', *Geophysical Research Letters*, 37(20), pp. 1-5. doi: 10.1029/2010GL044571.

Waltham, T. (2015), 'Sinking cities - An intergtrated approach towards solutions', *Deltares*, 18(3), pp. 95-100. doi: 10.1046/j.1365-2451.2002.00341.x.

Warren, L. A., Briggs, K. M. and McCombie, P. F. (2015), 'Advances in the assessment of drystone retaining walls-some case studies', *Geotechnical Engineering for Infrastructure and Development - Proceedings of the XVI European Conference on Soil Mechanics and Geotechnical Engineering, ECSMGE 2015*, 6, pp. 3583-3588. doi: 10.1680/ecsmge.60678.

Warrington, G. (2009), "Fluid Flow and Solute Movement in Sandstones", *The Onshore UK Permo-Triassic Red Bed Sequence*, The Geological Society Special Publications 263, Barker R. D. and Tellam J. H. (eds), p. 346.

Water Utilities Corporation (2019a), *Water levels for the Dukwi Wellfield*, 13pp.

Water Utilities Corporation (2019b), *Masunga Management Centre Monthly Abstraction Data*, 2pp.

Water Utilities Corporation (2019c), *Water Chemistry Results*, 13pp.

Wattez, A. (2020), "How does salinity increase with depth?" https://findanyanswer.com/How-does-salinity-increase-with-depth? Accessed: March 03, 2020.

Yihdego, Y. (2018), 'Engineering and enviro-management value of radius of influence estimate from mining excavation', *Journal of Applied Water Engineering and Research*, 6(4), pp. 329–337. doi: 10.1080/23249676.2017.1287022.

Younger, P. L. (2000), 'Simple generalized methods for estimating aquifer storage parameters P. L. Younger', pp. 127-135.

Zhdanov, M. S. (2015), 'Forward and Inverse Problems in Science and Engineering', *Inverse Theory and Applications in Geophysics*, pp. 3-31. doi: 10.1016/b978-0-444-62674-5.00001-3.

Zhou, Q., Bear, J. and Bensabat, J. (2005), 'Saltwater upconing and decay beneath a well pumping above an interface zone', *Transport in Porous Media,* 61(3), pp. 337-363. doi: 10.1007/s11242-005-0261-4.

Zreda, M. (2007), 'PART 10 Aquifers and aquitards', pp. 6.

APPENDIX A: Water Chemistry Results

Table A1. Dukwi Wellfield Phase II water chemistry results -July 2019 (Botswana Bureau of Standards, 2016; Water Utilities Corporation, 2019c; Department of Water Affairs, 2019c).

Parameter	Units	Borehole Number										
		BH 7674	BH 7675	BH 7687	BH 7678	BH 2985	BH 4649	BH 7516	BH 7521	BH 7639	BH 7546	BOS 262:2011
pH	-	7.16	7.63	7.17	7.23	7.21	7.23	7.52	8.69	7.12	7.14	5.5-9.5
Temp	^{o}C	19.7	19.4	19.5	19.7	20.1	19.3	18.5.	19.8	19.7	20.4	-
Conductivity(EC)	µS/cm	1530	1463	1549	1516	622.0	3096	1532	2408	1562	1532	1500
Turbidity	NTU	0.1400	0.17	0.19	0.17	0.57	0.68	0.82	0.24	0.53	0.23	5.00
Bromine	mg/l	0.60	0.93	1.27	0.90	0.14	3.12	0.56	1.01	1.03	1.43	-
Chloride	mg/l	354.0	197	205	231	40.1	480.4	223	256	250	254	200
Fluoride	mg/l	0.7800	0.85	0.97	0.79	1.86	0.860	0.450	12.3	0. 780	0.350	1.00
Nitrate	mg/l	2.79	1.16	1.53	2.78	2.43	2.32	1.43	0.68	1.23	1.35	50.0
Sulphate	mg/l	115.1	102.0	107.0	185.4	4.280	18.02	122.4	1.500	105.9	132.3	250.0
Carbonate	mg/l	31.60	36.56	43.73	81.12	56.43	41.96	43.96	0.4300	16.00	32.12	-
Aluminium	µg/l	0.84	14.5	4.15	6.52	7.87	5.52	4.42	3.52	4.39	6.32	200.0
Calcium	mg/l	113.7	80.75	41.54	88.68	92.32	236.7	62.41	4.180	99.70	88.42	150.0
Iron	µg/l	23.67	56.78	52.94	67.98	0.010	5.290	22.41	0.060	0.1900	23.46	300.0
Magnesium	mg/l	44.42	42.90	42.68	6.590	77.82	76.04	43.34	1.870	45.53	45.32	70.00
Potassium	mg/l	6.390	6.380	5.240	2.520	16.98	19.19	15.32	2.520	7.980	8.960	50.00

Sodium	mg/l	254.0	225.1	240.0	267.0	31.72	388.1	252.3	540.5	203.2	225.6	200.0
Manganese	µg/l	2.94	2.830	2.560	109	1.630	0.0200	1.310	1.430	0.0700	1.560	100.0
Copper	mg/l	7.87	7.56	6.65	7.82	7.76	6.78	6.56	5.25	6.54	6.56	2.00
Nickel	µg/l	1.14	1.12	1.26	5.66	6.58	3.68	5.52	5.53	1.54	1.35	70.0
Total Dissolved Solids(TDS)	mg/l	1167	951.0	1007	789.6	95.60	2024	1119	1588	918.0	832.5	1000

Table A2. Dukwi Wellfield Phase II water chemistry results- October 2019 (Botswana Bureau of Standards, 2016; Water Utilities Corporation 2019c; Department of Water Affairs, 2019c).

Parameter	Units	Borehole Number										
		BH 7674	BH 7675	BH 7687	BH 7678	BH 2985	BH 4649	BH 7516	BH 7521	BH 7639	BH 7546	BOS 262:2011
pH	-	7.14	7.24	7.27	7.64	7.23	7.09	7.69	8.51	7.14	7.17	5.5-9.5
Temp	^{o}C	23.2	25.2.	25.7	23.5	24.6	26.3	27.3	25.1	23.5	24.4	-
Conductivity (EC)	µS/cm	1457	1432	1553	1518	544.0	3097	1578	1542	1540	1421	1500
Turbidity	NTU	0.68	0.96	0.51	0.20	0.32	0.58	0.32	0.62	0.53	0.53	5.0
Bromine	mg/l	0.78	0.94	1.02	0.92	0.32	2.11	0.58	1.01	2.03	1.56	-
Chloride	mg/l	367	338	370	270	50.09	929	225.0	187	232	256	200
Fluoride	mg/l	0.92	0.64	0.78	0.82	1.9	0.37	0.47	9.7	0.89	0.46	1.0
Nitrate	mg/l	2.84	2.64	2.78	2.84	3.45	0.080	1.56	0.090	2.36	1.38	50.0
Sulphate	mg/l	118.3	112.5	121.9	125.6	5.250	88.78	124.6	1.070	108.9	136.3	250.0
Carbonate	mg/l	32.40	40.46	45.73	82.22	58.38	43.98	45.97	0.5200	18.00	35.22	-
Aluminium	µg/l	0.920	15.3	4.56	8.32	7.78	6.52	5.42	0.680	16.0	6.48	200
Calcium	mg/l	112.3	94.55	113.0	52.36	94.45	112.8	5.560	48.99	4.390	89.32	150.0
Iron	µg/l	23.76	58.78	51.56	82.75	0.0800	13.58	23.45	0.4300	99.70	25.31	300.0
Magnesium	mg/l	44.38	43.86	43.86	7.620	78.62	13.28	45.56	1.950	0.1900	46.32	70.00
Potassium	mg/l	6.53	5.51	5.51	2.56	21.4	18.6	16.3	15.3	45.5	9.35	50.0

Sodium	mg/l	238.1	256.0	238.0	272.0	33.52	752.2	256.3	562.3	238.0	228.4	200.0
Manganese	µg/l	3.21	2.83	2.68	109.4	1.83	0.020	1.31	1.62	2.03	0.070	100.0
Copper	mg/l	7.71	6.67	6.67	7.86	7.72	6.78	24.5	6.32	6.56	6.62	2.00
Nickel	µg/l	2.14	2.14	2.26	6.32	7.58	4.68	5.32	6.53	6.54	1.35	70.0
TDS	mg/l	1150	947.0	1009	1384	195.23	2026	872.3	858.6	855.2	840.6	1000

Appendix B: Geological logs of the monitoring and production boreholes in the study area (Department of Water Affairs, 2000).

Borehole Number	Completion date	Geology	Geological Formation
BH 2985	10/14/1974	0 - 7m: Calcrete & silcrete	Recent Deposits
		7 - 17m: Calcretised sandstone	Upper Tlapana
		17 - 22m: Rosty sandstone	Upper Tlapana
		22 - 36m: Light red sandstone	Upper Tlapana
		36 - 54m: Light red sandstone with clay	Upper Tlapana
		54 - 65m: Light red-pink sandstone	Upper Tlapana
		65 - 90m: Grey mudstone	Lower Tlapana
BH 4649	8/9/1984	0 - 12m: Decomposed material	Recent Deposits
		12 - 42m: Sandstone	Ntane Sandstone
		42 - 53m: Clay	Upper Tlapana
		53 - 78m: Shale	Lower Tlapana
		78 - 90m: Basalt	Stormberg Basalt
		90 - 132m: Quartzite	Mea Arkose
BH 7516	11/30/1993	0 - 1m: Soil	Recent Deposits
		1 - 2m: Light brown clay	Recent Deposits
		2 - 41m: Dolerite	Intrusive
		41 - 98m: Black carbonaceous shale	Lower Tlapana
		98 - 120m: Off-white arkose	Mea Arkose
		120 - 125m: Black, dull and shiny coal	Mea Arkose
		125 - 146m: Buff arkose	Mea Arkose
		146 - 170m: Black, dull and shiny coal	Mea Arkose
		170 - 177m: Off-white sandstone	Mea Arkose
		177 - 188m: Green-grey gneiss	Basement
BH 7521	1/15/1994	0 - 1m: Soil	Recent Deposits
		1 - 27m: Cream to off-white sandstone	Ntane Sandstone
		27 - 48m: Reddish brown mudstone	Upper Tlapana

		48 - 52m: Pale creamish pink sandstone	Upper Tlapana
		52 - 54m: Reddish brown mudstone	Upper Tlapana
		54 - 64m: Dolerite	Intrusive
		64 - 168m: Grey mudstone	Upper Tlapana
		168 - 240m: Dark black, shaly mudstone	Lower Tlapana
		240 - 256m: Black shales & sandstone	Lower Tlapana
		256 - 299m: Off-white sandstone	Mea Arkose
		299 - 305m: Dark grey to black shale	Mea Arkose
		305- 395m: Cream to off-white sandstone	Mea Arkose
		395 - 401m: Black shale	Mea Arkose
BH 7546	1/23/1994	0 - 1m: Soil	Recent Deposits
		1 - 8m: Pink silcrete	Recent Deposits
		8 - 23m: Pale yellow and pink sandstone	Ngwasha Formation
		23 - 39m: Pink-red to white clay	Ngwasha Formation
		39 - 53m: Pale yellow to beige sandstone	Ngwasha Formation
		53 - 73m: Brown to pale pinkish-grey clay	Ngwasha Formation
		73 - 84m: Pale grey to greenish grey mudstone	Upper Tlapana
		84 - 85m: Medium grey shale	Upper Tlapana
		85 - 146m: Pale grey mudstone	Upper Tlapana
		146 - 174: Carbonaceous mudstone	Lower Tlapana
		174 - 198m: Dolerite	Intrusive
		198 - 267m: Carbonaceous mudstone	Lower Tlapana
		267 - 303m: White to beige sandstone	Mea Arkose
		303 - 311m: Dark grey, carbonaceous mudstone	Mea Arkose
		311 - 403m: Pale grey sandstone	Mea Arkose
		403 - 415m: Siltstone & shale	Mea Arkose
BH 7639	6/3/1994	0 - 3m: Soil	Recent Deposits
		3 - 10m: White to cream calcrete	Recent Deposits
		10 - 61m: Pale greyish to beige mudstone	Upper Tlapana
		61 - 69m: Dark grey mudstone	Lower Tlapana

		69 - 76m: Shale	Lower Tlapana
		76 - 122m: Off-white to cream arkose	Mea Arkose
		122 - 127m: Black, carbonaceous shale	Mea Arkose
		127 - 132m: Cream to off-white sandstone	Mea Arkose
		132 - 135m: Black, carbonaceous shale	Mea Arkose
		135 - 160m: Off-white to grey sandstone	Mea Arkose
		160 - 169m: Tillite	Dwyka Formation
BH 7674	7/7/1994	0 - 1m: Soil	Recent Deposits
		1 - 9m: Calcrete with pinkish silcrete horizons	Recent Deposits
		9 - 10m: Beige clay	Upper Tlapana
		10 - 13m: Pink sandstone	Upper Tlapana
		13 - 51m: Pale greenish grey to yellow mudstone	Upper Tlapana
		51 - 60m: Mottled dark grey clay	Upper Tlapana
		60 - 79m: Dark brownish grey mudstone	Lower Tlapana
		79 - 81m: Black shale & mudstone	Lower Tlapana
		81 - 89m: Dark brownish grey to black mudstone	Lower Tlapana
		89 - 91m: Sandstone	Mea Arkose
		91 - 93m: Pale brown-beige mudstone	Mea Arkose
		93 - 112m: Pale grey sandstone	Mea Arkose
		112 - 115m: Medium to dark grey siltstone	Mea Arkose
		115 - 124m: Pale grey sandstone	Mea Arkose
		124 - 125m: Dark grey shale	Mea Arkose
		125 - 131m: Pale grey arkose	Mea Arkose
		131 - 133m: Pale grey sandstone	Mea Arkose
		133 - 134m: Dark grey-black shale	Mea Arkose
		134 - 138m: Brownish grey sandstone	Mea Arkose
		138 - 139m: Dark grey siltstone	Mea Arkose
		139 - 141m: Coarse grained arkose	Mea Arkose
		141 - 142m: Brownish grey sandstone	Mea Arkose
		142 - 152m: Dark to pale grey arkose	Mea Arkose

		152 - 165m: Dark grey-black mudstone	Mea Arkose
		165 - 167m: Dark brownish-grey sandy mudstone	Dwyka Formation
		167 - 172m: Pale greenish-grey siltstone	Dwyka Formation
		172 - 180m: Pale greenish-grey sandstone	Dwyka Formation
		180 - 192m: Dark to very pale greenish mudstone	Dwyka Formation
		192 - 197m: Siltstone & sandstone	Dwyka Formation
BH 7675	6/11/1994	0 - 1m: Soil	Recent Deposits
		1 - 9m: Light brown silcrete	Recent Deposits
		9 - 14m: Yellow-brown sandstone	Recent Deposits
		14 - 82m: Pale grey to pale greenish mudstone	Upper Tlapana
		82 - 99m: Dark brownish grey to black mudstone	Lower Tlapana
		99 - 100m: Pale grey arkose	Mea Arkose
		100 - 106m: Pale grey sandstone	Mea Arkose
		106 - 115m: Pale yellowish grey to white arkose	Mea Arkose
		115 - 159m: White to pale grey sandstone	Mea Arkose
		159 - 160m: White sandstone & shale	Mea Arkose
		160 - 165m: Black, carbonaceous mudstone	Mea Arkose
		165 - 166m: Pale grey sandstone	Mea Arkose
		166 - 171m: Black, carbonaceous mudstone	Mea Arkose
		171 - 179m: Black mudstone with sandstone	Mea Arkose
		179 - 186m: Black, carbonaceous mudstone	Mea Arkose
		186 - 187m: Pale grey sandstone	Mea Arkose
		187 - 188m: Pale grey siltstone	Mea Arkose
		188 - 192m: Black, carbonaceous mudstone	Mea Arkose
		192 - 194m: Pale grey sandstone	Mea Arkose
		194 - 196m: Pale grey sandstone & siltstone	Mea Arkose
		196 - 198m: Pale and dark grey mudstone	Dwyka Formation
BH 7678	6/23/1994	0 - 1m: Soil	Recent Deposits
		1 - 5m: White calcrete	Recent Deposits

		5 - 35m: Coloured mudstone	Upper Tlapana
		35 - 72m: Buff to yellow-brown arkose	Mea Arkose
		72 - 73m: Dark brown sandstone	Mea Arkose
		73 - 77m: Brown sandstone	Mea Arkose
		77 - 91m: off-white arkose	Mea Arkose
		91 - 98m: Pale purple to dark brown sandstone	Mea Arkose
		98 - 100m: Tillite	Dwyka Formation
		100 - 103m: Grey sandstone	Dwyka Formation
		103 - 119m: Mainly pale grey siltstone	Dwyka Formation
		119 - 125m: Schist	Basement
BH 7687	7/4/1994	0 - 1m: Soil	Recent Deposits
		1 - 2m: Medium brown, clayey sand	Recent Deposits
		2 - 5m: Creamy white-grey silcrete	Recent Deposits
		5 - 10m: Buff yellow sandstone	Recent Deposits
		10 - 49m: Coloured mudstone	Upper Tlapana
		49 - 59m: Grey-black, carbonaceous mudstone	Lower Tlapana
		59 - 110m: Pale grey to brown-red sandstone	Mea Arkose
		110 - 111m: Black, carbonaceous shale	Mea Arkose
		111 - 125m: White-brown to pale grey sandstone	Mea Arkose
		125 - 142m: Pale greenish grey metadolerite	Basement
		142 - 145m: Schist	Basement

Appendix C: Pumping test data of the production boreholes in the study area (1994) (Department of Water Affairs, 2000).

BH 7674			BH 7675		BH 7678		BH 7687	
t [min]	Dd [m]	Q [m^3/min]	Dd [m]	Q [m^3/min]	Dd [m]	Q [m^3/min]	Dd [m]	Q [m^3/min]
0.50	0.060	0.750	0.010	3.75	2.32	2.02	2.95	1.50
1.00	0.100	0.750	0.010	3.75	2.55	2.02	7.50	1.50
1.50	0.130	0.750	0.010	3.75	2.90	2.02	11.32	1.50
2.00	0.150	0.750	0.020	3.75	3.06	2.02	13.25	1.50
2.50	0.170	0.750	0.020	3.75	3.18	2.02	15.49	1.50
3.00	0.190	0.750	0.020	3.75	3.32	2.02	18.25	1.50
3.50	0.220	0.750	0.030	3.75	3.40	2.02	18.98	1.50
4.00	0.230	0.750	0.030	3.75	3.49	2.02	19.50	1.50
4.50	0.230	0.750	0.040	3.75	3.58	2.02	19.78	1.50
5.00	0.250	0.750	0.040	3.75	3.66	2.02	20.05	1.50
6.00	0.270	0.750	0.040	3.75	3.78	2.02	20.20	1.50
7.00	0.290	0.750	0.040	3.75	3.82	2.02	20.37	1.50
8.00	0.300	0.750	0.050	3.75	3.87	2.02	20.47	1.50
9.00	0.320	0.750	0.060	3.75	3.93	2.02	20.57	1.50
10.00	0.340	0.750	0.060	3.75	3.98	2.02	20.80	1.50
12.00	0.360	0.750	0.070	3.75	4.09	2.02	20.96	1.50
14.00	0.380	0.750	0.070	3.75	4.05	2.02	21.00	1.50
16.00	0.400	0.750	0.080	3.75	4.06	2.02	21.06	1.50
18.00	0.420	0.750	0.080	3.75	4.10	2.02	21.11	1.50
20.00	0.440	0.750	0.080	3.75	4.15	2.02	21.11	1.50
22.00	0.460	0.750	0.090	3.75	4.18	2.02	21.12	1.50
24.00	0.480	0.750	0.090	3.75	4.20	2.02	21.12	1.50
26.00	0.500	0.750	0.100	3.75	4.21	2.02	21.12	1.50

28.00	0.500	0.750	0.100	3.75	4.23	2.02	21.13	1.50
30.00	0.520	0.750	0.110	3.75	4.25	2.02	21.15	1.50
35.00	0.540	0.750	0.120	3.75	4.30	2.02	21.18	1.50
40.00	0.550	0.750	0.120	3.75	4.34	2.02	21.20	1.50
45.00	0.560	0.750	0.140	3.75	4.38	2.02	21.24	1.50
50.00	0.570	0.750	0.140	3.75	4.42	2.02	21.58	1.50
55.00	0.580	0.750	0.140	3.75	4.45	2.02	21.62	1.50
60.00	0.580	0.750	0.170	3.75	4.50	2.02	21.72	1.50
120.00	0.670	0.750	0.200	3.75	4.54	2.02	21.81	1.50

Notes:

t = time

Q = Discharge Dd = Drawdown

APPENDIX D: Hydraulic conductivities of unconsolidated sedimentary materials, sedimentary and crystalline rocks.

Table D1. Hydraulic conductivities of unconsolidated sedimentary materials (Duffield, 2020).

Material	Hydraulic Conductivity (m/min)
Gravel	1.8×10^{-2} to 1.8
Coarse sand	5.4×10^{-5} to 3.6×10^{-1}
Medium sand	5.4×10^{-5} to 3×10^{-2}
Fine sand	1.2×10^{-5} to 1.2×10^{-2}
Silt,loess	6×10^{-8} to 1.2×10^{-3}
Till	6×10^{-11} to 1.2×10^{-4}
Clay	6×10^{-10} to 2.82×10^{-7}
Unweathered marine clay	4.8×10^{-11} to 1.2×10^{-7}

Table D2. Hydraulic conductivities of sedimentary rocks (Duffield, 2020).

Rock Type	Hydraulic conductivity (m/min)
Karst and reef limestone	6×10^{-5} to 1.2
Limestone, dolimite	6×10^{-8} to 3.6×10^{-4}
Sandstone	1.8×10^{-8} to 3.6×10^{-4}
Siltstone	6×10^{-10} to 8.4×10^{-7}
Salt	6×10^{-11} to 6×10^{-9}
Anhydrite	2.4×10^{-11} to 1.2×10^{-6}
Shale	6×10^{-12} to 1.2×10^{-7}

Table D3. Hydraulic conductivities of crystalline rocks (Duffield, 2020)

Material	Hydraulic conductivity (m/min)
Permeable basalt	2.4×10^{-5} to 1.2
Fractured igneous and metamorphic rock	4.8×10^{-7} to 1.8×10^{-4}
Weathered granite	1.98×10^{-4} to 3.12×10^{-3}
Weathered gabbro	3.3×10^{-5} to 2.28×10^{-4}
Basalt	1×10^{-9} to 2.52×10^{-5}

Unfractured igneous and metamorphic rock	$1.8 \times 10\text{-}^{12}$ to 1.2×10^{-8}

APPENDIX E. Annual and monthly rainfall of the study area (Botswana Meteorological Services, 2019a).

Year	Month												Total (mm)
	Jan	Feb	Mar	April	May	June	Jul	Aug	Sept	Oct	Nov	Dec	
	Rainfall (mm)												
2010	82.4	80.1	48.9	128	2.6	0	0	0	0	0	0	12.3	354.3
2011	244.4	50	0.2	44.3	3.8	0	0	0	0	0	0	0	342.7
2012	4.9	120.5	26.6	0	0	0	0	0	0	11.5	78.8	15.3	257.6
2013	63.8	52.8	5.4	28.4	0	0	0	0	0	10.5	16.4	29.8	207.1
2014	25.9	18.5	22.9	0	0	0	0	0	0	0	8.3	28.2	103.8
2015	43.8	9.4	22.8	0	0	0	0	0	0	0	16.4	16.8	109.2
2016	119	74	38	57	0	0	0	0	0	20	58.2	54	420.2
2017	30.2	52.6	33.5	13.2	0	0	0	0	12	0	23.5	36.2	201.2
2018	86.5	28.5	39	13.8	0	0	0	0	0	0	0	32.5	200.3
2019	92.2	28.6	23.2	21.3	0	0	0	0	0	0	0	36.2	201.5
Average	**79.31**	**51.5**	**26.05**	**30.6**	**0.64**	**0**	**0**	**0**	**1.2**	**4.2**	**20.16**	**26.13**	**273.6**

APPENDIX F: Average minimum and maximum temperatures of the project area (2010-2019) (Botswana Meteorological Services, 2019b).

Year	Maximum Temperature (˚C)	Minimum Temperature (˚C)
2010	31.56	15.63
2011	31.01	14.63
2012	31.62	13.98
2013	31.32	14.99
2014	30.40	14.29
2015	31.90	16.11
2016	31.52	16.28
2017	29.44	15.14
2018	28.30	14.00
2019	31.30	16.36
Average	30.84	15.14

APPENDIX G: Average porosities of different rocks and sediments (Manger, 1963; Freeze and Cherry, 1979; Anon., 2006; Warrington, 2009; Barrett, Froggatt and Land, 2012).

Geological material	Average Porosity (%)
Clay	52.5
Silt	45
Sand	35
Gravel	30
Shale	10
Sandstone	17.5
Limestone	15.05
Basalt	0.5
Granite	1.0
Slate	0.5
Schist	0.5
Siltstone	31
Arkose	7.35
Calcrete	20.5
Tillite	20
Mudstone	17.1

APPENDIX H: Fractions of effective porosity considered for by Specific yield in different geological materials (Younger, 2000).

Geological Material	Fraction of Porosity considered for by specific yield in different geological materials
Coarse gravel	0.80
Medium gravel	0.75
Fine gravel	0.73
Coarse Sand	0.69
Medium Sand	0.70
Fine Sand	0.53
Clay	0.07
Silt	0.17
Till	0.18
Peat	0.48
Loess	0.37
Coarse grained sandstone	0.73
Medium grained sandstone	0.64
Fine grained sandstone	0.54
Limestone	0.74
Fracture microporous (or non-porous rock)	0.80
Tuff	0.51

APPENDIX I: Statistical significance of trends for monitoring wells and production boreholes at the wellfield area.

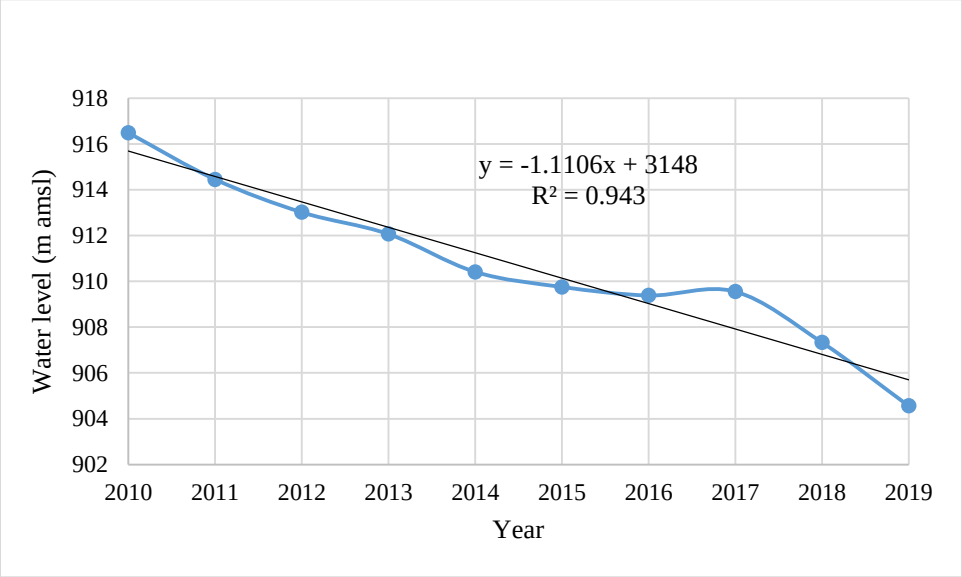

Figure I1. Annual average water level fluctuations and statistical significance of trend for Production Borehole BH 7675.

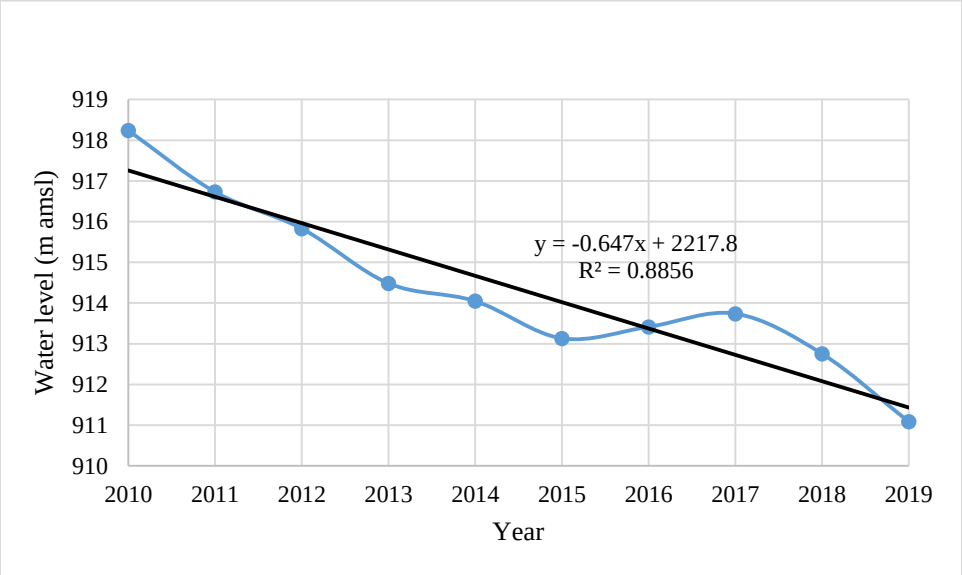

Figure I2. Annual average water level fluctuations and statistical significance of trend for Production Borehole BH 7674

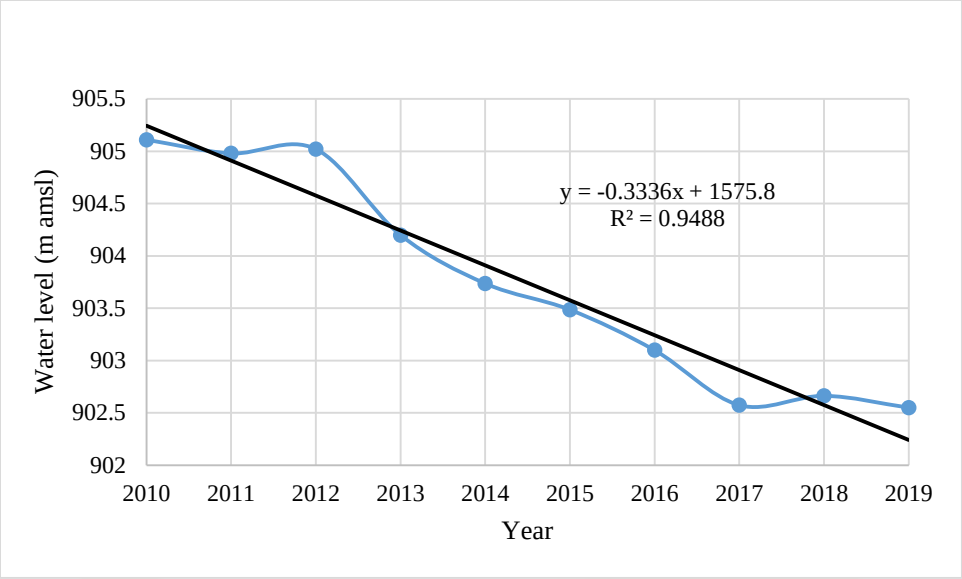

Figure I3. Annual average water level fluctuations and statistical significance of trend for Production Borehole BH 7678

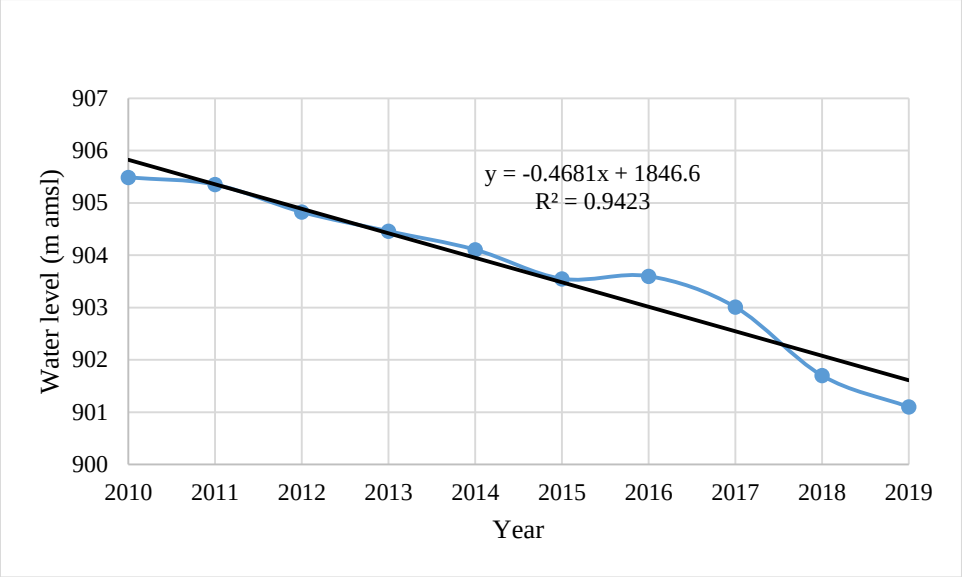

Figure I4. Annual average water level fluctuations and statistical significance of trend for Production Borehole BH 7687

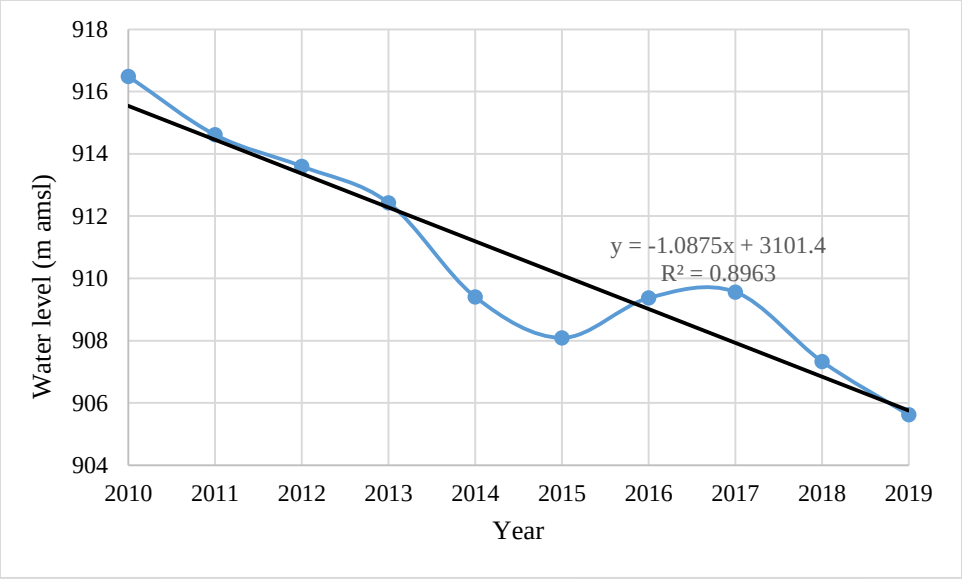

Figure I5. Annual average water level fluctuations and statistical significance of trend for Production Borehole BH 7516

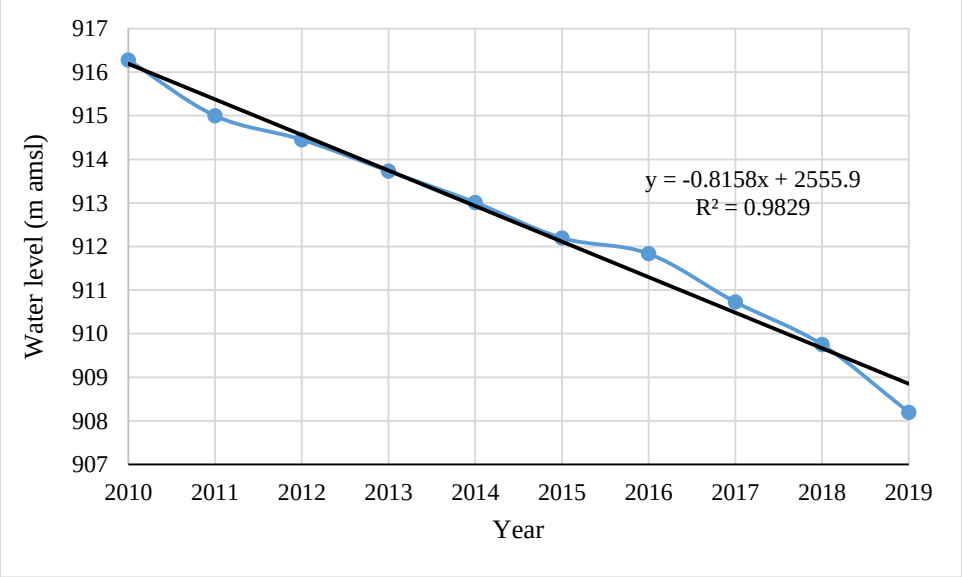

Figure I6. Annual average water level fluctuations and statistical significance of trend for Production Borehole BH 7520

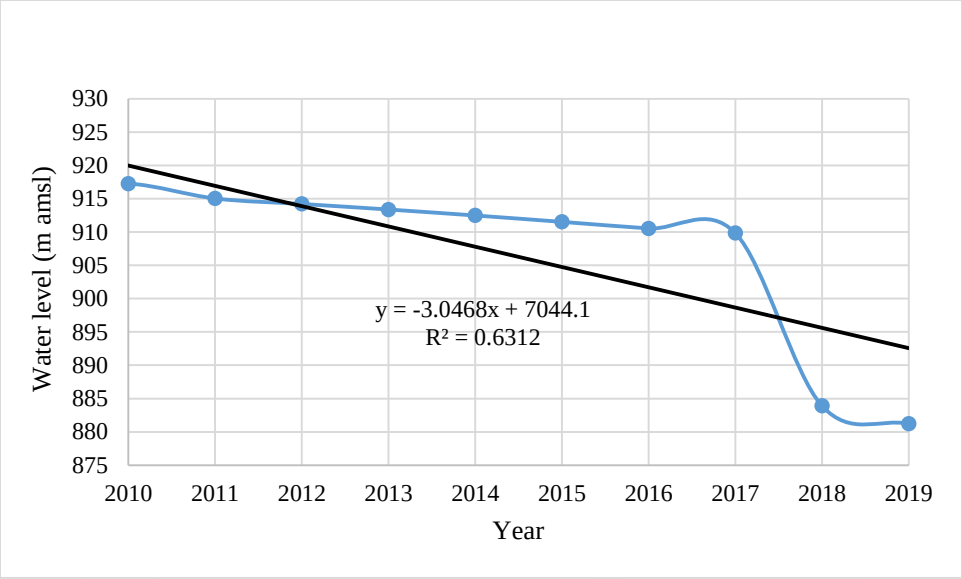

Figure I7. Annual average water level fluctuations and statistical significance of trend for Production Borehole BH 7546

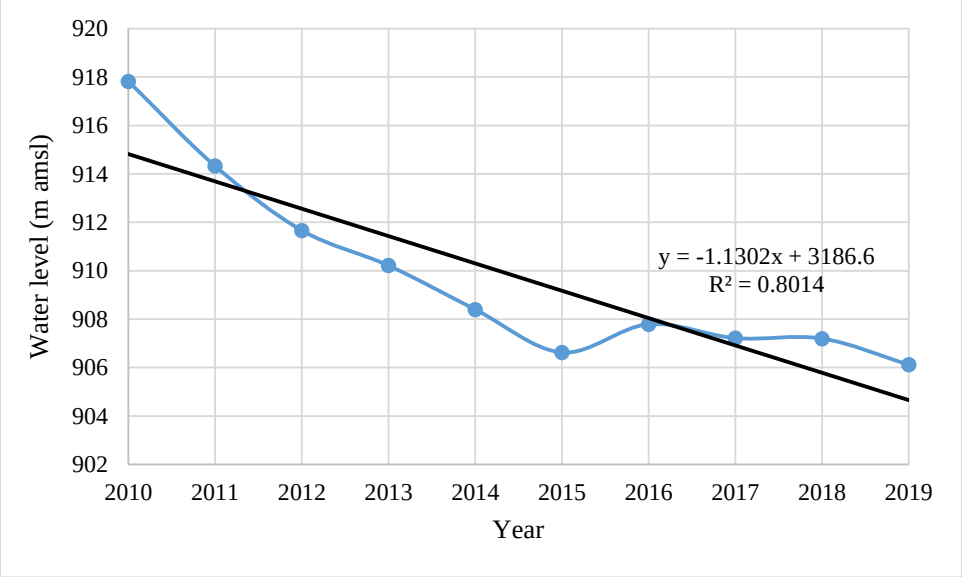

Figure I8. Annual average water level fluctuations and statistical significance of trend for Production Borehole BH 7639

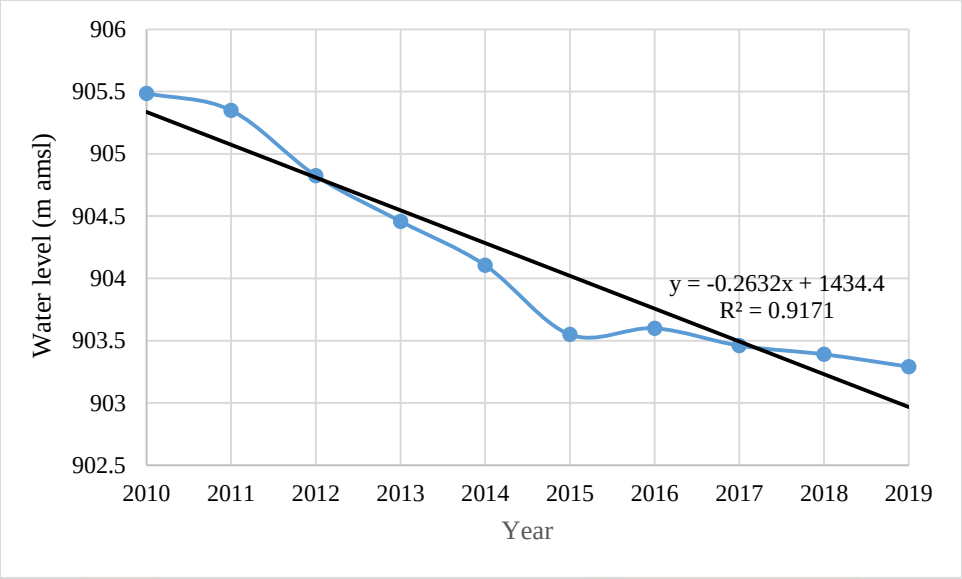

Figure I9. Annual average water level fluctuations and statistical significance of trend for Production Borehole BH 7641